DEVELOPMENT OF NANO-SCALE AND BIOMIMETIC SURFACES FOR BIOMEDICAL APPLICATIONS

A Dissertation

by

JAMES EDWARD HENRY

Submitted to the Office of Graduate Studies of
Texas A&M University
in partial fulfillment of the requirements for the degree of

DOCTOR OF PHILOSOPHY

August 2005

Major Subject: Chemical Engineering

DEVELOPMENT OF NANO-SCALE AND BIOMIMETIC SURFACES FOR BIOMEDICAL APPLICATIONS

A Dissertation

by

JAMES EDWARD HENRY

Submitted to the Office of Graduate Studies of
Texas A&M University
in partial fulfillment of the requirements for the degree of

DOCTOR OF PHILOSOPHY

Approved by:

Co-Chairs of Committee,	Theresa Good
	Daniel Shantz
Committee Members,	Gerard Coté
	Rosana Moreira
Head of Department,	Kenneth Hall

August 2005

Major Subject: Chemical Engineering

ABSTRACT

Development of Nano-scale and Biomimetic Surfaces

for Biomedical Applications. (August 2005)

James Edward Henry, B.S.; M.S., University of Arkansas

Co-Chairs of Advisory Committee: Dr. Theresa Good
Dr. Daniel Shantz

The work described in this dissertation details the development of a biomimetic materials for use in sensors and therapeutics, based on new advances in material science. The sensors developed herein target neurodegenerative diseases. Two of the diseases, the transmissible spongiform encephalopathies (TSEs) and Alzheimer's disease (AD), are diseases associated with the abnormal folding of a protein, thus detecting the disease is dependent upon developing structure specific sensor technologies. Both sensors developed in this work take advantage of the unique optical properties associated with nanoscale metal particles, however they use different types of spectroscopies for optical detection of the presence of the disease associated abnormal protein, and different types of recognition elements that bring the disease associated proteins close to the nanoscale metal particles. In the case of TSEs, the recognition element was a commercially available antibody. In the case of AD, the recognition element was a molecular scale self-assembled surface. A therapeutic for AD was developed based on the molecular scale materials developed for the AD biosensor. Mathematical models were developed

that facilitated the rational design of the biosensors described in this work that could also be used in future biosensor development.

To my wife, Kasey

ACKNOWLEDGMENTS

I would like to thank the FDA and NIH for funding on this project. Secondly, I would like to thank all my lab mates for their help and support through all the work. I would also like to thank Dr. Justin Baba, Dr. Mary Cloninger, Dr. Stephanie Mabry and Dr. Ram Hosmane for their guidance and expertise. Additionally, I would like to thank my committee for their patience and guidance in helping to complete this project. A special thank you to Dr. Theresa Good, my advisor. She has been an outstanding, leader, colleague, and, most of all, friend. Her strength, wisdom, and understanding are the hallmark by which I will measure myself. Finally, I would like to thank my wife, Kasey Henry, for her patience, perseverance, and love through all the trials. I could not have accomplished any of this without her.

TABLE OF CONTENTS

CHAPTER Page

Page

LIST OF FIGURES

FIGURE Page

FIGURE Page

LIST OF TABLES

CHAPTER I

INTRODUCTION

In the past decade, advances in material science have led to the development of new materials that can be used in biotechnology and medicine as part of sensors and therapeutics. Two areas in particular have had breakthroughs in technology, the development of nanoscale materials and the development of self-assembled molecular surfaces.

Nanoparticles are any particle-like structure that is on the nanometer scale. Some of these nanoparticles are formed from a metal or metal complex. The small size of these particles causes them to exhibit unique properties. Currently, the unique electrochemical properties of nanoparticles are exploited for use in catalysis and gas sensing [1, 2, 3]. Nanoparticles are also used in magnetic resonance imaging (MRI) and electron microscopy imaging [4, 5, 6]. Furthermore, there has been some work expanding into the area of using nanoparticles as carriers for use in protein introduction *in vitro,* to protect the protein from degradation [7]. However, the most interesting property of nanoparticles in how they apply to this work is how the electromagnetic field of these particles, when in the presence of a light source, can greatly alter the optical properties of objects close to the nanoparticle (a few nanometers away).

This thesis follows the style of the Journal of Analytical Biochemistry.

To fully take advantage of the unique optical properties of metal nanoparticles in sensor development, we had to create a way to selectively bind the target analyte to the nanoparticles to achieve the appropriate distance. Monoclonal antibodies are the most commonly used material which binds with high affinity and specificity to a protein or biological material, however, they are of relatively large molecular dimensions, on the order of 8 nm, which limits their utility in nanoparticle based sensor applications. It is this requirement for small molecular size of a recognition or binding element that led us to the development of self-assembled molecular surfaces with small molecular size but high affinity for the target analyte that are described in this work.

Self-assembled molecular surfaces are any materials that naturally align themselves into a well-ordered, structured surface. This behavior is described by such phenomena as the formation of self-assembled monolayers by alkanethiols and polymers, the formation of micelles by phospholipids, or the assembly of peptides into tertiary structures. Self-assembling peptides and polymers have been used as adhesion substrates in tissue engineering [8, 9, 10]. Additionally, thiol-based monolayers are used to form coatings to prevent corrosion and oxidation of metals and other surfaces [11, 12]. Finally, self-assembled materials have been used as substrates for micropatterning and sensing platforms, generally used in surface plasmon resonance [13-23].

While the advances in the material sciences alone are important, to design and build them into useful devices, such as biosensors or therapeutics, requires an interdisciplinary understanding of several scientific fields. The work described in this dissertation details the development of a biomimetic materials for use in sensors and

therapeutics, based on these new advances in material science. The sensors developed herein target neurodegenerative diseases. Two of the diseases, the transmissible spongiform encephalopathies (TSEs) and Alzheimer's disease (AD), are diseases associated with the abnormal folding of a protein, thus detecting the disease is dependent upon developing structure specific sensor technologies. Both sensors developed in this work take advantage of the unique optical properties associated with nanoscale metal particles, however they use different types of spectroscopies for optical detection of the presence of the disease associated abnormal protein, and different types of recognition elements that bring the disease associated proteins close to the nanoscale metal particles. In the case of TSEs, the recognition element was a commercially available antibody. In the case of AD, the recognition element was a molecular scale self-assembled surface. A therapeutic for AD was developed based on the molecular scale materials developed for the AD biosensor. Mathematical models were developed that facilitated the rational design of the biosensors described in this work that could also be used in future biosensor development.

CHAPTER II

LITERATURE REVIEW

Introduction

There have been several recent advances in material science that have impacted biotechnology and bioengineering. Among these advancements, two standout as influential and are relevant for the work discussed here: nanoparticles and self-assembled molecular surfaces. These advances in material science have led to advances in biotechnology and medicine such as more rapid sequencing of the genome, new technologies for tissue engineering, and development of biomimetic surfaces.

Nanoparticles

Nanoparticle development

Nanoparticle based sensor systems have been in development since about the early 1980's [24, 25]. The development started with the reports that certain metals and semiconductor colloidal suspensions showed unusual optical properties [26]. However, this phenomenon seemed to be most pronounced with particles on the nanometer scale [24]. As an extension of this phenomenon, semiconductor nanocrystals showed the ability to produce fluorescence that was up 20 times more intense and 100 times more stable than conventional fluorophores [25]. It was also found that nanoscale metal

particles of certain noble metals could dramatically alter the natural spectra of nearby molecules [26].

The principles that lead to the interesting optical effects associated with nanoparticles arise from the physical characteristics of the nanoparticles. The changes in optical properties relate back to the plasmons and resonant frequencies of the particles. Surface enhanced fluorescence occurs when the excitation of the fluorescent compound is coincident to the surface plasmon frequency of the particle. The nanoparticle "focuses" the excitation source that is incident to the particle surface. When the fluorophore is in close proximity, the nanoparticle can transfer the absorbed excitation energy to the fluorophore, in turn increasing the excitation energy delivered to the fluorophore and increasing the fluorescence. This creates the effect of increasing the quantum efficiency (ratio of energy absorbed to energy emitted) of the fluorophore, leading to an increased signal [27-29]. Most spectroscopic techniques using fluorescence modification in the presence of nanoparticles involve the use of molecular beacons for the detection of DNA and RNA [30-34]. However, this shift in optical properties can be tied to other techniques.

Surface enhanced Raman spectroscopy (SERS) relies on gold or silver nanoparticles for their ability to increase Raman spectra of target analytes in a solution or on a surface. This technique relies on the same physical properties discussed earlier, with the exception that instead of increasing fluorescence, the particles increase the Raman scatter of the target. However, SERS generally relies on nonspecific aggregation of these nanoparticles to the target of interest. We propose that by attaching a

recognition molecule to these SERS substrates, we can produce a specific SERS sensor [35 – 40].

Surface plasmon resonance (SPR)

Surface plasmons are charge density waves propagating along the interface of a metal and a dielectric media [41]. For metals to exhibit strong surface plasmon resonance, the free electrons associated with the metal must be mobile (have low electrical resistance). This property makes silver and gold the best options for SPR. While gold features a good chemical stability, silver provides sharp SPR resonance peaks. Kretchmann's method is the most predominant method used in SPR. This method uses the phenomenon of total reflection [42]. The method relies on the partial penetration of light as it passes through the interface of two media of different optical densities. The partial penetration of light (one wavelength in depth) creates an evanescent wave that excites molecules near the material media interface. In SPR, the evanescent wave couples with the free oscillating electrons (plasmons) of a thin metal film placed at the interface. Adsorption and desorption from the metal film creates shifts in the resonance angle of the plasmon. It is this angle shift that is detected [42, 43].

Surface modified fluorescence

Surface modified fluorescence relies on the interaction of a fluorophore or other fluorescent compound with some surface or particle with electrons available for interaction. This behavior is related to the surface plasmon of the material and the

resonant frequency of the modifier [44]. Förster resonance energy transfer (FRET) is a form of surface-modified fluorescence that relies on the photonless transfer of energy from one fluorophore to another (when the donor emission overlaps the receiver excitation) [44]. For both systems, there is a very strong dependence on distance.

A variety of assays that exploit changes in fluorescence in the vicinity of a nanosurface have been developed recently. Most of these have been used in the form of molecular beacons. Recent work indicates the use of this technique for the detection of prostate-specific antigens [26] and blood-glucose levels [45]. This broad application of the technology allows it to be an excellent cross-material sensing platform.

Surface enhanced Raman spectroscopy (SERS)

Surface enhanced Raman spectroscopy (SERS) is a Raman spectroscopic technique that provides greatly enhanced Raman signal from analyte molecules that have been adsorbed onto certain specially prepared metal surfaces. Increases in the intensity can be as high as 10^8 and 10^{14} for some systems [46, 47]. Raman is ineffective for analyte studies at low concentration due to weak vibrational modes being undetectable over background signal. SERS selectivity of surface signal results from the presence of surface enhancement mechanisms only at the surface. Thus, the surface signal overwhelms the bulk signal. The majority of this enhancement is attributed to electromagnetic effects (EME) at the metaled surface [48]. The structural and molecular identification power of Raman combined with the EME makes SERS useful for the detection of trace molecules [46]. SERS is observed primarily for analytes adsorbed

onto coinage (Au, Ag, Cu) or alkali (Li, Na, K) metal surfaces, with the excitation wavelength near or in the visible region [49]. However, many metals would be capable of exhibiting SERS. Metals such as Pd or Pt exhibit enhancements of about 10^2-10^3 for excitation in the near ultraviolet [47]. The importance of SERS is that the surface selectivity and sensitivity extends Raman utility to a wide variety of interfacial systems previously inaccessible to Raman due to low surface sensitivity. In addition to the positives previously discussed, SERS can be conducted under ambient conditions and has a broad wavenumber range [50]. Unlike other vibrational spectroscopies, SERS can be performed in the presence of water, as Raman is most sensitive to non-polar molecules. SERS shows higher enhancement on roughened metal surfaces [51]. The features are generally less than 100nm (which is quite small compared to the wavelength of the excitation source) [47, 52]. The small size of the particles allows the excitation of the metal particle's surface plasmon to be localized. The resultant electromagnetic energy density on the particle is the source of the EME, the primary contributor to SERS. It is SERS and surface-modified fluorescence that we use in the development of the sensors described in this work.

Self-assembled molecular surfaces

Self-assembled molecular surfaces can be formed from a number of materials. These include the use of biological materials such as phospholipids and peptides. More expansively, the use of alkanethiols and polymers on different surfaces has been investigated extensively. Uses for these materials are numerous.

As discussed previously, self-assembling peptides and polymers have been used as adhesion substrates in tissue engineering [8 - 10]. Self-assembled materials have been used as substrates for corrosion prevention, micropatterning and sensing platforms. The sensing platforms are generally used in surface plasmon resonance and focus on the assembly of the monolayer itself and not what is happening external to the monolayer [11 - 23]. Relying on works performed by Laibinis and others, we intend to look at how to take advantage of the monolayer for assembly of and recognition surface substrate [53 - 55]. Some work has been done in this field, generally in the area of tissue engineering.

Self-assembled materials have been used to guide cell growth and adhesion in tissue engineering [56 - 59]. These self-assembled materials (particularly peptides) have been analyzed for cytocompatability [8]. Expanding on this, work applying these self-assembled materials for direct tissue replacement is underway involving both hard and soft tissue replacement [60].

Some of the most interesting and applicable work is in area of microarrays for biosensing. Little work has been done in the area, with most of it involving the use of immobilized antibodies for use microarrays [61]. However, this technique does not take advantage of properties of the self-assembling materials. The assembled material is simply a tethering molecule. We propose and prove that by using self-assembled monolayers we can block nonspecific binding, create surface flexibility, minimize distance, and mimic biological surfaces [62 - 64]. Many bio micro electric mechanical systems (bioMEMS) use the self-assembled materials structurally; however, this neglects the fact that self-assembled materials (particularly self-assembled monolayers

(SAMs)) can serve not only structural, but functional purposes as well. SAMs can allow for close assembly to a substrate for sensing purposes (i.e. SERS) where simply tethering a biological receptor or antibody would prove fruitless (due to distance constraints and the large size of receptors and antibodies). It is this area of self-assembly that we exploit in this work.

Rationale for sensor modalities

Sensors in food and pharmaceutical industry

Food-borne illnesses are an increasing threat in today's society. The food pathogen testing/biosensor market is expected to grow to approximately $200 million in 2005, with common pathogens such as E. coli and Salmonella and conventional microbiological assays and DNA/PCR based methods still important [65]. Compounding the situation with food-borne illnesses is the immergence of new threats (i.e. Bovine Spongiform Encephalopathy) requiring the development of practical and robust detection methods [66, 67].

Bovine spongiform encephalopathy (BSE)

No disease has captured public awareness or scientific concern quite like bovine spongiform encephalopathy or as it is more commonly known, mad cow disease. Public anxiety grew as more and more information came forward about this illness. Officials in the United Kingdom made public on March 20, 1996, a possible link between BSE and what was believed to be a new, lethal human illness called new variant Creutzfeldt-

Jakob disease (vCJD). In the statement, the officials stated that 10 people in the UK had been diagnosed with vCJD in the previous 14 months [66]. Similarly, around the same time, a case of vCJD was reported in France [67]. By October, 1997, there were 10 additional cases in the UK [66]. Upon further investigation, it was proposed that the onset of vCJD was caused by the ingestion of BSE contaminated meat. Based on reports from the Center for Disease Control, as of the end of 2003, there have been a total of 158 cases of vCJD worldwide (147 in the UK) [68].

With no current known treatment for vCJD, the only way to control the spread of this disease is to eliminate the consumption or use of BSE contaminated materials in food products or pharmaceuticals. While measures are in place to prevent the spread of BSE to countries outside of the UK, and to eliminate infected cattle, no system is fool-proof as evidenced by the recent report of BSE infected cattle in Alberta, Canada. In order to prevent the spread of vCJD in humans, sensitive and robust sensor technologies are needed to detect the transmissible agent in BSE.

Bovine Spongiform Encephalopathy (BSE) and new variant Creutzfeldt-Jacobs Disease (vCJD) are both transmissible spongiform encephalopathies (TSE). They are fatal, neurodegenerative diseases that can affect both animals and humans. The diseases are characterized by protein aggregate deposits in the brains of the infected organism. The most distinguishing characteristic of both of these conditions is that they are transmitted via infectious proteins, or prion, rather than bacteria or viruses [69]. These infectious proteins are resistant to heat, ultraviolet radiation, ionizing radiation, and most normal disinfectants (i.e. formaldehyde and gluteraldehyde) [70].

Prions (PrP) are defined as proteinaceous infectious particles that lack nucleic acid. The normal cellular form of the prion is called PrP^{C} and is readily digested by proteases. The pathogenic form of the prion is called PrP^{SC} and is partially resistant to proteases [71]. PrP^{C} is found in healthy neuronal tissue and is encoded by a single copy host gene [70]. It appears to be involved in dendritic extension, antibody-antigen trapping [72], and possibly in calcium control [73]. PrP^{C} has a molecular weight of 35kDa and is a membrane bound protein whose secondary structure consists of approximately 42% α–helical and 3% β–sheet. PrP^{SC}, however, has a molecular weight of only 27-30kDa and has a secondary structure that is about 30% α–helical and 43% β–sheet [74]. It is this increased β–sheet structure of the PrP^{SC} that leads to aggregation and protease resistance. When PrP^{SC} comes into contact with PrP^{C}, the infectious protein causes the normal prion to refold itself into the infectious form. This is how the protein propagates.

New variant Creutzfeldt-Jacobs Disease (vCJD) occurs in people ages 19-39 years of age. This disease exhibits a number of psychiatric and/or sensory symptoms. Theses symptoms include, but are not limited to: fatigue, disordered sleep, decreased appetite, memory loss, loss of vision, and loss of various mental and physical abilities [75]. The symptoms continue to worsen until eventual death (a length of approximately 14 months from onset). vCJD is often misdiagnosed as Alzheimer's disease (however because of the early onset age, this is less common now) [76]. The only definitive way to diagnose vCJD is by histological examination of the brain of the infected person [70]. Upon examination, the brain exhibits deposition numerous PrP amyloid plaques in

multiple cortical and subcortical regions [77]. This has been shown to lead to diffuse neuronal degeneration and glial cell proliferation, giving rise to the typical spongiform (or sponge-like) appearance of infected brain upon autopsy [76].

Current detection methods – hamster model

Bioassays are the traditional assays for prion protein detection since the discovery of transmissible spongiform encephalopathies. This style of assay involves injecting material into the brain of some host animal and watching for symptoms of prion infection. After some set period of time that is defined by the incubation period of the host animal (the shortest being 60 days is the case of the golden Syrian hamster), the host animal is killed and its brain is examined for signs of prion infection (i.e. protein plaque formation). The first useful form of these bioassays was the transmission of scrapie from mouse to golden Syrian hamsters, hence the name the "Hamster Model" [78].

Current detection methods – immunoassay approaches

While there are several different variations of immunoassays that have been developed, they all generally rely on the same principles. These assays use either monoclonal or polyclonal antibodies to detect the presence of prion proteins. In the general ELISA form of immunoassays, the sample is immobilized in a well on a microplate. The well is washed carefully and then treated with an antibody to the target prion (primary antibody). The well is then washed again and treated with an antibody

against the primary antibody (secondary antibody). The secondary antibody is normally labeled with an enzyme to some substrate that will give a colorimetric response depending upon the concentration of the secondary antibody. The enzyme normally used in horseradish peroxidase [79].

The second form of immunoassays used for prion detection rely on a standard Western blot technique do detect the infectious prion. This process is performed by first treating the samples with proteinase K, and then performing a western blot on the digested sample. The monoclonal antibody used in this technique will only bind to the undigested fragments that showed some resistance to protease K. These prion pieces are from the infectious form of the prion [80].

While both these techniques have shown acceptable detection limits (down to approximately 5 pg / ml or 185 fM), they have certain shortcomings [80]. Both techniques take moderately long periods of time to obtain results (2 to 4 days). Also, these techniques take rather substantial levels of specialized training. Finally, these techniques, due to the response being visual, are semiquantitative. This leads to the need for a simple, robust, rapid, and sensitive method for the detection of prion proteins in foodstuffs [69].

In addition to foodstuff concerns, we must also become more aware of the expanding use of biological products in the pharmaceutical industry. Recombinant protein products are becoming much more prominent in today's pharmaceutical manufacturing procedures (such as cell culture based pharmaceuticals and tissue engineering materials). With this expansion comes the need for even greater safety

measures in the event of cross-species contamination from opportunistic viral agents. This leaves a substantially large opportunity for biosensor development.

Sensors in the medical industry

There is also a growing need for detection methods to be used in biomedical applications (i.e. diagnostics). With the advent of molecular medicine, advances in disease treatment are being made faster than advances in diagnosis [81]. For some diseases such as Alzheimer's disease (AD), when definitive diagnosis can only be made post mortem, the need for new diagnostic technology is apparent. Further compounding this need for an AD diagnostic tool are the costs facing the U.S. and other countries for AD patient care.

Alzheimer's disease

Alzheimer's disease is a neurodegenerative disease that is characterized the by the aggregation and deposition of β-amyloid (Aβ) in the brain. It is the leading cause of neurodegradation in the United States. As of 2003, there were 4.5 million cases in the United States. This number is expected to grow to greater than 14 million by 2050 [81].

The large number of AD patients in the United States leads to medical costs of an estimated $100 billion per year, with $61 million incurred by U.S. businesses. Most of this cost can be attributed to long-term care of patients that can no longer take care of themselves [81].

Progression of the disease starts with the aggregation of Aβ in the entorhinal cortex of the brain, the memory processing center. This aggregation is marked by the formation of senile or neuronal plaques between neurons and neurofibrillary tangles inside neurons. The disease progresses to the hippocampus (responsible for complex memory), and finally the neocortex (top, responsible for sorting stimuli and orchestrating behavior), with both senile plaques and neurofibrillary tangles accompanying the neurodegeneration. In addition to the plaques and tangles, there is noted mass loss and rutting of the brain. This progression eventually leads to death (on average 9 years after the onset of symptoms [82]. AD can only be diagnosed definitely by post-mortem analysis of the brain [81].

Aβ is the primary protein component of senile plaques. Aβ is produced from the proteolytic processing of amyloid precursor protein (APP). This processing is performed by two proteolytic enzymes, β-secretase and γ-secretase. Upon cleavage, a peptide sequence ranging form 39 to 43 amino acids long (~4100 Da) is created. In healthy adults, this protein is cleared easily. This clearance is made possible by cleavage of the protein by α-secretase. However, in AD brains, the protein aggregates (forms β-sheet structures). These structures progress on to protofibrils (fibril precursors) and eventually fibrils (long, thin protein microtubules). All known genetic mutations that lead to familiar AD are associated with the processing and aggregation of Aβ [81].

Aβ detection techniques

Diagnosis of Alzheimer's disease (AD) is done by clinical analysis of symptoms (dementia, loss of memory, etc.). Unfortunately, this form of diagnosis is not absolute, since any neurological disease that causes the same symptoms could be misdiagnosed as AD. This means that the only way definitively diagnose AD is by post-mortem analysis of the victim's brain. During the autopsy, certain hallmarks are analyzed to verify the pre-mortem diagnosis (amyloid fibrils, senile plaques, neurofibrillary tangles, loss of brain mass, severe rutting and degradation).

There is currently a major push in academic research to develop other methods for Aβ detection. One area of interest is using amyloid-reactive dyes that to bind to the fibrils and plaques [83]. This technique would be used to image the brain. While excellent for imaging, this technique creates two major problems. First, the issue of crossing the blood-brain barrier has to be overcome. Second, these dyes are not specific to Aβ fibrils. This means that any amyloid based neurological disease would be labeled by the dye. It's important to be able to distinguish one disease from another to institute the proper treatment. This is especially important as new advances in AD treatment such as vaccines and Aβ aggregation inhibitors are on the horizon [84, 85].

Other than dyes, most techniques revolve around standard laboratory analysis techniques. One method is via immunoprecipitation-HPLC-Mass spectroscopy [86]. This method is not used for in-patient detection and relies on standard ELISA technology. However, the immunoprecipitation step creates a dilemma. It's known that Aβ changes structures based on the ionic strength, acidity, temperature, etc. of the

environment in which it is placed. This means that the sample that is being analyzed at the end of the procedure is not the same sample that was pulled from the patient. Furthermore, this technique requires a substantial amount of time and training (up to a week for sample preparation and analysis). Since this is just an extension of ELISA, the same argument can be made for any immunoassay that is used.

Other methods that are suggested use standard MRI to detect both mass loss in the brain and the formation of amyloid plaques [87, 88]. However, MRI systems can only detect unusually large plaque formations (therefore only able to detect very advanced cases). Additionally, while plaques are a hallmark of the disease, the mechanism for neuronal degradation from Aβ is not completely understood. Current beliefs indicate that the toxic species is not the plaques, but some precursor (which will have already been present for a substantial length of time prior to plaque formation) [89, 90]. Using PET scans has also been suggested, but this requires the use of radioactive substrates for imaging and can only tell a loss of metabolic activity in the brain (so it can only detect once the brain is wasting) [91]. By the time either of these techniques is useful, treating the patient is purely academic, with little hope of major improvement.

With the difficulties of detecting Aβ directly, many people are looking for markers that are related to Aβ formation. The markers include amyloid precursor protein, presenilin-1 [92], mitochondrial damage [93], tau protein, ptau protein [94], and insulin degrading enzyme (IDE) [95]. These markers can all be found in cerebrospinal fluid, with the exception of mitochondrial damage. The fact that these markers do not require brain tissue samples for detection indicates a legitimate potential for the

detection of these markers to be used in a diagnostic procedure for AD. However, the relationship between these markers and the development of AD has not characterized to the point necessary to rely on these markers alone. Conversely, the link between Aβ fibrils and AD has been substantially studied and is widely accepted [96 - 100]. It is for this reason we feel that a sensor or assay based on detection of structure specific forms of Aβ is superior to what else is being developed. A SERS based assay that was specific for Aβ would provide both the concentration and structure information thought needed for diagnosis of AD and monitoring of disease progression.

AD therapeutic techniques

Most clinically used treatments for AD that have been developed to date have nothing to do with actually treating the cause of the disease, or even preventing or slowing further neurodegeneration. They focus on treating the symptoms to improve the quality of life. One example is the use of acetyl cholinesterase inhibitors to increase the amount of acetylcholine in patients with AD (acetylcholine is responsible for transmitting the signals involved in memory and cognition). While this helps with memory, the neuronal degradation continues. This is why it is important to treat the underlying cause of the disease.

Most researchers believe that Aβ is the (or one of the) causative agents in AD. It has been shown to be neurotoxic both *in vivo* and *in vitro* when aggregated [96]. Overexpression of APP with mutations that lead to Aβ production results in the development of AD like symptoms in transgenic mice [89]. Vaccines that sequester

aggregated Aβ appear to reduce AD like symptoms in transgenic models of the disease [84].

Agents which either sequester Aβ or interfere with Aβ interaction/binding to cells have been sought after as a means to reduce the pathological effects of Aβ [97, 101 - 104]. We believe that the same biomimetic materials developed that provide molecular scale high affinity interaction with Aβ for sensing might also be developed into a therapeutic which interferes with Aβ-cell interactions to prevent Aβ induced neurodegeneration.

Sensor design

Sensors are an important combination of two fields. The first is the development of some recognition unit toward an analyte of interest, be it a protein, peptide, cell, compound or single element (such as in oxygen sensors). The second step is developing some sort of signaling technique. These range from optical based (absorbance, fluorescence, etc.) to electrical transduction as is found in enzymatic sensors. The challenge lies in how to link these two in way that can be used as a sensor. It is this challenge that requires the incorporation of multiple disciplines and ideas.

Recognition methods for sensors

With any sensor, it is required to have high specificity and affinity. ELISA-like assays use antibodies (which have very high specificity and affinity) as recognition molecules. Applying the use of antibodies, we have been able to develop a solution-

based sensor for the detection of Bovine Spongiform Encephalopathy (BSE) prions. This sensor shows lower recognition limits on the order of 1nM (approximately equal to the equilibrium binding coefficient for the antibody) with high specificity.

In parallel, the recent development of mini-mAbs (bacterially produced light chain antibodies of monoclonal antibodies) greatly expands the possibilities of these sensors [105]. With these mini-mAbs showing much smaller molecular weights than antibody fragments (25-30kDa compared to 50kDa), there use in highly dependant distance-based sensors (FRET, SERS, surface-modified fluorescence based) is attractive. For distance-based sensors, the measured variable varies by one over distance to the sixth. Therefore, every bit of distance that can be eliminated helps.

Another option for recognition molecules includes the use of cell surface receptors to develop sensors for serum-based measurements. Elevated levels of serum analytes have been linked to several diseases (soluble IL2 receptor for hepatitis C or glucose levels in diabeties) [106, 107]. When the use of these surface receptors is not possible, it is important to be able to develop something that can be used in its place, a biomimetic structure. We were able to do just that when constructing sialic acid modified dendrimers to mimic cell surface gangliosides for both sensing Aβ and preventing Aβ toxicity. Using an expansion of this principle, it would be possible to immobilize the cell membranes from a desired cell to a sensor surface to keep intact an entire receptor complex and not just a single receptor.

Recognition molecules

While the options for recognition molecules are substantial, there has been little done to expand into new recognition detection areas. Most work being done in sensor recognition is in the area of either immuno-based recognition, enzymatic recognition, or cell receptor-based recognition.

Immuno-assays range in use from standard ELISA techniques to immobilized antibodies for use in SPR. While antibodies show excellent affinity values (10^9 M^{-1}), they have limitations in that their size (~150 kDA) can cause interference in size-dependant assays. Furthermore, if the target analyte is a protein, then IR, Raman, and rayleigh scatter can have overlapping (interfering) signatures [108 - 112].

Enzymatic recognition has many similar characteristics to immunological recognition, but with smaller protein size. Enzymes also have the bonus that they can perform auto-amplification (as in colorimetric assays and electrical based recognition). However, when destruction of the desired analyte is not acceptable, this leads to enzymatic sensing being a hindrance. Additionally, enzymes have substantially lower binding coefficients than antibodies (10^6 M^{-1}) [113 - 118].

Cell receptors have the similar characteristics to antibodies. While surface receptors produce extremely high affinity (10^7 - 10^{10} M^{-1}), harvesting these receptors can be extremely difficult [119 - 121]. In addition, because cell surface receptors are typically found in the context of the cell membrane, the solubility and/or stability of cell receptors in solution is sometimes problematic.

Electrical-based detection methods

Biosensors based on electrical transducers are the most commonly used for clinical analyses and the most frequently cited in the literature. Amperometry is the electrochemical technique usually applied in commercially available biosensors. Amperometry is an electrochemical technique taking advantage of the fact that certain chemical species are oxidized or reduced (redox reactions) at metal electrodes when exposed to a constant potential. Related to amperometry is coulometry. Coulometry is an electrochemical technique where the amount of charge passing between two electrodes is measured. The amount of charge passing between the electrodes is proportional to oxidation or reduction of an electroactive substance at one of the electrodes [45, 122 - 124]. The technique has been applied to glucose detection in cell cultures [125].

Potentiometry is the measurement of the potential difference between two electrodes when the current is zero. The two electrodes are known as the indicator and reference electrodes. The indicator electrode develops a variable potential depending on the activity or concentration of a specific analyte in solution. The difference in potential between the reference and indicator electrode is related to concentration of the analyte. Ion-selective electrode (ISE) a potentiometric technique routinely used in clinical chemistry for the detection of electrolytes. A change in solution conductivity has also been used in enzyme-based biosensors. When an alternating potential is applied between two inert electrodes, the conductance of the solution is measured. Some

enzyme reactions, producing a change in the ionic strength of the sample, may be monitored by conductometric devices [126 - 128].

Piezoelectric detection is a technique that relies on a change in the oscillatory properties of a polymer or crystal substrate in the presence of a target analyte. This system relies on the change in frequency of oscillation of the polymer/crystal due to increased mass upon absorption of some target analyte. This increased mass leads to a decrease in the oscillation rate of the polymer which can be measured. This technique has great promise due to its low detection limits (picograms), but is limited by immobilization and processing issues. [129 - 132] In particular, the mass of the absorbed analyte must be significant with respect to the mass of the recognition unit, such that the change in mass is detectable above system noise.

Optical-based detection methods

To expand this idea into enzyme detection systems, enzyme based sensors (amperometric) have been explored extensively. However, little work has been done in the area of SERS, FRET, and surface-modified fluorescence based enzyme sensors. Much of the chemistries involved in immobilizing enzymes for amperometric detection could be used in the construction of surface based detection systems like the one listed above. This would allow for redundant sensor systems for verification.

Finally, if the target is an organism (or virus), modifying these systems for DNA detection is simple. Many of the techniques required for this modification are based on the work that has been developed in the area of molecular beacons (fluorescence based

DNA detection system). Many of these systems could be altered to be used for positive or negative detection (increase or decrease in signal, respectively). The choice of which method to use would be dictated by the system being developed.

As for the bio-optical sensors side of the system, this is where the incorporation of ideas from several disciplines is important. Knowing our limitations, we rely heavily on the expertise of Dr. Gerard Coté. His extensive work in bio-optics has allowed us to incorporate some unusual and creative ideas into the design of the recognition substrates [133, 134].

Modeling in sensor design

Sensor design is challenging in many aspects. When designing a sensing system, it is important to understand the characteristics of the system thoroughly. Things to consider are the response of the sensor in the presence of analyte, the binding affinity of the sensing molecule to the target of interest, the specificity of the sensor, and the influence of background on detection capabilities. To experimentally determine these characteristics can be extremely time consuming and expensive. This is where the use of modeling is crucial.

Most modeling today is done post-experimentation. Modeling is used as an empirical way to describe the results achieved through experimentation. While it is useful to be able to understand the trends of the data after collection, this completely neglects another aspect of modeling, intelligent experimental design. Often modeling can allow you to eliminate conditions or sensor designs that will not function in an

acceptable manor in the conditions available. It is this trend in current sensor design that we took advantage of in this project [135 - 140].

CHAPTER III

MODELING FOR INTELLIGENT SENSOR DESIGN

Introduction

In any developmental research, trial-and-error approaches prove often to be both time consuming and financial restrictive. However, without large amounts of *a priori* information, a certain amount of guesswork is required. Making these attempts "educated guesses" is what's important. By performing modeling of the sensor system before hand, one can quickly rule out sensor schemes that are far from optimal and focus on the more viable candidates.

Currently, we're looking at detection techniques for amyloid proteins. These proteins are the causative agents and/or toxic species of interest in Mad Cow disease (prion), Creutzfeldt-Jakob disease (prion), Alzheimer's (Aβ), Huntington's disease (huntingtin), and several others. The diseases are characterized by the neurodegeneration due to the aggregation and formation of amyloid fibrils by the species of interest (as indicated in parenthesis). The requirements of the sensor are that it be sensitive to levels found *in vivo*, selective for amyloid proteins, and provide structure information for the analyte of interest.

While the molecules we wish to detect and the sensor application define the physical constraints of the biosensors we will develop, the models that we describe to evaluate their feasibility are broadly applicable. In each model developed, we assume

that the analyte of interest binds to a recognition molecule with a given binding affinity, and that the binding of the analyte to the recognition molecule results in a detectable change in signal. Our particular biosensor applications are based on surface modified spectroscopic techniques, thus the signal is assumed to be either an emission or absorption intensity. The signal is either generated by binding the analyte directly or via the displacement of a competing molecule. Equilibrium and dynamic cases of these types of sensors are explored.

Materials and methods

Materials

All models were derived based on standard chemical and biochemical kinetic principles and equations. The models were solved under desired conditions using MATLAB v. 7.0.1 (The MathWorks, Inc. Natick, MA). The resulting data were compiled and plotted using Microsoft (Seattle, WA) Excel 2002.

Competitive (indirect) equilibrium model

With a competitive sensing system, there are three major components. These components are the recognition unit (R), the first target (signal unit (S)), and the second target (analyte (A)). For a standard equilibrium competition system, the recognition unit and signal unit are combined and allowed to come to equilibrium. Upon equilibration, the sample of interest is added. If the target is present, the system will come to new equilibrium conditions with the analyte (in turn displacing a fraction of the signal unit).

This displacement will lead to a new equilibrium condition between the recognition unit and the signal unit. The result will be a change in the signal intensity from the original equilibrium situation. It is the change that is measured to determine the analyte concentration. Figure 3.1 demonstrates this system (schematic of competitive sensor).

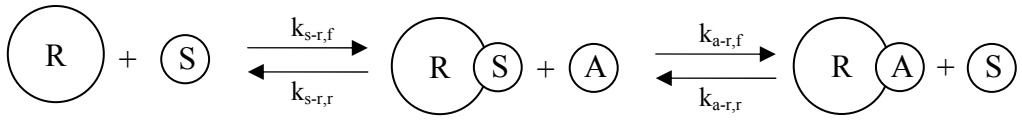

Fig 3.1 Schematic of competitive equilibrium sensor. The recognition unit (R) binds to the signal unit (S). This leads to some baseline signal. Upon introduction of the target analyte (A), A displaces some of the S bound to R, creating a new signal

Based on this model, there are several variable of interest to consider. Aside from concentrations of signal unit, recognition unit, and analyte (which can be easily controlled), there are three major variables of interest. The first is the equilibrium binding conditions between the signal unit and recognition unit. This is governed by the equilibrium binding coefficient for these two units ($K_{s\text{-}r}$). The second variable is the equilibrium binding between the analyte and recognition unit (and in turn the equilibrium binding coefficient for these two ($K_{a\text{-}r}$). The final variable is how the signal intensity of the signal unit changes upon binding with the recognition unit (F_b).

Taking into account just the kinetics of the system, we arrive at a system of equations as follows:

$$\frac{d(SR)}{dt} = k_{s-r,f} * S * R - k_{s-r,r} * SR \qquad (3.1)$$

$$\frac{d(AR)}{dt} = k_{a-r,f} * A * R - k_{a-r,r} * AR \qquad (3.2)$$

$$K_{s-r} = \frac{k_{s-r,f}}{k_{s-r,r}} \qquad (3.3)$$

$$K_{a-r} = \frac{k_{a-r,f}}{k_{a-r,r}} \qquad (3.4)$$

Where: SR = Concentration of recognition unit / signal unit complex

AR = Concentration of analyte / signal unit complex

S = Concentration of signal unit

A = Concentration of analyte

R = Concentration of signal unit

$k_{s-r,f}$ = Reaction constant for S / R association

$k_{s-r,r}$ = Reaction constant for S / R dissociation

$k_{a-r,f}$ = Reaction constant for A / R association

$k_{a-r,r}$ = Reaction constant for A / R dissociation

K_{s-r} = Equilibrium coefficient for formation of the SR complex

K_{a-r} = Equilibrium coefficient for formation of the AR complex

The independent forward and reverse rates dictate how quickly equilibrium is achieved. However, these rates do not affect the actual concentrations of the system at equilibrium.

While kinetics dictate the system, the signal determines usability. Looking at signal intensity as a function of different of concentration of different species (R and SR are the only species of interest when determining signal; the other species do not contribute to signal), we arrive at the following equation:

$$I_{total} = I_{bound} * SR + I_{free} * R \qquad (3.5)$$

Where: I_{total} = Total signal intensity of the system

I_{bound} = Signal intensity of bound signal unit

I_{free} = Signal intensity of free signal unit

Normalizing the system by the intensity of the free signal unit (I_{free}) we arrive at the final form of the equation:

$$\frac{I_{total}}{I_{free}} = \frac{I_{bound}}{I_{free}} * SR + \frac{I_{free}}{I_{free}} * R \Rightarrow I_{total,norm} = F_b * SR + R \qquad (3.6)$$

Where: $I_{total,norm}$ = Normalized total signal intensity of the system

F_b = Fractional change in signal upon binding

The system of equations (3.1 – 3.4 and 3.6) were solved simultaneously using MATLAB v. 7.0.1 (The MathWorks, Inc. Natick, MA). Normalized signal intensity as a function of analyte concentrations were evaluated at equilibrium (the time derivative of all concentrations were equal to zero). The sensitivity of normalized intensity to model parameters ($K_{a\text{-}r}$, $K_{s\text{-}r}$, and initial concentrations of R, and S) was investigated

Competitive (indirect) dynamic model

This competitive sensing field is similar to the one described in the previous section except for the caveat the equilibrium with the final sample cannot be achieved due to the degradation of the target to some final product. An example of such a system is an enzyme based detection of some target analyte. Figure 3.2 depicts such a system.

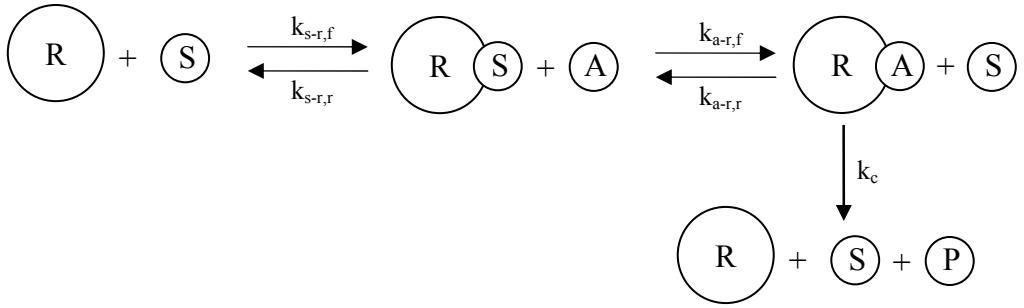

Fig 3.2 Schematic of competitive dynamic sensor (enzymatic). The recognition unit (R) binds to the signal unit (S). This leads to some baseline signal. Upon introduction of the target analyte (A), A displaces some of the S bound to R, creating a new signal. An additional complication occurs due to the regeneration of R by the conversion of A to product (P).

The equations governing the system are as follows:

$$\frac{d(SR)}{dt} = k_{s-r,f} * S * R - k_{s-r,r} * SR \qquad (3.7)$$

$$\frac{d(AR)}{dt} = k_{a-r,f} * A * R - k_{a-r,r} * AR - k_c * AR \qquad (3.8)$$

$$\frac{dP}{dt} = k_c * AR \qquad (3.9)$$

$$K_{s-r} = \frac{k_{s-r,f}}{k_{s-r,r}} \qquad (3.10)$$

$$K_{a-r} = \frac{k_{a-r,f}}{k_{a-r,r}} \qquad (3.11)$$

$$I_{total} = I_{bound} * SR + I_{free} * R \qquad (3.12)$$

$$\frac{dI_{total}}{dt} = I_{bound} * \frac{d(SR)}{dt} + I_{free} * \frac{dR}{dt} \qquad (3.13)$$

Where: P = Concentration of product formed from analyte degradation

k_c = Reaction constant for degradation of analyte to product

Again, normalizing the system by the intensity of the free signal unit (I_{free}) we arrive at the final form of the equation:

$$\frac{dI_{total}}{dt} = \frac{I_{bound}}{I_{free}} * \frac{d(SR)}{dt} + \frac{I_{free}}{I_{free}} * \frac{dR}{dt} \Rightarrow \frac{dI_{total,norm}}{dt} = F_b * \frac{d(SR)}{dt} + \frac{dR}{dt} \qquad (3.14)$$

By monitoring the rate of change in fluorescence intensity, we can determine the concentration of target analyte in the sample. Equations (3.7 – 3.11 and 3.14) were solved simultaneously using MATLAB 7.0 and the rate of change in fluorescence as a function of analyte concentration was determined at different model parameter values.

Direct equilibrium model

Direct sensors rely on a change in some measurable variable upon the interaction of the analyte of interest with the recognition molecule in the system. In the system we describe, the sensor relies on a change in the optical properties of the system upon binding of analyte. More specifically, the model is based on the surface-enhanced Raman spectroscopy (SERS). In SERS, the target analyte exhibits an increase in spectroscopic signal upon interacting with some enhancing substrate (i.e. gold). The enhancement factor can be as high as 10^{12}. A schematic of the biosensor system is seen in Figure 3.3.

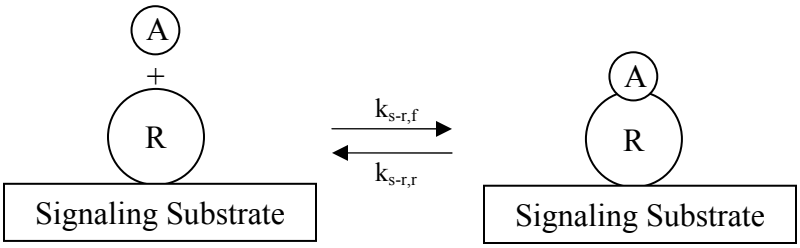

Fig 3.3 Schematic of direct equilibrium sensor. The recognition unit (R) is immobilized to a signaling substrate. Upon introduction of the target analyte (A), A binds to R, creating a signal.

The equations governing this system are very similar to those above. However, the system is simpler since it doesn't rely on a secondary molecule for the detection. The governing equations are as follows:

$$\frac{d(AR)}{dt} = k_{a-r,f} * A * R - k_{a-r,r} * AR \qquad (3.15)$$

$$Signal = I_{free} * A + F_{enh} * F_{dist} * AR \qquad (3.16)$$

Where: Signal = Spectroscopic signal

F_{enh} = Enhancement factor upon binding

F_{dist} = Distance factor for analyte to enhancer distance

The enhancement factor upon binding is a function of electromagnetic properties of the enhancing surface, wavelength of light used to excite the surface, other physical properties of the system. The distance factor for analyte to enhancer distance is a function of the thickness of the enhancing surface and the dimensions of the recognition molecule given by the function shown in Equation 3.17.

$$F_{dist} = \left(\frac{r_o}{d + r_o} \right)^n \qquad (3.17)$$

Where: r_o = Radius of curvature of enhancement substrate

d = Distance from analyte to enhancing surface, typically of the dimensions of the recognition molecule.

Results and discussion

The models developed were analyzed based on the variables of interest for the different systems. For both the competitive equilibrium sensor and the competitive dynamic sensor, the values of R_o, S_o, $K_{s\text{-}r}$, and $K_{a\text{-}r}$ were varied to determine the effect of those variable on the sensor behavior. Comparatively, for the direct equilibrium sensor, R_o, $K_{a\text{-}r}$, enhancement factor, and the ratio of distance to diameter were varied.

Competitive equilibrium model – effects of varying $K_{s\text{-}r}$

The equilibrium binding constant ($K_{s\text{-}r}$) represents the ratio of R-S complex to unbound R and S. Increasing the value of $K_{s\text{-}r}$ increases the amount of R-S complex, with the converse also being true. Figure 3.4 shows the effect of varying $K_{s\text{-}r}$ on the response of the sensor.

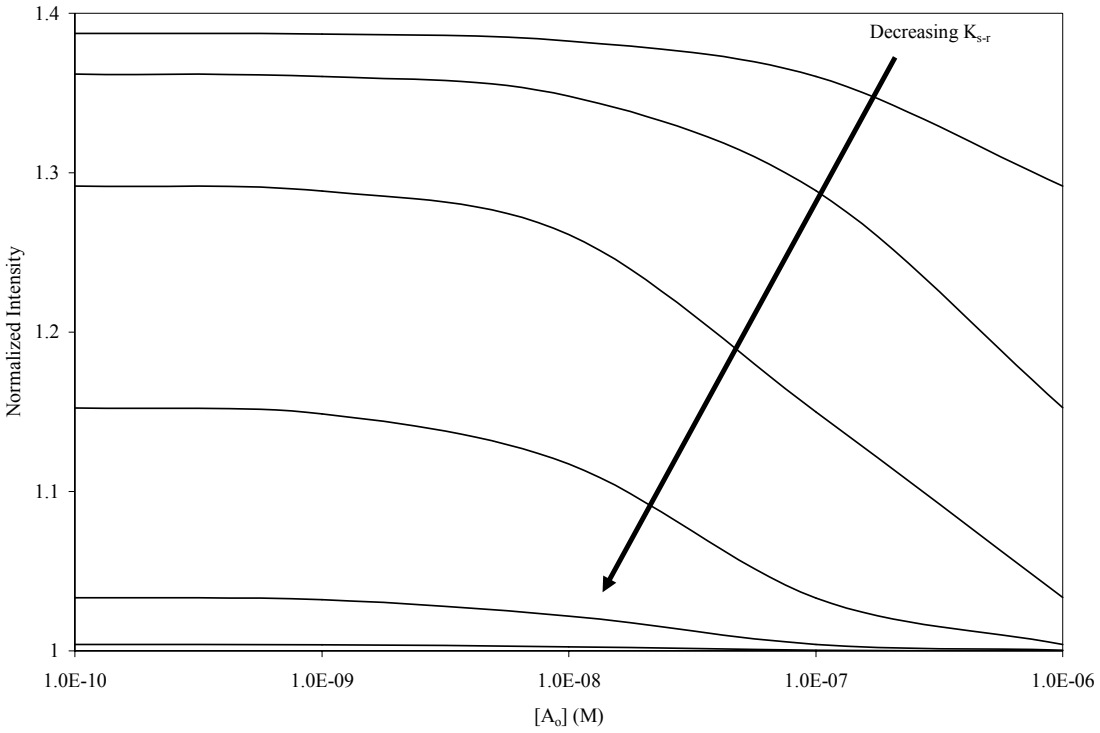

Fig 3.4 Equilibrium competitive sensing system response to changes in K_{s-r}. Values of K_{s-r} ranging from 10^6 to 10^{11} M^{-1} (decreasing as you move down the graph). $K_{a-r} = 10^8$ M^{-1} , $R_0 = S_0 = 10^{-8}$ M

As can be seen from the figure, as K_{s-r} increases, the linear response region of the sensor expands in both the active range of substrate concentrations and in the magnitude of the fluorescence intensity change that occurs. However, increasing K_{s-r} shifts the lower limit of the linear region to higher values of substrate. Therefore, maximizing K_{s-r} does not necessarily lead to optimized biosensor performance. The value of K_{s-r} to use is dependant upon the substrate region of interest and the sensitivity of the equipment being used.

Competitive equilibrium model – effects of varying K_{a-r}

Much as K_{s-r} represents the ratio of R-S complex to free R and S, K_{a-r} represents the ratio of R-A complex to R and A. Again, increasing K_{a-r} increases the amount of R-A complex. Figure 3.5 shows the effect of varying K_{a-r} on the response of the sensor.

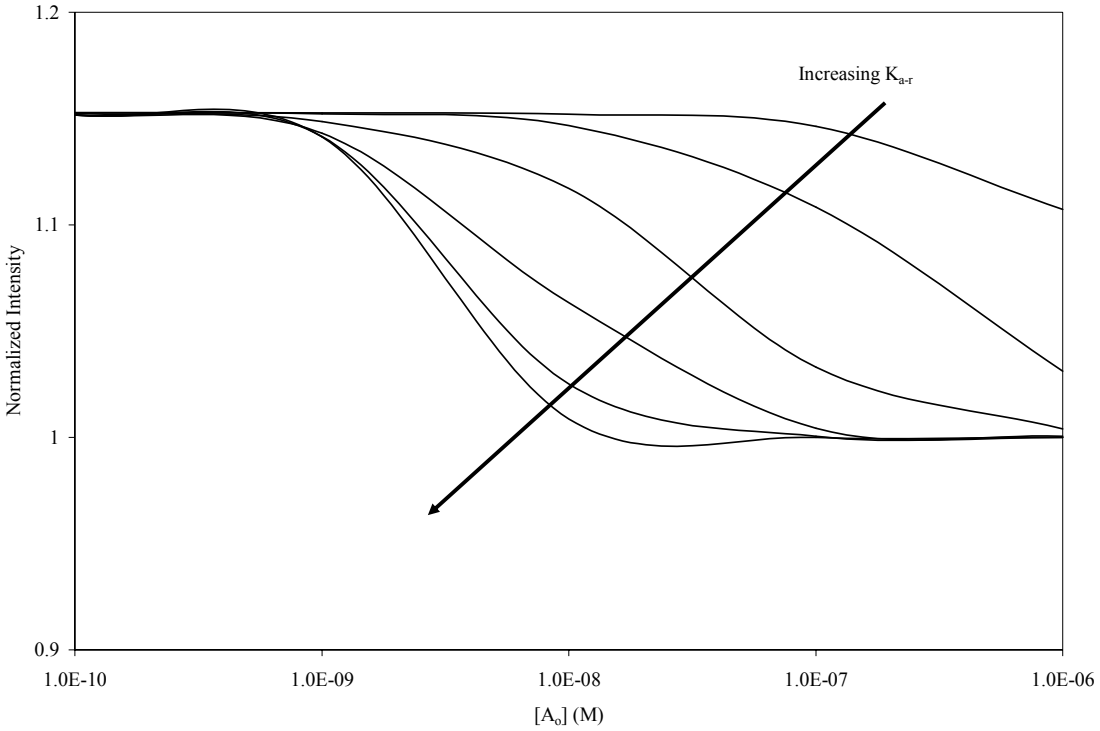

Fig 3.5 Equilibrium competitive sensing system response to changes in K_{a-r}. Values of K_{a-r} ranging from 10^6 to 10^{11} M^{-1} (increasing as you move down the graph). $K_{s-r} = 10^8$ M^{-1} , $R_0 = S_0 = 10^{-8}$ M

From Figure 3.5, we see that increasing K_{a-r} decreases the lower limit of the linear response region of the sensor. However, increasing K_{a-r} narrows the linear region. Again, maximizing the value of K_{a-r} will not necessarily produce the optimum sensor performance. As with K_{s-r}, the desired value of equilibrium binding constant for the

analyte to the recognition element is function of the desired sensor range for the application.

Competitive equilibrium model – effects of varying S_0

The initial amount of signaling unit (S_0), also has direct consequences on equilibrium concentrations of free and bound analyte and signal molecule, thus will affect the performance and sensitivity of the biosensor. Figure 3.6 shows this relationship.

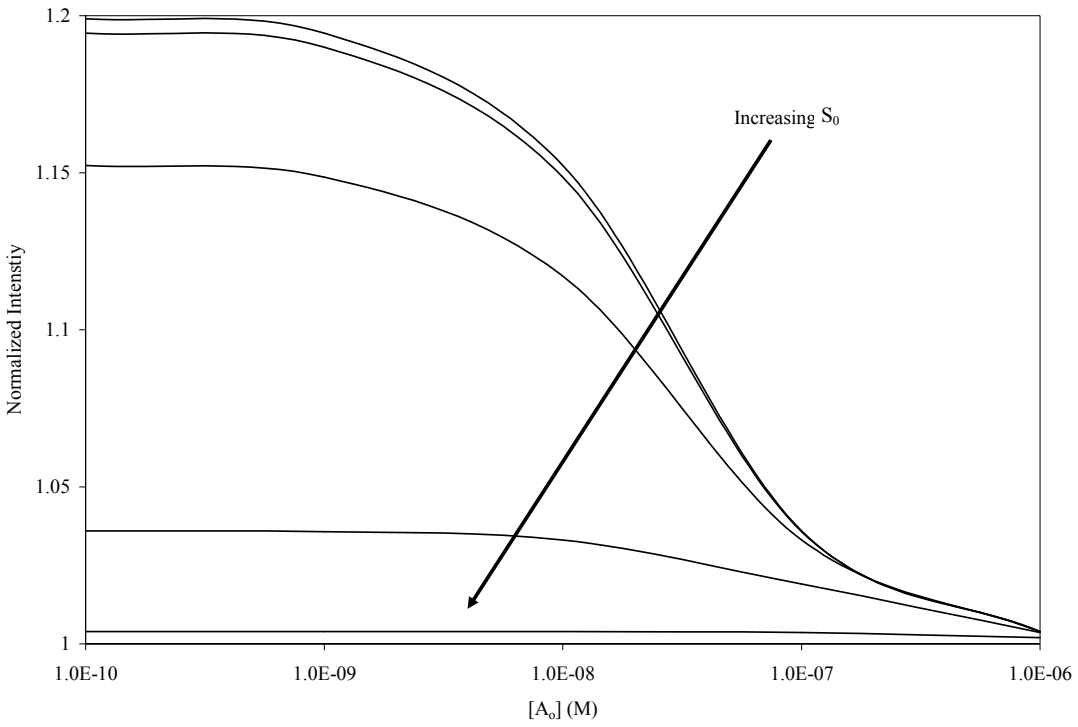

Fig 3.6 Equilibrium competitive sensing system response to changes in S_0. Values of S_0 ranging from 10^{-6} to 10^{-10} M (increasing as you move down the graph). $K_{a\text{-}r} = K_{s\text{-}r} = 10^8\ M^{-1}$, $R_0 = 10^{-8}$ M

As is apparent from the figure, increasing S_0 reduces the amount of signal possible from the sensor, as the excess free signaling unit both shifts the concentration at which the analyte of interest can displace the decoy to higher concentrations and leads to greater background signal such that the enhancement of signal caused by binding of the signaling molecule to thee recognition molecule is obscured. However, increasing concentrations of S_0 also expands the range of concentrations of analyte detectable in the linear region of the sensor.

Competitive equilibrium model – effects of varying R_0

The effect of R_0 on equilibrium is similar to the effect of S_0. Greater concentrations of R_0 leads to lower concentrations of free S in system at equilibrium and a greater shift of the fluorescence intensity from basal value. However, more R_0 in the system results in R being available to bind A without displacing S, which decreases the effectiveness of the sensor. Figure 3.7 demonstrates this effect.

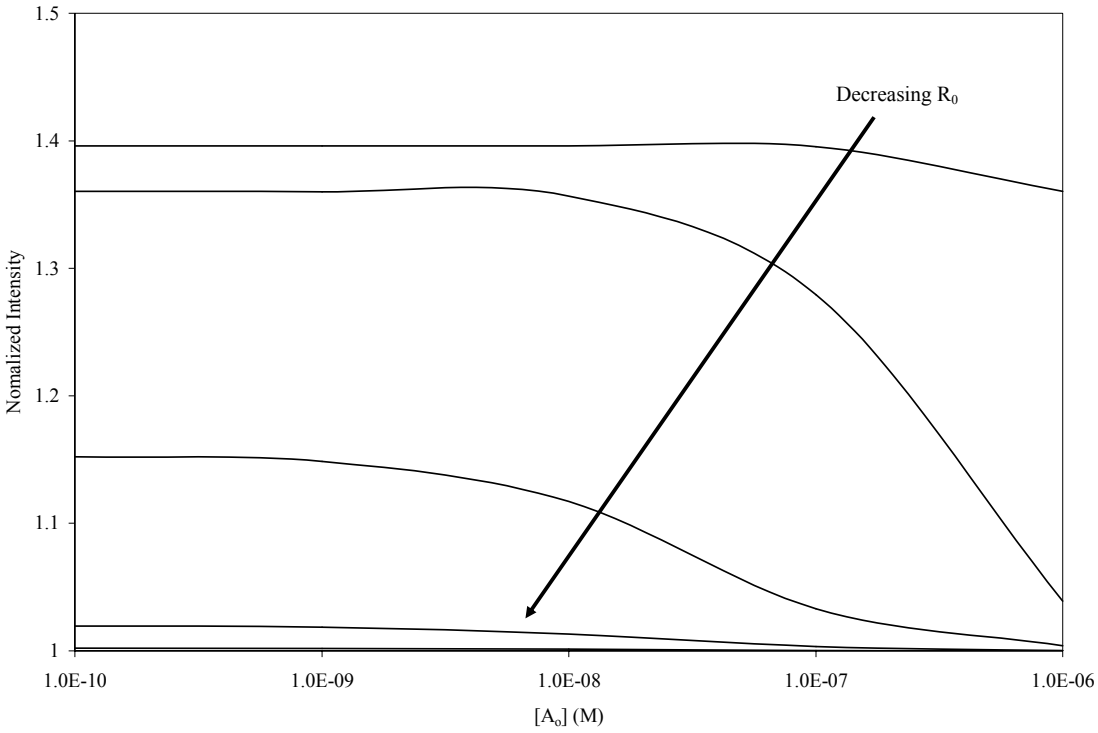

Fig 3.7 Equilibrium competitive sensing system response to changes in R_0. Values of R_0 ranging from 10^{-6} to 10^{-10} M (decreasing as you move down the graph). $K_{a\text{-}r} = K_{s\text{-}r} = 10^8\ M^{-1}$, $R_0 = 10^{-8}$ M

Summary of competitive equilibrium model results

In general, the lower limit of detection for the sensor is governed by $K_{a\text{-}r}$, with the limit of detection of analyte approaching the inverse of the value of $K_{a\text{-}r}$. However, to achieve those detection limits, values of $K_{s\text{-}r}$, R_0, and S_0 must be matched to $K_{a\text{-}r}$. If $K_{s\text{-}r}$ is within an order of magnitude of $K_{a\text{-}r}$, then the detection limits of the sensor remain approximately the inverse of $K_{a\text{-}r}$, with larger $K_{s\text{-}r}$'s resulting in greater signal to noise and somewhat larger range of concentrations of analyte leading to linear sensor response. For lowest limits of detection, both R_0 and S_0 should be within an order of magnitude of the inverse of $K_{a\text{-}r}$, with deviations from these values leading either to a loss in

sensitivity or loss in signal to noise. Experimental verification of these findings are seen in Chapter IV.

Competitive dynamic model

Unlike the competitive equilibrium sensor, in the competitive dynamic sensor, while the same signal generation mechanism is used (surface modified fluorescence in this example), the analyte of interest is degraded by the recognition element. Therefore, fluorescence intensity changes with time in the sensor, and this rate of change in fluorescence intensity can be used to infer analyte concentrations.

Competitive dynamic model– effects of varying $K_{s\text{-}r}$

As seen in Figure 3.8, an increase in $K_{s\text{-}r}$ leads to a decrease in the rate of change in signal intensity, dI/dt, (due to the increased binding affinity of the signal unit for the recognition molecule). The decrease in dI/dt would result in a decrease in signal to noise, experimentally. Conversely, as $K_{s\text{-}r}$ increases, the lower limit of detection decreases. As with the equilibrium sensor, and optimum value of $K_{s\text{-}r}$ exists which maximizes signal to noise while minimizing the concentration at which analyte is detectable.

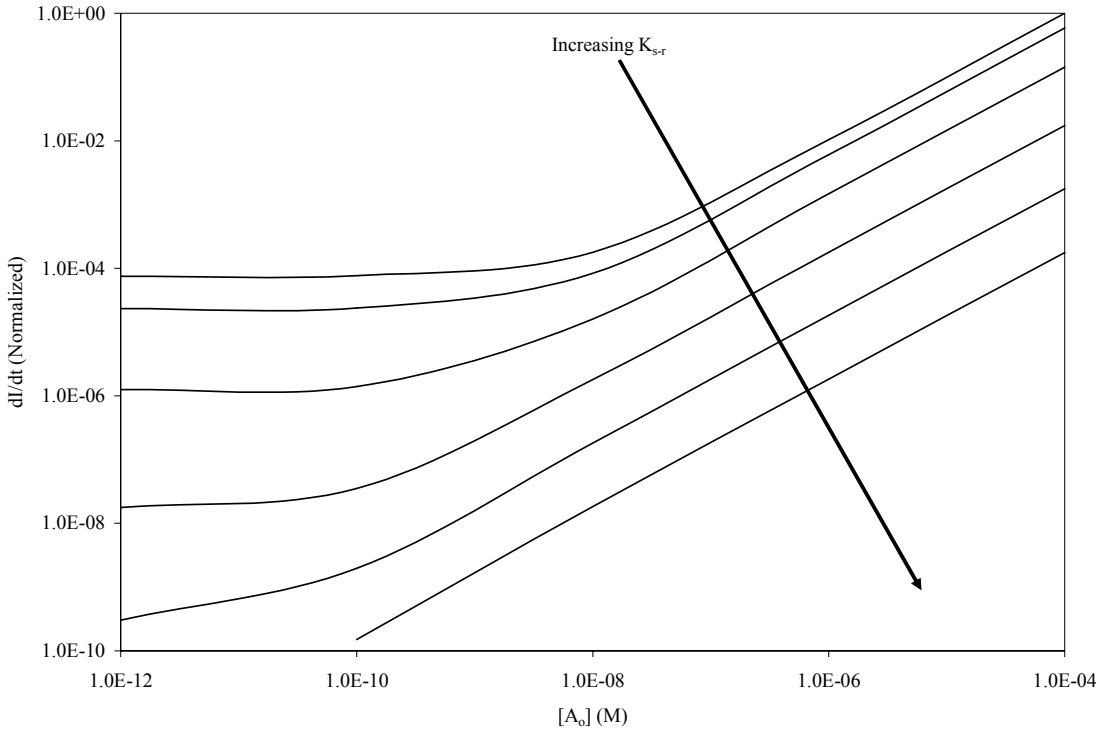

Fig 3.8 Dynamic competitive sensing system response to changes in K_{s-r}. Values of K_{s-r} ranging from 10^4 to 10^9 M^{-1} (increasing as you move down the graph). $K_{a-r} = 10^7$ M^{-1}, $R_0 = S_0 = 10^{-8}$ M

Competitive dynamic model – effects of varying K_{a-r}

Within the range of parameters explored, it appears that the major effect of varying K_{a-r} is to increase signal to noise (dI/dt) as the value of K_{a-r} increases, with possibly a modest effect on the upper limits of detection of the system (Figure 3.9). K_{a-r} appears to have much less effect on system sensitivity and limits of detection in the dynamic sensor than in the equilibrium sensor.

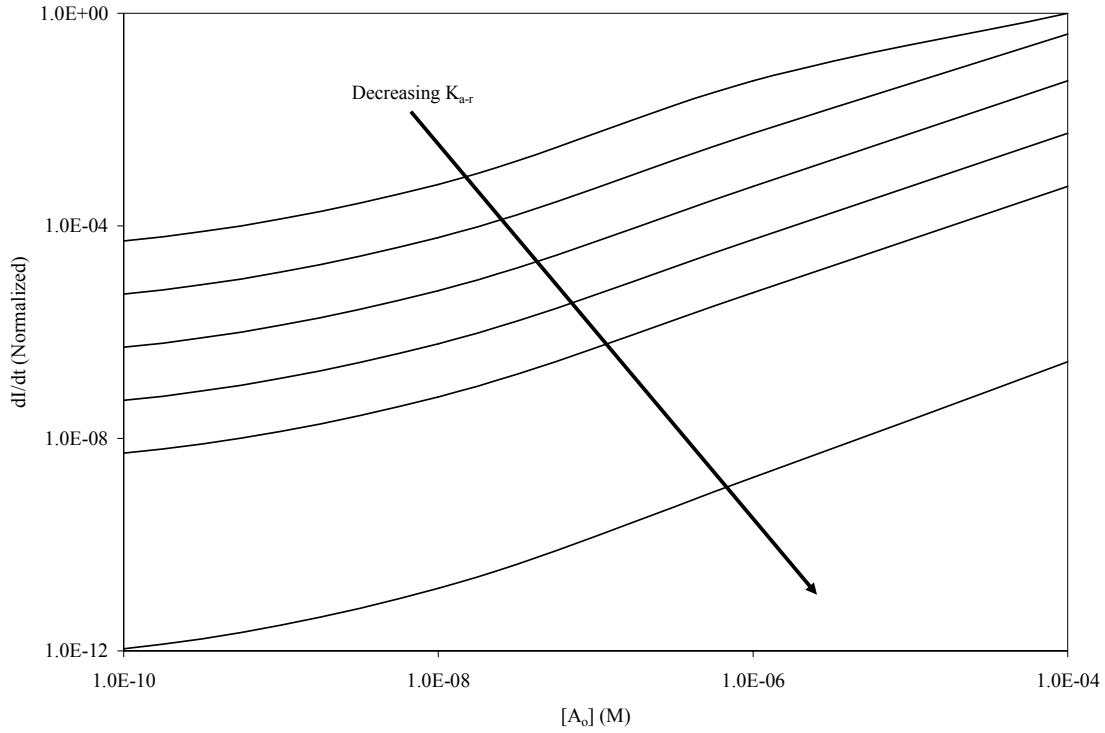

Fig 3.9 Dynamic competitive sensing system response to changes in K_{a-r}. Values of K_{a-r} ranging from 10^4 to 10^9 M^{-1} (decreasing as you move down the graph). $K_{s-r} = 10^7$ M^{-1} , $R_0 = S_0 = 10^{-8}$ M

Competitive dynamic model – effects of varying S_0

Varying the amount of decoy available varies the intrinsic fluorescence of the system. Greater concentration of decoy indicates greater fluorescence. This allows for easier detection of signal, but makes the rate of fluorescence change a much smaller fraction of the total signal. Figure 3.10 shows this effect.

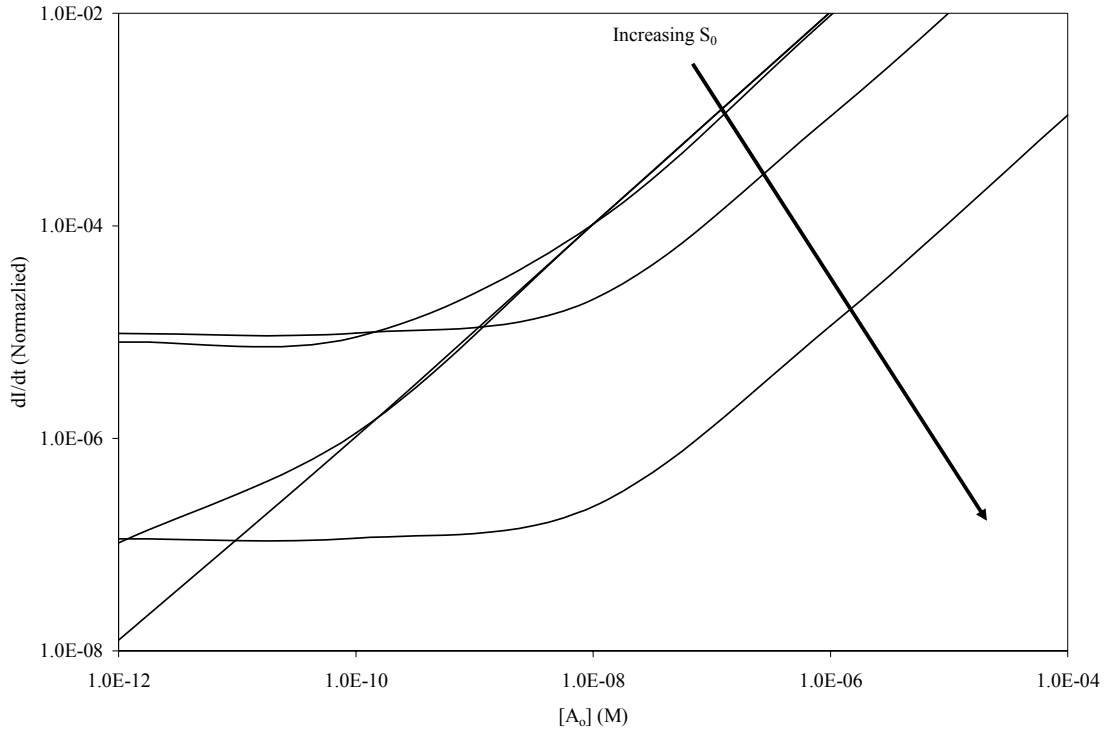

Fig 3.10 Dynamic competitive sensing system response to changes in S_0. Values of S_0 ranging from 10^{-r} to 10^{-12} M (increasing as you move down the graph). $K_{a\text{-}r} = K_{s\text{-}r} = 10^7$ M^{-1} , $R_0 = 10^{-8}$ M

Figure 3.10 demonstrates how decreasing the decoy concentration leads to greater values for dI/dt. Additionally, decreasing the decoy concentration gives better lower detection limits. As previously mentioned, the caveat is that as decoy concentration decreases, so does total signal, placing the burden of limitations on the equipment being used.

Competitive dynamic model – effect of varying R_0

As discussed in the equilibrium model, increasing R_0 increases the amount of bound decoy and free recognition unit. This has the possible positive effect of

increasing the total fluorescence of the system, but with the possible negative attribute that the free recognition unit will decrease the sensitivity of the sensor. Figure 3.11 emphasizes these possible effects.

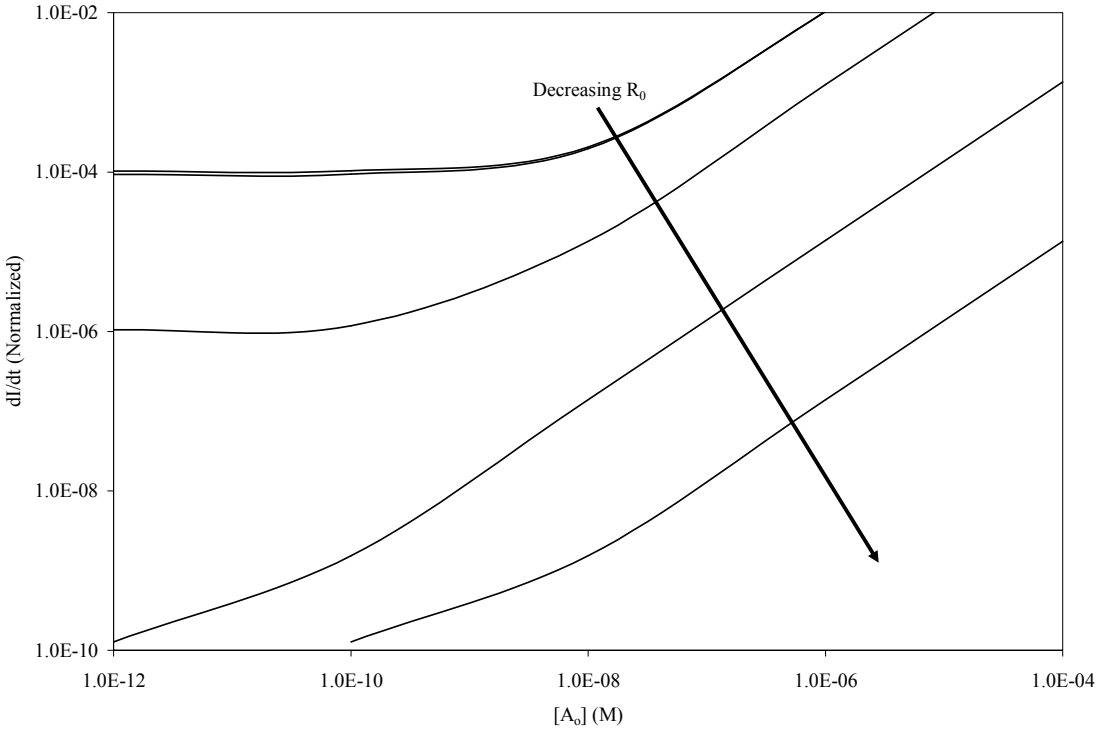

Fig 3.11 Dynamic competitive sensing system response to changes in R_0. Values of R_0 ranging from 10^{-4} to 10^{-12} M (decreasing as you move down the graph). $K_{a\text{-}r} = K_{s\text{-}r} = 10^7\ M^{-1}$, $S_0 = 10^{-8}$ M

From the figure we can see that decreasing the initial concentration of recognition unit improves the lower detection limits of the system. However, decreasing R_0 also decreases the total signal available for analysis. This creates the same problem that the lower limits of R_0 are governed by the equipment available.

Summary of competitive dynamic model

For a given value of $K_{s\text{-}r}$, you are limited to using concentrations of R_0 greater than or equal to the inverse of $K_{s\text{-}r}$. This is caused by the drastic shift of equilibrium toward dissociation, due to R values less than the limits just set. Additionally, the same limitation hold true for the concentration of S (for the same reasons). Since equilibrium limitations still apply, the limits of detection are limited by the value for $K_{a\text{-}r}$. The inverse of this value also dictates R_0 in addition to A_0 concentrations that may be used or detected, respectively. Since there are major economic limitations that are placed on the system by the cost of gold substrate, we are required to work at exceptionally low volumes (<20μL) to achieve the necessary concentration. This is created by the fact that most enzymes operate with moderately low values of $K_{s\text{-}r}$ (10^6 – 10^7 M^{-1}). These limitations are demonstrated in Chapter IV.

Direct equilibrium model - effect of varying R_0

Unlike the two previous models described, with a direct sensor, signal is generated by binding of the analyte of interest directly to the recognition molecule on the surface. Since the concentration of recognition molecule on the surface, R_0, is directly related to the amount of total possible bound analyte, model results suggest, as expected, that total signal intensity, signal to noise, and range of detectable concentrations would be greatest when the highest concentrations of recognition unit possible were bound to the surface (Figure 3.12).

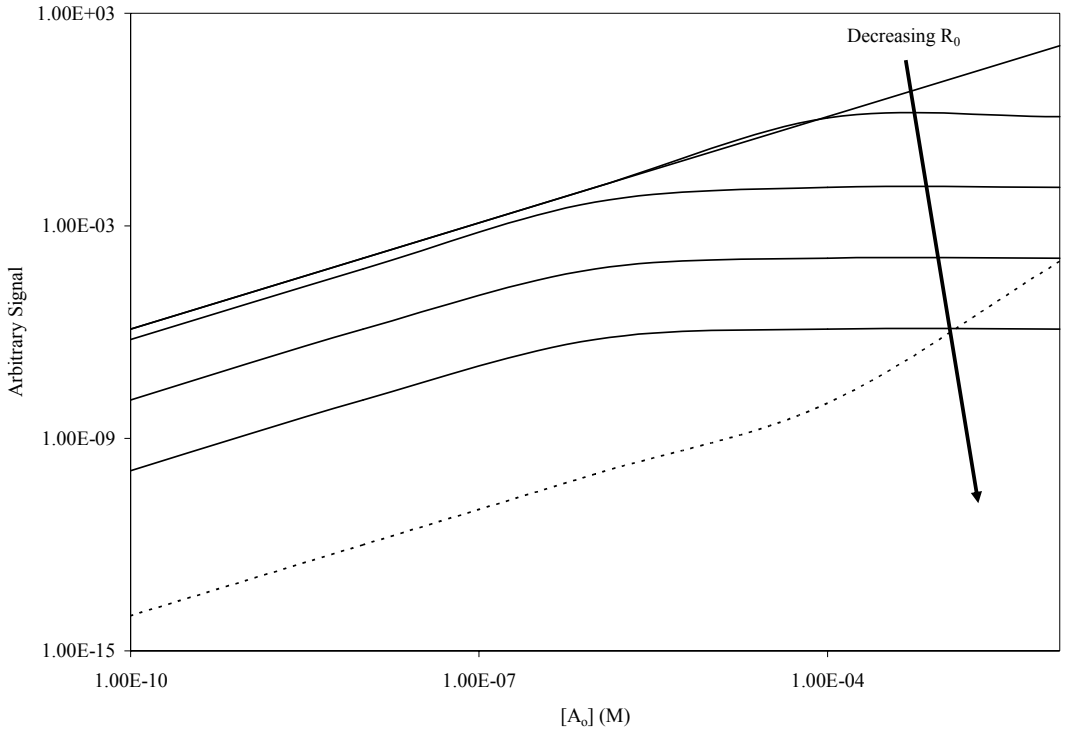

Fig 3.12 Equilibrium direct sensing system response to changes in R_0. Values of R_0 ranging from 10^{-2} to 10^{-10} M (decreasing as you move down the graph, solid lines). Signal from the free decoy represented by the dashed line. $K_{a\text{-}r} = 10^6$ M^{-1}, Enfac = 10^6, Dist/Dia = 3.33.

As described early, the system is more effective (more signal) with increasing values of R_0. However, there is one more interesting artifact. As R_0 increases, the upper detection limits of the system increase. This further supports the idea that the maximum concentration of recognition unit should be used in the sensor.

Direct equilibrium model – effect of varying enhancement factor

With the same predictability of varying R_0, increasing the enhancement factor (Enfac, the increase in signal of the analyte upon binding to the surface relative to that free in solution) increases the effectiveness of the sensor. This is obvious from the fact

that increasing Enfac directly increases the bound signal without influencing the kinetics of the system. Figure 3.13 exemplifies this effect.

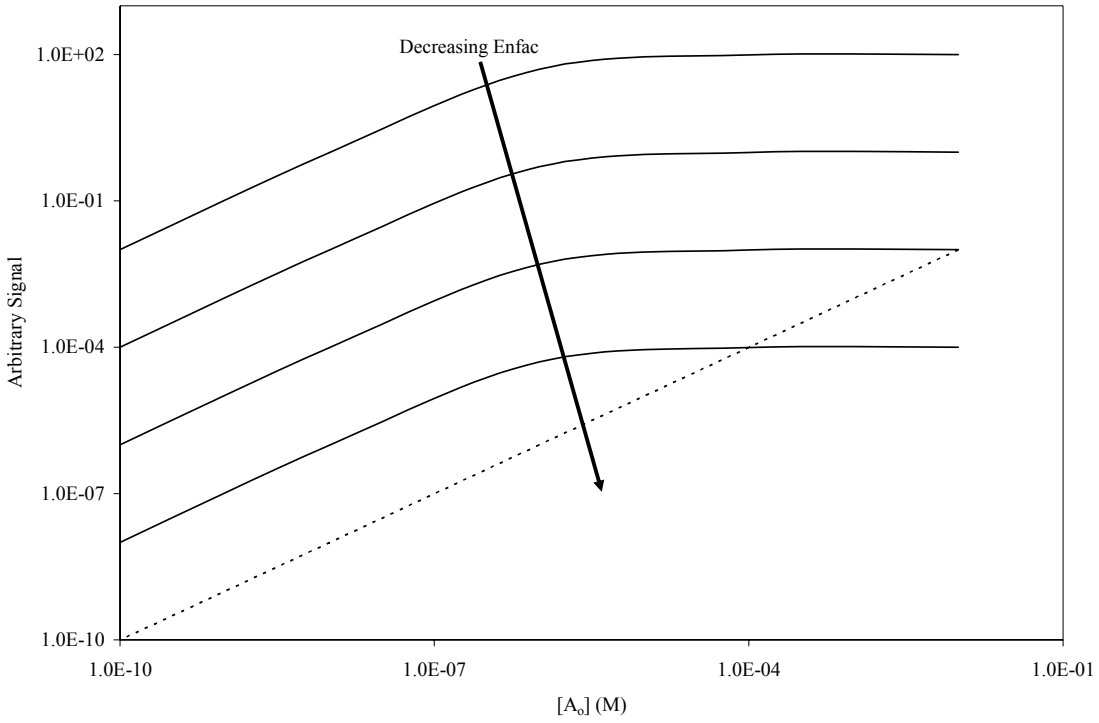

Fig 3.13 Equilibrium direct sensing system response to changes in enhancement factor (Enfac). Values of Enfac ranging from 10^6 to 10^{12} M (decreasing as you move down the graph, solid lines). Signal from the free decoy represented by the dashed line. $K_{a\text{-}r} = 10^6\ M^{-1}$, $R_0 = 10^{-10}$ M, Dist/Dia = 0.

Direct equilibrium model – effect of varying distance/diameter ratio

As the distance/diameter ratio (Dist/Dia) decreases, which physically implies that the recognition unit becomes smaller and the analyte comes closer to the enhancing surface, it is expected that the bound signal in the system will increase. For the purposes of this paper, a third order decay in signal as distance increased was assumed, based on theoretical estimates of the decay of the electromagnetic field [46, 47] and

experimental measurements with different surfaces (Chapter VI). Figure 3.14 demonstrates the distance effects.

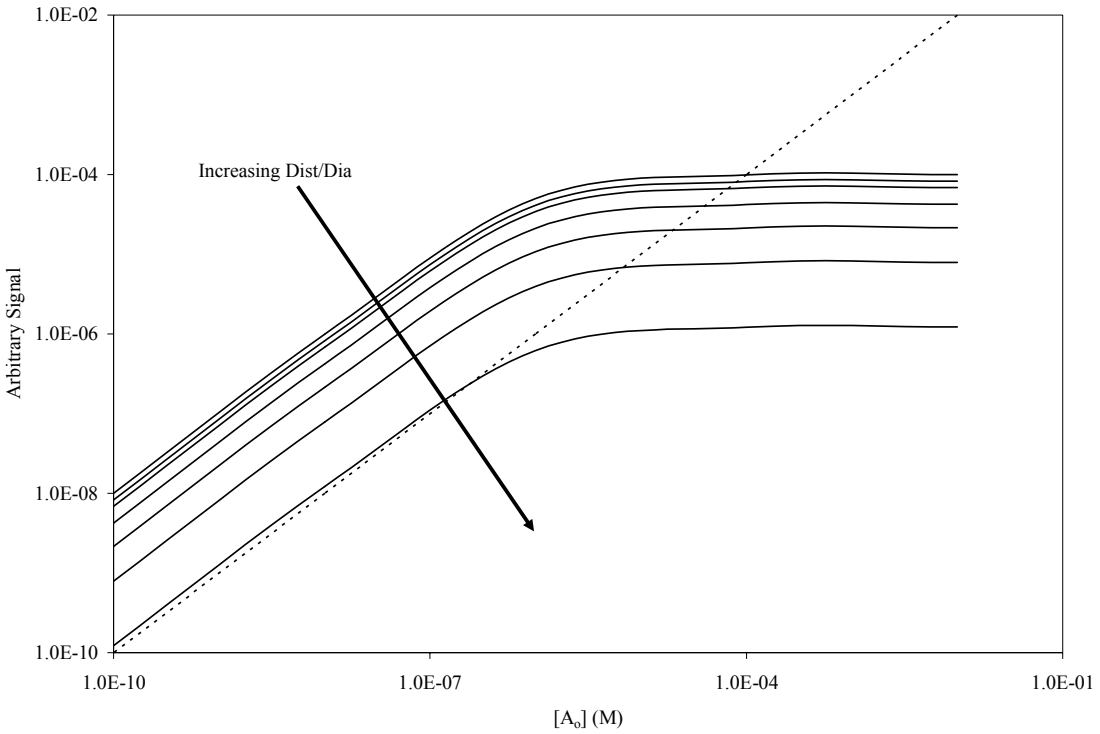

Fig 3.14 Equilibrium direct sensing system response to changes in ratio of distance from surface to diameter of curvature (Dist/Dia). Values of Dist/Dia ranging from 0 to 3.33 (increasing as you move down the graph, solid lines). Signal from the free decoy represented by the dashed line. $K_{a\text{-}r} = 10^6\ M^{-1}$, Enfac = 10^6, $R_0 = 10^{-10}$ M.

Direct equilibrium model – effect of varying $K_{a\text{-}r}$

Varying $K_{a\text{-}r}$ directly affects the equilibrium conditions in the system in the same way as discussed in the competitive equilibrium model. Therefore, it would stand to reason that by increasing the value of $K_{a\text{-}r}$, the amount of bound substrate would increase. This will lead to increased signal and easier detection, as illustrated in Figure 3.15.

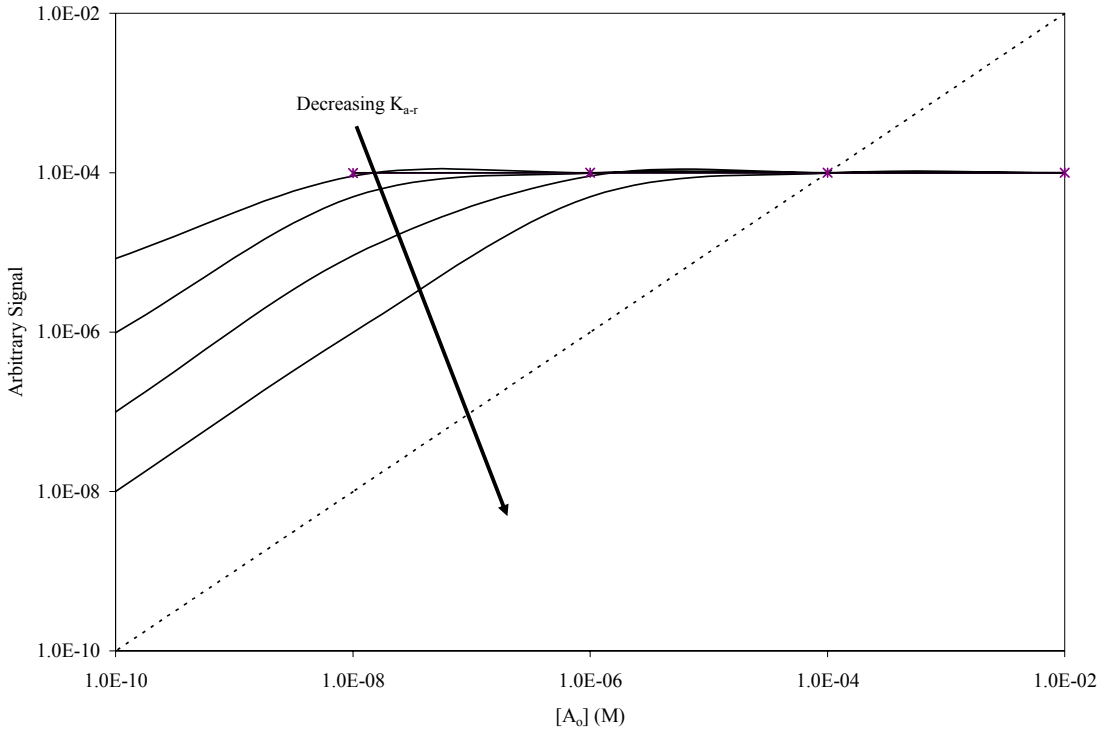

Fig 3.15 Equilibrium direct sensing system response to changes in K_{a-r}. Values of K_{a-r} ranging from 10^6 to 10^{11} M^{-1} (decreasing as you move down the graph, solid lines). Signal from the free decoy represented by the dashed line. $R_0 = 10^{-10}$ M, Enfac = 10^6, Dist/Dia = 0.

While the increase in signal is apparent from the figure, there is another interesting artifact. As K_{a-r} increases, the upper detection limit decreases because the surface saturates.

Summary of direct equilibrium sensor

In general, the direct sensing platform is much simpler than the competitive platforms, but somewhat more difficult experimentally to realize. Success depends on high surface coverage of the recognition unit, a physically small recognition unit (such that the distance from the analyte to the surface is low), and a high binding affinity of the

recognition unit for the analyte. Antibodies bind with high specificity and reasonably high binding affinity (10^9 to 10^{12} M^{-1}), but are molecularly rather large (4-5 nm in diameter). The large size both decreases the distance of the analyte for the surface and decreases possible surface coverage of the recognition unit.

We show, with some novel molecular surfaces, that surface coverage at picomole levels are possible (near 10^{-8}M for R_0), with binding affinities in the range of 10^8 M^{-1}, and at distances near 10 nm from the surface (Dist/Dia=0.067). Our collaborators have generated surfaces with enhancement factors near 10^6 or greater. Thus, with instrument sensitivity optimized (high power input, high sensitivity detector), analyte at concentrations below 10 nM should be detectable. Higher concentrations of analyte, up to near 10 μM, should be distinguishable from signal arising from analyte free in solution, but signal will not increase with increasing concentration as the sensor surface would be saturated. The feasibility of engineering the direct sensor, as described, is detailed in Chapter VI.

Conclusions

Competitive equilibrium model

While the trends discussed give an idea of how the system depends on each of these variables, the true determination of what $K_{a\text{-}r}$, $K_{s\text{-}r}$, R_0, and S_0 to use greatly depend on the range of concentrations of substrate for which detection is desired. However, it does appear that matching R_0 and S_0 concentrations seems to give the best response with the least loss of signal. Furthermore, it appears that the limiting components of the

system will probably be the equipment being used for detection and the binding affinity of the recognition molecule for both analyte and signal molecule.

Competitive dynamic model

The results of this model are significantly easier to discuss. As is the case for all the variables R_0, and S_0, lower is better. However, since decreasing R_0 and S_0 seems to fight the trends of each (it is not the lower value but the change in the ratio), it would be most beneficial to, again, match the concentrations to one another. Conversely, maximizing $K_{a\text{-}r}$ and $K_{s\text{-}r}$ seems to be the most beneficial. Limitations on the possible performance of the sensor are the binding affinities obtainable for the recognition molecule, the limits of equipment detection (which are limited both by power input into the sample and detector efficiency), and the cost constraints associated with putting enhancing particles (gold for example) on the recognition element.

Direct equilibrium model

For this system, one should maximize R_0 and Enfac while minimizing Dist/Dia. This will give the highest bound signal available. As for $K_{a\text{-}r}$, it is important that the value of $K_{a\text{-}r}$ matches the concentration range of interest (since increasing $K_{a\text{-}r}$ decreases the upper detection limits, but decreasing $K_{a\text{-}r}$ decreases total signal).

Summary

Keeping all of these factors in mind when designing a sensor system (regardless of style) can help create a much more efficient design and understanding of the system. Furthermore, by using models for "intelligent design", one can fine tune the system to better match the capabilities and limitations of the equipment available, the biology or chemistry of the recognition units available, and the optical of the surface modifying metal particles used in biosensor development. Furthermore, incorporating models along with experimentation, you can decrease the number of experiments by "testing" some parameters with simulation, reject certain designs because the models show they are not feasible, and speed up optimization process associated with biosensor development.

CHAPTER IV

DEVELOPMENT OF A NANOPARTICLE-BASED SURFACE-MODIFIED FLUORESCENCE ASSAY FOR THE DETECTION OF PRION PROTEINS*

Overview

A nanoparticle-based immunoassay for the detection of recombinant bovine prion protein (PrP) was developed as a step in the development of screening tools for the prevention of the spread of transmissible spongiform encephalopathies. The assay is based on the competitive binding between PrP and a peptide–fluorophore to a nanoparticle-labeled antibody which is specific for a conserved prion sequence. The fluorophore, when bound to the antibody, is subject to surfaced-modified fluorescence, enabling detection of changes in the concentration of bound fluorophore in the presence of prion protein. Important factors considered during the development of the assay were ease of use, robustness, and detection level. The effects of pH and nanoparticle conjugation chemistry on surface-modified fluorescence observed in the assay were explored. Effects of concentrations of antibody and fluorophore on reproducibility and detection limits were examined. At present, the detection limits of the system are approximately equal to the antibody–peptide fluorophore equilibrium dissociation

---

*Reprinted from the Journal of Analytical Biochemistry, 334, James Henry et al., "Development of nanoparticle-based surface-modified fluorescence assay for the detection of prion proteins," 1-8, Copyright 2004, with permission from Elsevier. doi:10.1016/j.ab.2004.07.008

constant, which is near one nanomolar concentration. Improved assay performance could be obtained by optimization of the nanoparticle surface resonance effects. The simplicity of the assay and ease of use may make the type of assay described in this report attractive for screening purposes in the food industry.

Introduction

Prion proteins (PrPs) are thought to be the causative agent in transmissible spongiform encephalopathies (TSEs), a group of fatal neurodegenerative diseases that include chronic wasting disease and bovine spongiform encephalopathy (BSE) in nonhuman animals and Creudzfeld Jakob disease in humans [80]. The diseases are highly contagious in certain species, with transmission from nonhuman animals to humans thought to be possible, at least for BSE [80].

Until methods of treatment or prevention of the diseases have been established, the best hope of preventing the spread of TSEs is through surveillance of animals and animal products including foods and pharmaceutical materials. Current screening methods involve the use of immunological assays such as ELISAs and Western blots with high sensitivity (down to the picomolar range or below), but these require considerable time and skill [80]. The other major screening method for the detection of infectious prions is the ‘‘Hamster Model’’ [78], which examines the ability of a sample to transmit infection to a golden hamster. This method is the only assay capable of definitively determining whether a sample is capable of transmitting disease; however, the incubation period for the hamster screening method is approximately 60 days,

prohibitively long for the screening of foodstuffs and the detection limits are uncertain. Simple, robust, rapid, and sensitive methods for the detection of prion proteins are needed for use in the food and pharmaceutical industries.

In this paper, the development of a simple nanoparticle-based surface-modified fluorescence assay for the detection of prions is described. The assay developed is based on phenomena associated with the high number of surface electrons associated with metal nanosurfaces [141]. A variety of assays that exploit changes in optical properties in the vicinity of a nanosurface have been developed recently [142], including surface-plasmon-resonance-based assays [143] and surface-enhanced resonance Raman assays [144]. These assays have been used in the detection of proteins including the estrogen receptor alpha [145], human serum albumin [146], and wheat germ agglutinin and epidermal growth factor [147]. Use of surface-modified fluorescence has been reported recently for the detection of prostate-specific antigens [148].

A variety of analytical techniques have been developed which exploit changes in fluorescence properties of a molecule in different environments, whether those changes be quenching [149], Förster resonance energy transfer [150], or surface-modified fluorescence in which the energy absorbed by the nanoparticle or nanosurface either quenches or enhances the fluorescence of fluorophore, depending upon the distance between the excited surface and the fluorophore [151]. In this work, an assay utilizing surface-modified fluorescence for prion detection is described. The assay is based on the competitive binding of a fluorophore to a nanoparticle-labeled prion-specific antibody. As currently implemented, the assay is simple to perform, requires minimal skill, and

can be used to detect recombinant prion proteins down to 2 nM. With optimization, including steps for the discrimination between infectious and noninfectious prion, this assay could be used as a rapid and simple screening tool to prevent the introduction of TSEs into the food and pharmaceutical supply.

Materials and methods

Materials

The fluorescent peptide fluorescein-GABA-QYQRES-COOH, referred to as decoy, was custom synthesized and purified by Multiple Peptide Systems (San Diego, CA). Peptide purity was 85% as indicated by mass spectrometry and reverse-phase HPLC provided by the manufacturer. The recombinant prion protein (Calbiochem, San Diego, CA) was a histidine-tagged protein expressed in Escherichia coli containing amino acids 25–244 of the bovine PrP sequence. The anti-PrP monoclonal antibody (derived from cell line F99/97.6.1 from VMRD, Pullman, WA) was used in sensor development. The antibody was specific for the sequence QYQRES, a conserved sequence in human, bovine, and elk PrPs.

The 1.4-nm gold nanoparticles for labeling of the antibody at specific residues were purchased from Nanoprobes (Yaphank, NY). The particles had only one attachment site per gold cluster with the attachment site being dependant upon the type of gold nanoparticles used. All other chemicals, unless specifically indicated, were supplied by Sigma–Aldrich (St. Louis, MO).

Antibody purification

The anti-PrP monoclonal antibody (MAb) was purified on an rProtein A column (Amersham Biosciences, Piscataway, NJ) before use. A 2.5-mL-bed-volume column was used to purify approximately 7 mg of antibody. The column was .rst washed with 10 mM borate buffer, pH 8.9, with 3 M NaCl, before use. The impure MAb, diluted 1:1 in pH 8.9, 3 M NaCl buffer, was loaded onto the column. The column was then washed with 10 bed volumes of 50 mM borate buffer, pH 8.9, 3 M NaCl, followed by 10 bed volumes of 10 mM borate buffer, pH 8.9, 3M NaCl. Purified MAb was eluted with the 100 mM glycine buffer, pH 3.0. MAb was detected in fractions via absorbance at 280 nm using the Beckman DU620 spectrophotometer (Beckman Coulter, Fullerton, CA). Antibody was neutralized with 1/10 volume 1 M Tris buffer, pH 8, containing 0.02% sodium azide. Bovine serum albumin was added to the antibody to a concentration of 2 mg/mL to improve stability during storage.

Preparation of fAb fragment

The antibody fragments (FAb) were prepared using the ImmunoPure FAb Preparation Kit (Pierce Biotechnology, Rockford, IL). The procedure used was provided by Pierce Biotechnology [152].

Nanogold attachment

Three different gold nanoparticle attachment chemistries were used, monomaleimido, mono-NHS, and monoamino, to specifically attach the gold

nanoparticles to the anti-PrP MAb at sulfhydryl, amine, and carbohydrate residues, respectively. The sulfhydryl attachment chemistry was also performed using FAb fragments. The procedure for the attachment of the monomaleimido nanogold to both whole MAb and antibody fragments at reduced sulfhydryl groups was performed according to the IgG and FAb attachment procedures provided by Nanoprobes with the following modification: 80 mM dithiothreitol was used in place of 100 mM MEA as a disulfide bond reducing agent [153]. The procedures for the attachment of mono-NHS nanogold to primary amines on the anti-PrP MAb and monoamino nanogold to oxidized carbohydrate chains on the Fc region of the anti-PrP MAb were performed according to the IgG attachment procedure provided by Nanoprobes without modification [154,155].

Separation of labeled antibodies from unbound nanogold particles was performed by ultrafiltration using Millipore (Billerica, MA) Microcon 30,000 MWCO filters. Gold to protein mole ratios of the nanoparticle-labeled antibody or antibody fragments were determined by measurement of sample absorption at 280 and 420 nm. Gold to Ab (or FAb) mole ratios were in the range of 1.6:1 to 4.2:1, or approximately 2–4 gold particles per antibody molecule. Less than 1% of total gold in each sample was unbound.

Sample mixing

The samples were mixed from stock solutions of decoy, gold-labeled MAb, recombinant PrP, and buffer. Stock solutions of decoy and antibody were prepared in phosphate buffer. Stock solutions of PrP were prepared in deionized water to avoid PrP aggregation. The buffer used for fluorescence measurements was 0.1 M phosphate

buffer, pH 7, unless otherwise specifically indicated. The samples were placed in sealed foil pouches and mixed for times ranging from 4 to 24 h depending on the concentrations of the samples. Independent fluorescent measurements were taken at various times to ensure that mixing times were sufficient for samples to reach equilibrium. No attempt was made to remove unbound decoy from samples prior to fluorescence measurements. Measurements were recorded from equilibrium mixtures of bound and free decoy, antibody–gold conjugate, and prion.

Sample testing

The fluorescence of samples was measured using a fluorometer from Photon Technologies International (Lawrenceville, NJ) outfitted with a 25 mW argon laser from Spectra-Physics Lasers and Photonics (Mountain View, CA). A 500 nM long-pass filter was placed in the emission light path to reduce the effects of scattered excitation light. Samples were excited at 488 nm and the emission was scanned from 500 to 600 nm. Fluorescence intensity at 514 nm was recorded. Normalized fluorescence intensity, reported here, refers to the fluorescence intensity of the sample at 514 nm divided by the fluorescence intensity of the fluorescein-labeled peptide (decoy) alone at the same concentration and same pH condition as that of the sample.

Statistical and modeling analysis

Data are presented as the mean plus or minus the standard deviation (or standard error) of n independent measurements where n is 3 or greater. To determine the

statistical difference of two samples or a sample from a control, a Student t test was performed. When multiple measurements were compared, a Tukey test was used to determine the statistical difference in data. Unless otherwise indicated, $P < 0.05$ was used.

To estimate the range of conditions that should be tested to optimize assay performance, a simple equilibrium model of antibody–decoy and antibody–prion binding was constructed in which it was assumed that the equilibrium binding constants to both decoy and prion were the same. The decoy–antibody equilibrium binding constant, 2.5×10^9 M^{-1}, was estimated independently [156]. The resulting set of nonlinear equations was then solved using Polymath or Maple to determine free and bound decoy concentrations. Fluorescence intensity was assumed to be a linear combination of the fluorescence emission of the free decoy and that of the bound decoy and was assumed to be directly proportional to the concentrations of fluorescing species. While linearity of fluorescence intensity with free decoy concentration was confirmed experimentally, other assumptions in model development were not tested directly.

Results and discussion

A novel assay for the detection of PrP in buffers that was rapid and simple to use was developed. A simple schematic of the assay can be seen in Figure 4.1.

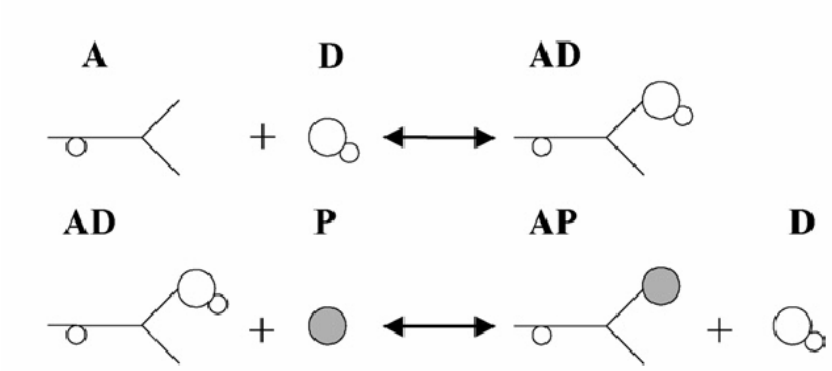

Fig. 4.1. Schematic of the prion detection system. Two reactions occur in the assay mixture. A fluorescent peptide decoy (D) can bind to an antibody–gold conjugate (A) forming an antibody–decoy complex (AD) or a prion protein (P) can bind to the antibody–gold conjugate forming an antibody–prion complex (AP). The fluorescence intensity of the decoy changes when bound to the antibody–gold complex relative to that of the free decoy. If, when the complex forms, the fluorophore is close to the gold nanoparticle (approximately 10 nm or less), the fluorescence is quenched relative to that observed in the free decoy. If the fluorophore is at an intermediate distance from the gold nanoparticle when bound (approximately between 10 and 40 nm), fluorescence is enhanced relative to that of the free decoy. The change in fluorescence of the assay mixture upon addition of prion is used to indicate the prion concentration in the sample.

While there are prion assays with high sensitivity in current use, the level of expertise required for these methods and the length of time required to perform such assays can be a major hindrance in food manufacturing and processing environments [80, 79]. The assay described here was based on the competitive binding of PrP and a fluorescent peptide or decoy to a monoclonal antibody specific for a conserved sequence in several PrP species including sheep, goat, cattle, mink [157], and deer [158]. The sequence is near the C terminus of the prion protein, which is believed to be accessible to antibodies on both infectious and noninfectious prions and is unlikely to be cleaved by protease pretreatment of the infectious protein [80]. The fluorescence of the decoy was modified when bound to the antibody because of the presence of a gold nanoparticle on the antibody.

Since the assay developed here is based on competitive binding, the detection limits of the system will be related to the relative amounts of fluorescent decoy bound to the antibody and free in solution and to the differences in fluorescence intensity of the bound and free species. The distance between the gold nanoparticles and the fluorophore will greatly affect the fluorescence of the bound fluorophore as at short molecular distances nonradiative energy transfer to the metal leads to fluorescence quenching, while at longer distances (generally between 10 and 45 nm) enhancement is seen as a result of surface resonance effects [151]. Local pH will also affect the fluorescence of bound and free species. In addition, concentrations of all species participating in assay reactions along with equilibrium constants for those reactions will determine the relative concentrations of bound and free species. The effects of these parameters were explored to elucidate the working range and detection limits of the assay developed.

Structural comparison

The first step in the assay development was to quantify the effective change in peptide decoy fluorescence upon binding with gold–MAb (or gold–FAb) conjugate as a function of location or type of gold nanoparticles attachment. Binding of gold-labeled antibody to fluorescent decoy did not alter the shape of the emission spectra or wavelength of emission maximum but simply led to changes in intensity of fluorescence. Results from these experiments are shown in Figure 4.2.

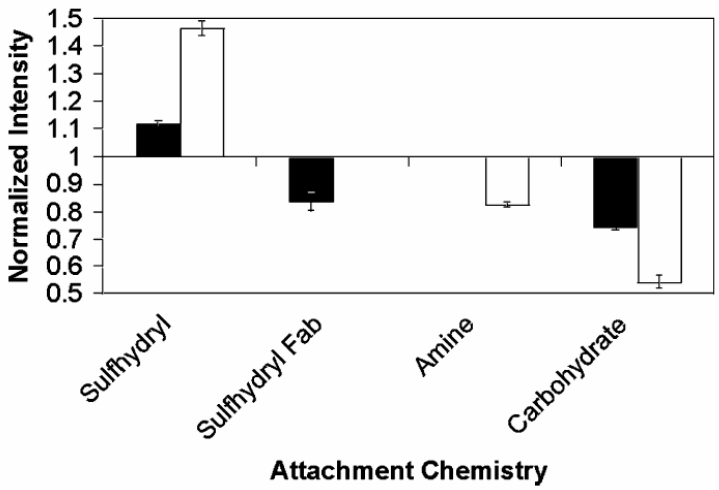

Fig. 4.2. Effect of nanoparticle attachment chemistry on surface modified fluorescence. The filled bars and empty bars are 200 nM antibody, 200 nM decoy, and 10 nM antibody, 10 nM decoy, respectively. Normalized intensity is the fluorescence of the antibody decoy pair divided by the fluorescence intensity of the free decoy at the same concentration. Error bars represent the standard deviation of three or more independent measurements.

As seen in the figure, fluorescence intensity of the decoy bound to the antibody relative to that free in solution was a strong function of the method of gold attachment. The sulfhydryl–FAb, amine–MAb, and carbohydrate–MAb chemistries led to a decrease in fluorescence, or quenching, while the sulfhydryl–MAb chemistry led to an increase in fluorescence, or enhancement, of the decoy when bound to antibody relative to that of free decoy without antibody present. Significant variability in enhancement and quenching observed was noted when different batches of antibody were used in experiments. However, for the same batch of antibody, but different conjugation reactions, reproducible enhancement and quenching were observed. We assumed that the variability in enhancement and quenching seen with different batches of antibody were associated with differences between batches in stability/purity of the antibody and not

with differences in concentration at which the reactions were carried out. One possible explanation for the variation in the fluorescence modification behaviors observed with the different chemistries is that the different attachment chemistries led to different molecular distances between the nanoparticle and the bound decoy (fluorophore). For the sulfhydryl–FAb attachment chemistry, the average molecular distance between nanoparticle and fluorophore may be relatively small, leading to quenching of fluorescence, while for the same attachment chemistry to the whole antibody, the average molecular distance between nanoparticle and fluorophore was greater, leading to a fluorescence enhancement. For the amine attachment chemistry, considerable heterogeneity in molecular distances would be expected because of the relatively large number of possible surface amines for attachment, giving rise to small changes in fluorescence because of averaging of both enhancement and quenching effects. Similar arguments could be made about molecular distances with the carbohydrate attachment chemistry (small molecular distances, leading to quenching). No direct measurements of distances between gold attachment sites and fluorophore binding sites were attempted.

pH effects

Given that fluorescein, the fluorophore attached to the decoy used in the assay, is known to be pH sensitive [159], we examined the role of pH on the relative enhancement or quenching behavior observed when the decoy was bound to the gold-labeled MAbs prepared with the three different attachment chemistries (Figure 4.3).

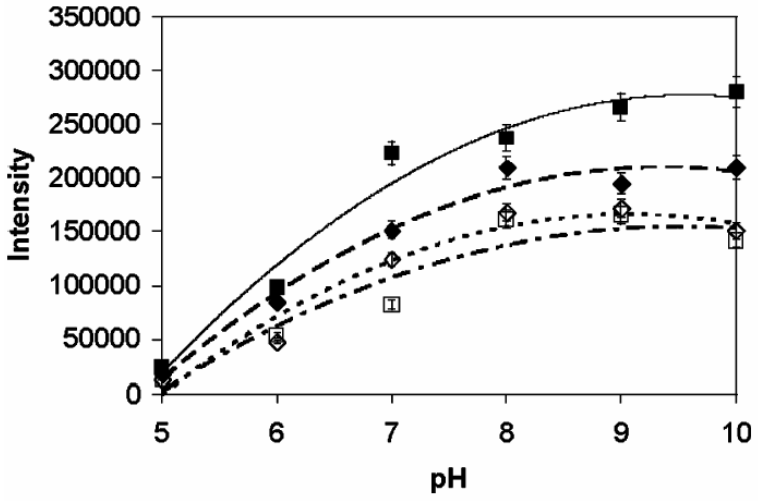

Fig. 4.3. Effect of solution pH on fluorescence intensity of decoy and decoy/antibody pairs. The concentration of decoy was 10 nM. The concentration of antibody–gold conjugates was 8 nM. The following symbols were used to represent different attachment chemistries: ■, sulfhydryl; □, carbohydrate; ♦, free decoy; ◊, amine. Error bars represent the standard deviation of three or more independent measurements.

The FAb–sulfhydryl attachment was eliminated as it provided no noticeable advantage over other available chemistries. No obvious shifts in fluorescence dependence upon pH with respect to control were observed with nanogold-labeled antibodies relative to that of the free decoy (Fig. 4.3), suggesting that the binding showed no pH dependence. For subsequent experiments, pH 7 was used. Since the sulfhydryl and carbohydrate chemistries showed the most promise, they were the only chemistries used in further testing.

Decoy:Ab ratio

As seen in Figure 4.4, we explored the effect of the relative ratio of decoy to gold-labeled antibody on normalized fluorescence intensity. We expected, based on stoichiometric arguments, that optimal enhancement or quenching would be observed

when decoy to antibody ratios were between 1:1 and 2:1. A maximum was observed for the sulfhydryl attachment chemistry at a decoy to antibody ratio of 1.25:1 (Fig. 4.4).

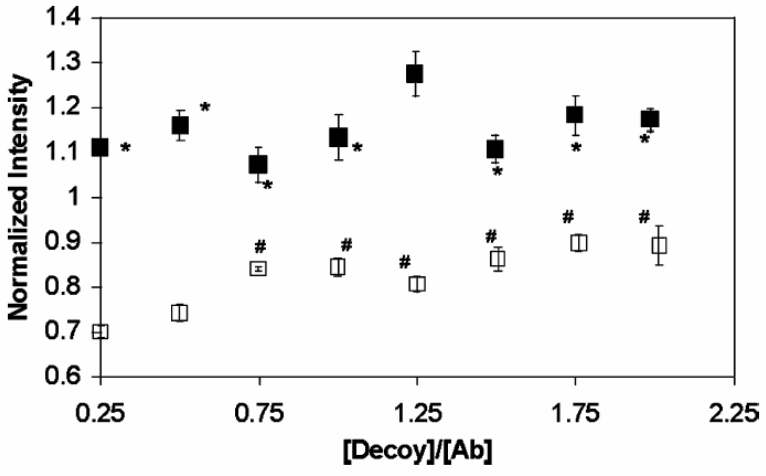

Fig. 4.4. Effect of decoy to antibody mole ratio on normalized fluorescence intensity for different conjugation chemistries. The following symbols represent different attachment chemistries: ■,sulfhydryl; □, carbohydrate. Points labeled with like symbols are statistically equivalent (Tukey, $P < 0.05$).

There were no significant changes in normalized fluorescence intensity in the range of ratios between 1:1 and 2:1 when the carbohydrate attachment chemistry was used. The 1.25:1 decoy to antibody ratio was used in all subsequent experiments.

Whether this represents the true mole ratio of decoy to antibody under conditions that yield maximum changes in fluorescence signal or whether the observed optimal ratio was due to some uncertainty in our measurements of antibody or decoy concentrations is not clear. However, it should be noted that these results were observed consistently with multiple batches of antibody–nanoparticle conjugations.

Detection limits

Using the optimum decoy to antibody ratios, we then determined the minimum concentrations of decoy and antibody that could be used and still reveal a significant difference between the fluorescence intensity of decoy bound to the gold-labeled antibody and that of free decoy. Results from those experiments are seen in Figure 4.5.

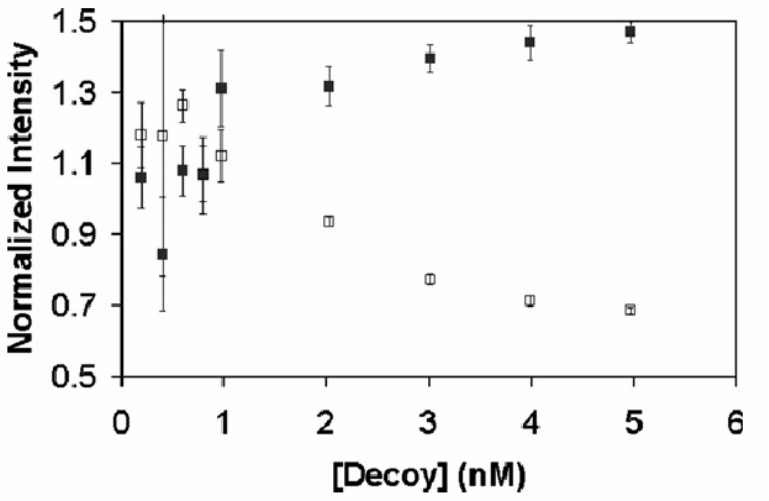

Fig. 4.5. Effect of decoy/antibody pair concentration on normalized fluorescence intensity for different attachment chemistries. The following symbols were used to represent different attachment chemistries: ■, sulfhydryl; □, carbohydrate. The normalized fluorescence intensities for sulfhydryl-labeled Ab and carbohydrate-labeled Ab were statistically different from the normalized control value (1.0) for concentrations at and above 2 and 3 nM, respectively (Student's t test, $P < 0.01$).

At concentrations below 2 nM decoy for the sulfhydryl chemistry and below 3 nM decoy for the carbohydrate chemistry, no differences between free and bound decoy were detectable ($P < 0.01$). The concentrations at which no statistical difference between free and bound decoy could be detected approaches the equilibrium dissociation constant for the Ab:Decoy system (approximately 4×10^{-10} M) [156].

Prion displacement

The principle of the assay under development was that of competitive binding of the decoy and prion to the antibody. Thus, in the absence of the prion, the decoy would bind to the antibody and its fluorescence would be modified by the gold nanoparticle. However, in the presence of the prion, the decoy would be displaced, and fluorescence would return to unmodified levels. A number of experiments were performed to test the ability of the prion to displace the decoy and whether the assay could be used to detect recombinant prion in the system (Figure 4.6).

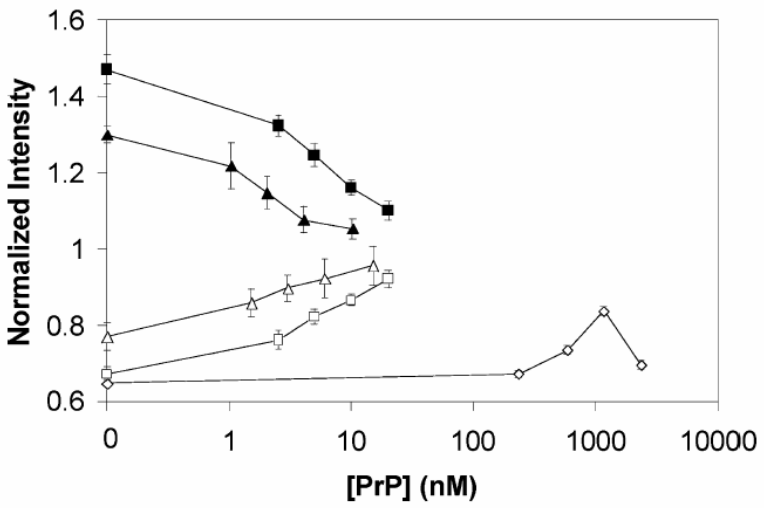

Fig. 4.6. Normalized fluorescence intensity as a function of recombinant prion concentration in solution. Sulfhydryl attachment chemistry is indicated with filled symbols. Carbohydrate attachment chemistry is indicated with open symbols. All measurements were performed at pH 7.0. Diamonds, 200 nM decoy, 160 nM antibody. All values (other than 0 nM PrP) are statistically different from the 0 nM PrP value (Student's t test, $P < 0.05$). Squares, 5 nM decoy, 4 nM antibody. All values of fluorescent intensity except 20 nM PrP (carbohydrate attachment chemistry only) samples are statistically different from the fluorescence intensity of free decoy (normalized intensity of 1). All values of fluorescence intensity are statistically different from the 0 nM PrP values, indicating that all concentrations tested could be distinguished from zero prion concentration (Student's t test, $P < 0.05$). Triangles, 2 and 3 nM for sulfhydryl and carbohydrate attachment chemistries, respectively, 1.25:1 decoy:antibody ratio. Fluorescence intensities of prion-containing samples are statistically different from that of free decoy for concentrations less than 5 nM PrP. Fluorescence intensities of prion-containing samples 3 nM and above can be distinguished from the fluorescence intensity of zero prion samples (Student's t test, $P < 0.05$).

The first attempt was performed at high decoy and antibody concentrations (200 nM decoy concentration, pH 7, 1.25 decoy to antibody ratio, diamond symbol). As prion was added to solution, the fluorescence intensity of the decoy increased from that of the quenched level of decoy bound to gold-labeled antibody toward the fluorescence intensity of free decoy (in the absence of antibody). The normalized fluorescence of the 200 nM prion sample was significantly different from that of the decoy–antibody controls ($P < 0.05$). However, at very high prion concentrations, 2 μM, the fluorescence decreased relative to that at lower prion concentrations, possibly due to prion aggregation in high-ionic-strength solution [160]. The histagged prion protein did not appear to aggregate at lower concentrations unless stored in high-ionic-strength buffers.

Further prion displacement assays were performed at lower decoy and antibody concentrations to improve the limits of sensitivity of the assay. When decoy concentrations of 5 and 2 or 3 nM were used (keeping the decoy to antibody ratio fixed at 1.25 to 1), the assay could be used to distinguish 2 nM prion from zero prion in the sample as opposed to the 200 nM lower limit observed when 200 nM decoy was used (based on a Student t test with $P < 0.05$). The observed trend of the limits of detection of prion, corresponding roughly to the decoy concentration used in the assay, was expected based on simple equilibrium models of the reactions taking place in the assay. The working range of the assay was 2–10 nM (for carbohydrate chemistry) or 20 nM (for sulfhydryl chemistry) when 5 nM decoy was used (squares), while it was 2–5 nM when the lower decoy concentrations were used (triangles).

The equilibrium model was used to estimate normalized fluorescence intensity for an enhancement-based assay, analogous to the system employing sulfhydryl chemistry described here, as a function of concentration of prion at different concentrations of antibody and decoy (Figure 4.7).

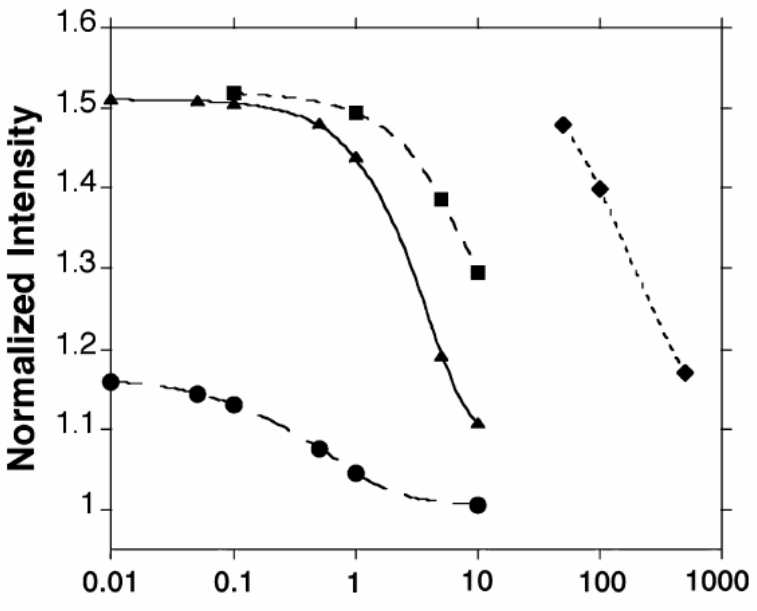

Fig. 4.7. Equilibrium model estimates of normalized fluorescence intensity as a function of prion concentration for an enhancement based assay. In model calculations, the equilibrium binding constants for both antibody to decoy and antibody to prion were assumed to be 2.5 x 10^9 M^{-1}. The maximum possible enhancement was assumed to be 1.6 times the fluorescence intensity of the unbound decoy. Equimolar decoy and antibody concentrations were assumed at 200 nM (diamonds), 10 nM (squares), 1 nM (triangles), and 100 pM (circles).

The equilibrium models showed that the limits of detection of the system corresponded to the equilibrium dissociation constant for the antibody to the decoy, that the limits of detection for each antibody and decoy concentration corresponded approximately to the decoy concentration used, and that at very low antibody and decoy concentrations (below the dissociation constant), normalized fluorescence intensity decreased,

suggesting that the signal to noise ratio would also decrease. These observations are consistent with experimental data shown in Fig. 4.6. To reduce further the detection limits of the assay, the equilibrium binding coefficient would have to be increased, either by finding a different antibody or by altering the ionic strength and temperature at which the assay was performed [161, 162] or both.

Detection was also limited by background fluorescence of free decoy or decoy bound to antibody, for enhancement and quenching chemistries, respectively, which increased the noise in the system. Improved surface-modified fluorescence effects might be obtained through use of silver deposition on the gold nanoparticle, which would both increase surface roughness and alter the absorbance of the particles such that they would better match the excitation source [151]. For better enhancement specifically, outside of better control of molecular distances and resonance effects, it would be necessary to change to a lower-quantum-efficiency fluorophore [151].

Conclusions

It has been demonstrated that it is feasible to detect nanomolar concentrations of recombinant prion protein in a simple and reproducible assay that uses surface-modified fluorescence. The strengths of the method are its simplicity, ease of use, and relative speed which are appropriate for screening technologies for the food industry. However, we were not able to achieve the femtomolar detection limits of current detection methods (ELISAs) [79, 80]. To further increase the sensitivity of a surface-modified fluorescence-based system beyond the limits of the affinity of the antibody, it would be

necessary to create an assay that was no longer competition based. In addition, with the current system, the natural fluorescence of biological molecules (along with the scattering effects of a serum-based sample) would create significant ‘‘noise’’ in the output leading to a decreased sensitivity of the assay. This problem could be addressed by shifting to a longer-wavelength fluorophore to reduce the effects of scatter and the intrinsic fluorescence of biological samples. Finally, the current method as described would require modifications to the sample to allow for the discrimination between infectious and noninfectious prions. This could be accomplished by pretreating the samples with proteinase K or other selective proteases prior to sample analysis [163]. This step would, of course, increase the difficulty and time required for the assay to be performed.

In summary, surface-modified fluorescence assays such as the one described here can be used for the detection of biologically important proteins. The method is simple and fast and has a sensitivity approximately equal to the antibody–antigen equilibrium dissociation constant. In applications where very high-affinity antibodies are available, where the sensitivity needs are on the order of nanomolar concentrations, or where ease of operation are important, assays such as the one that we have described may be appropriate.

CHAPTER V

PRELIMINARY WORK TOWARDS THE DEVELOPMENT OF AN ORGANOPHOSPHATE ENZYMATIC SENSOR

Introduction

The wide spread use of neurotoxic organophosphates (OP) in the environment for insect and pathogen control and recent threats of OP based chemical warfare agent involvement in ground based warfare and terrorist attacks necessitate the development of simple and specific methods for OP detection. Organophosphorus (OP) neurotoxins comprise a unique class of contaminants and chemical warfare agents (CW) that generally show low environmental persistence, but they have a high acute toxicity and a wide range of biological activities. Some members of this class are extremely toxic to mammals (e.g. the human oral lethal dose for paraoxon = 16 mg/kg, and VX is lethal at 1 mg if ingested or 100 mg-min/m^3 if inhaled); they are powerful inhibitors of enzymes, such as Acetyl- and Buturyl-Cholinesterases or Neurotoxic Esterase, which are involved in nerve function. Moreover, low doses, but long-term exposure of these neurotoxins may lead to the development of cancer, genetic diseases, and other dangerous effects. OP neurotoxins are capable of producing organophosphate-induced delayed neurotoxicity (OPIDN) in man and susceptible species. Recovery from these complex and poorly understood diseases is usually poor and there is no specific treatment, as observed for many Gulf War participants.

A variety of methods including gas, liquid, and thin-layer chromatography with mass spectrometry or other sophisticated spectroscopic detection methods have been used for organophosphate identification and detection. These approaches are very sensitive but require expensive equipment and are not specific for organophosphates. Another approach has been the use of biosensors that use specific enzymes such as acetylcholinesterase or butyryl cholinesterase as the recognition element [164 - 166]. Organophosphate neurotoxins inhibit the activity of the enzymes, thus inhibition of their activity can be used as an indirect measure the "total anticholinesterase activity" of a sample (with sensitivity up to 10^{-10} M) but are prone to interference by a environmental contaminants such as heavy metals or phenols.

Another approach has been to use organophosphate hydrolase as the principle component of biosensors for the direct detection of organophosphates [167 - 169]. The enzymatic hydrolysis of OP neurotoxins by organophosphate hydrolase (OPH) generates two protons in each hydrolytic turnover through a reaction in which P-O bonds are cleaved. Several strategies, potentiometric and fluorescence, have been used to detect the generation of protons, with sensitivity down to 1 μM [170, 171]. While sensitive, these sensors are very sensitive to the buffering capacity of the sample.

In this work, we examine the feasibility of developing a biosensor using organophosphate hydrolase as a recognition element, and surface modified fluorescence spectroscopy as a detection method for a variety of organophosphate neurotoxins. This work builds on our previous success in the development of a surface modified fluorescence method for the detection of prions [172], preliminary work of our

collaborators on the development of a nanoparticle based sensor for organophosphate detection [173], and our modeling efforts detailed in Chapter III.

The system uses a fluorescent competitive inhibitor of OPH as the detection analyte. By isolating the enzyme in close proximity to a fluorescence modifier (e.g. gold), we can alter the fluorescence intensity of the inhibitor upon it binding to OPH. Because the reaction is enzymatic, rate of change of fluorescence can then be used as an indicator of the presence of organophosphate neurotoxin. This differs significantly than sensor methods that we have previously developed. In addition, the gold-laden OPH will be produced either through direct gold-labeling of the enzyme, or by creating a gold-rich hydrogel in which the enzyme is contained. The end goal of the work is to develop a detection methodology that is portable and affordable, such that communities can monitor their water/soil for OP pesticide contamination and/or OP chemical warfare agents.

Materials and methods

Materials

The OPH was supplied by Dr. Jim Wild from the Department of Biochemistry and Biophysics at Texas A&M University. Paraoxon was purchased from Chem Service (West Chester, PA). Nanogold was purchased from Nanoprobes, Inc (Yaphank, NY). *N*-dodecyl-*N,N*-dimethylamine *N*-oxide (DDAO), DDAO phosphate, and Texas Red were purchased from Molecular Probes (Eugene, OR). Acryloyl polyethylene glycol N-hydroxysuccinimide (Acryloyl-PEG-NHS) was purchased from Nektar Therapeutics

(Huntsville, AL). Irgacure 2959 photoinitiator was acquired from Ciba Specialty Chemicals (Tarrytown, NY). The Spectroline EN-180 Longwave UV Lamp was purchased from Spectronics Corporation (Westbury, NY). Fluorescence and absorbance was measured using an Applied Photophysics (Leatherhead, Surrey, UK) PiStar system equipped with stopped-flow capability. Centrifugal filter units were purchased from Millipore Corporation (Billerica, MA). All other chemicals and supplies were purchased from Sigma-Aldrich (St. Louis, MO).

Gold labeling of OPH – all gold types

Three different gold nanoparticle attachment chemistries were used, monomaleimido, mono-NHS, and monoamino, to specifically attach the gold nanoparticles to the organophosphate hydrolase (OPH) enzyme at sulfhydryl, amine, and carbohydrate residues, respectively. The procedure for the attachment of the monomaleimido nanogold was performed according to the large protein attachment procedure provided by Nanoprobes with the following modification: 200 mM dithiothreitol was used in place of 100 mM MEA as a disulfide bond reducing agent [153]. The procedures for the attachment of sulfo-NHS nanogold to primary amines and monoamino nanogold to oxidized carbohydrate moieties were performed according to the protein and glycoprotein attachment procedure, respectively, provided by Nanoprobes without modification [154, 155].

Determination of kinetic constants for OPH enzyme in the absence and presence of inhibitors DDAO phosphate and coumarin-1.

Enzyme activity in the absence of inhibitors was determined mixing equal volumes of 20nM OPH in PBS (pH=7.0) and solutions of varying concentrations of paraoxon. The absorbance of the mixture was measured at 340nm to monitor the production of p-nitrophenol (the degradation product of paraoxon by OPH) as a function of time. The data were then analyzed to find initial rates of paraoxon hydrolysis as a function of substrate concentration. K_m and k_{cat} were then estimated by fitting initial rate data to a standard Michaelis –Menton kinetic expression.

DDAO phosphate was mixed in varying concentrations ranging from 10 to 100μM with 20nM OPH in PBS (pH=7.0). Paraoxon stock was made by dissolving paraoxon in DMF to a concentration of 100 mM. The stock was diluted in PBS to varying concentrations ranging from 10 to 1000μM. DMF was added to a concentration of 4% (v/v). The OPH/DDAO phosphate solution and the paraoxon solution were mixed in equal volumes using the stopped-flow attachment for the PiStar system. The absorbance was measured at 340nm to monitor the production of p-nitrophenol as a function of time. The data were then analyzed to find initial rates of paraoxon hydrolysis as a function of substrate and inhibitor concentration. K_m, k_{cat}, and K_I were then estimated by fitting initial rate data to a standard Michaelis –Menton kinetic expression that included competitive inhibition. Analogous experiments were performed to determine an inhibition constant (K_I) for OPH with coumarin 1.

Fabrication of hydrogel for enzyme/dye immobilization

Polymer precursors were made by producing a PEG-DA solution containing 0.5% Irgacure 2959 and 10% acryloyl-PEG-NHS. Texas Red, coumarin 1, and gold-labeled OPH were added in varying concentrations to the polymer mixture. From the resulting mixture, a 10 μL dot was applied to a thin strip of polystyrene. The dot was placed under the UV curing lamp at a distance of ½ inch for 10 minutes (~260 mW/cm^2).

Measurement of gold-modified fluorescence of OPH-coumarin 1 system

The hydrogel dot was placed at a ~45^o to the light path in the fluorometer. The emission intensity of the coumarin 1 was monitored at 468nm while exciting at 390nm. Texas red was used for normalization (since the exact sample volume in the path could not be maintained from one slide to the next). This was done by measuring the emission intensity of Texas red at 610nm while exciting at 510nm. The value for the emission of coumarin 1 was then divided by the emission intensity of Texas red to compensate for difference in the material light paths.

Results and discussion

OPH temperature study

The first concern we had when working with OPH was creating the best environment for the sensor and the enzyme. We knew that temperature would effect the system and attempted to find the ideal working temperature (with reasonable laboratory operating conditions being somewhere between 5^{o}C and 25^{o}C. From this work, we can

to the conclusion that within that range, 25°C was the best conditions for operation. This was due to the increased reaction rates allowing for quicker detection.

OPH-DDAO phosphate inhibition study

In order to develop a surface modified fluorescence assay for organophosphates, a suitable fluorescence inhibitor must be identified. By recommendation of Dr. Alex Simonian at Auburn University, we tested DDAO phosphate as an inhibiting dye for the sensor system. This was performed as described previously. Figure 5.1 shows the results of this study.

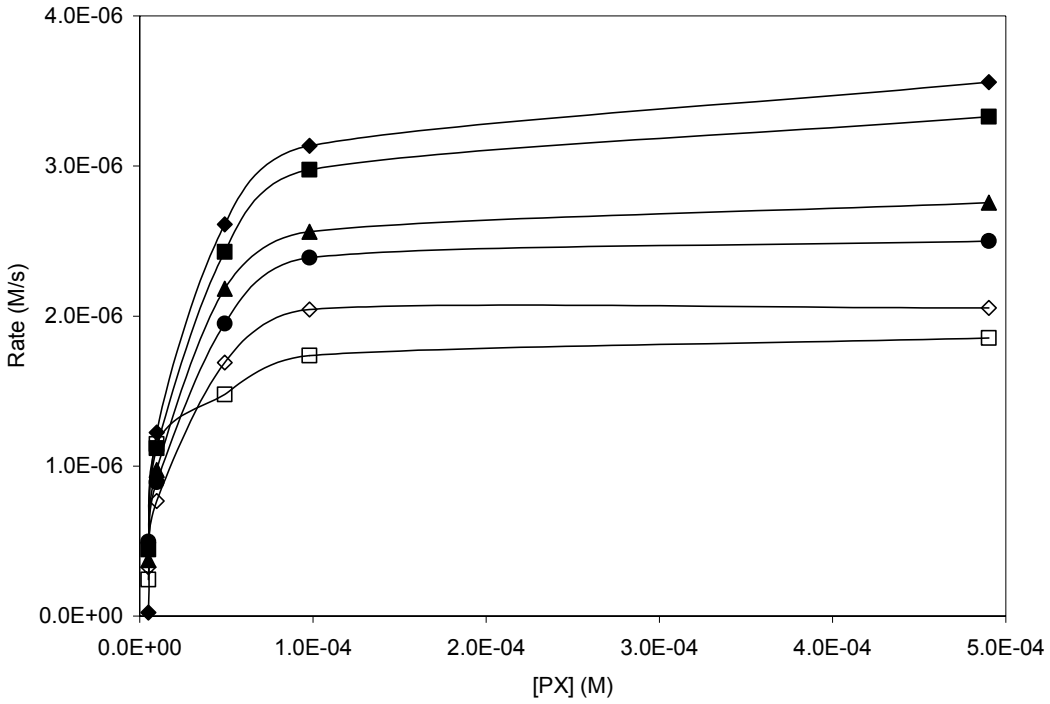

Fig 5.1. DDAO phosphate inhibition results. This figure shows how the enzymatic reaction curve varies with DDAO phosphate concentration. The rates reported are initial rates measured within the first minute of reaction. The resulting data was analyzed to find the linear region closer to time zero. The DDAO phosphate concentration for each curve is as follows: ♦ - 0 µM, ■ – 4.90 µM, ▲ – 8.17 µM, ● – 16.34 µM, ◊ - 32.68 µM, and □ – 49.02 µM.

From this figure, it is apparent that the inhibition effect from DDAO phosphate is not competitive (as expected or desired). With a competitive inhibitor we would expect a constant value for V_{max}, with K_m increasing with increasing inhibitor concentration. This is not what is happening here. This is further exemplified by Figure 5.2.

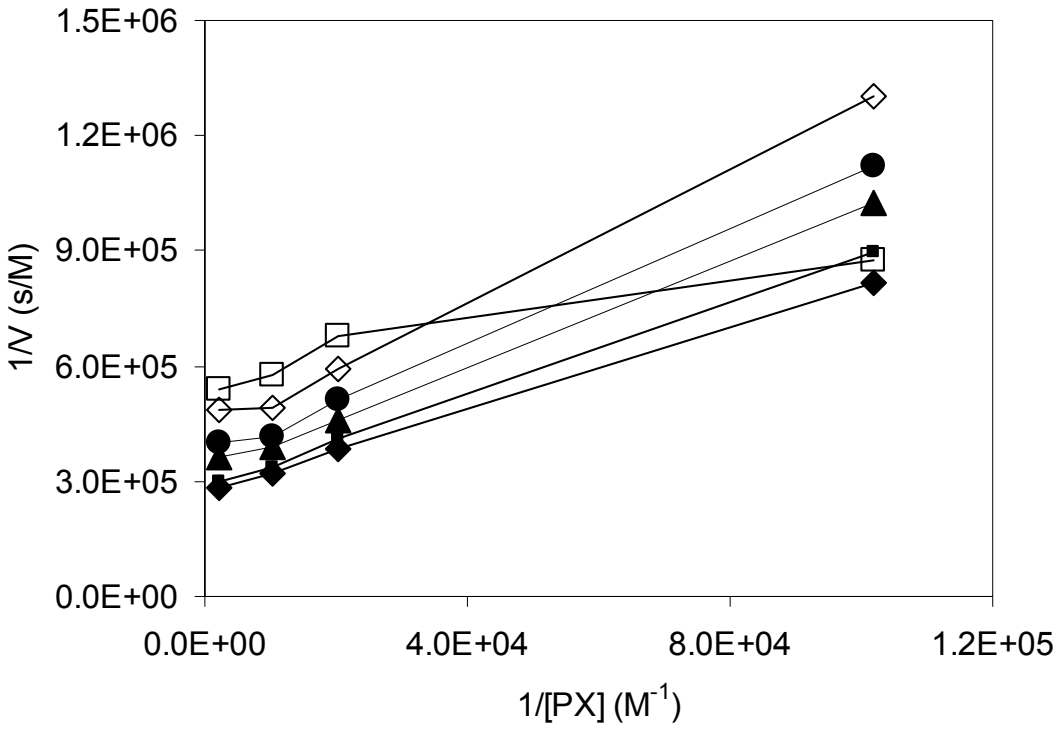

Fig 5.2. Lineweaver-Burke analysis of DDAO phosphate inhibition. Plotting 1/V vs. 1/[PX], allows for the calculation of V_{max} (and in turn, k_{cat}) from the inverse of the y-intercept and the calculation of K_m by multiplying the slope by V_{max}. The DDAO phosphate concentration for each curve is as follows: ♦ - 0 μM, ■ – 4.90 μM, ▲ – 8.17 μM, ● – 16.34 μM, ◊ - 32.68 μM, and □ – 49.02 μM.

Neglecting the highest DDAO phosphate concentration (there were problems with DDAO phosphate solubility), we can analyze the curves to obtain the values for K_m and V_{max} for each curve. From this, we obtain the following (Table 5.1):

Table 5.1. Summary of Lineweaver-Burke analysis

[PX] (μM)	V_{max} (M/s)	K_m (M)
0	3.72×10^{-6}	2.00×10^{-5}
4.90	3.52×10^{-6}	2.10×10^{-5}
8.17	3.02×10^{-6}	2.05×10^{-5}
16.34	2.75×10^{-6}	2.03×10^{-5}
32.68	2.32×10^{-6}	1.97×10^{-5}

From Table 5.1, it is apparent that V_{max} is a function of DDAO phosphate concentration. This, however, is not true for K_m, which remained constant over all values of DDAO phosphate. This indicates that, unlike previously believed, DDAO phosphate is a noncompetitive inhibitor and, therefore, not useful for this system. The led us to pursue other possible inhibitors.

Dr. Jim Wild recommended the use of coumarin derivatives as possible inhibitors. On the recommendation by Dr. Alex Simonian that coumarin 1 was a competitive inhibitor; we investigated coumarin 1 for its fluorescent properties. We found that coumarin 1 has an excitation maximum at 390 nm and an emission maximum at 468 nm.

We gold labeled the enzyme and tested the enzyme activity. We found that the enzyme had lost >90% of the activity upon labeling for all gold attachments. With such

low activity it was difficult to quantify exact values. An important thing to note is that it is possible that activity loss does not necessarily indicate loss of binding. So it is possible that enzyme will still be useful as a sensor with no catalytic properties. If not then we will need to address other ways of introducing gold into the system. This could be done by immobilizing both the enzyme and gold colloid into a hydrogel network that would encapsulate the enzyme/gold mixture, but still allow for diffusion of target and decoy into the hydrogel. Another problem with the system is that we require moderately high concentrations of gold-labeled enzyme in the system (>100 μM, assuming that the binding affinity has not be decreased). During the production of the gold-labeled enzyme, the enzyme solution is only around 1μM. However, this can be overcome by concentrating the enzyme via centrifuge filtration, and then immobilizing a small volume in the light path of the fluorometer (to compensate for the very low required volume). To do this, we had to incorporate a second, noninterfering fluorophore into the mixture to allow for normalization. For this, Texas Red was chosen (ex: 510 nm, em: 615 nm).

Initial attempts at performing the hydrogel immobilization have been unsuccessful. While coumarin 1 has responded well to the polymeric environment, Texas Red appears to be quenched by the polymer. Furthermore, creating a thin, immobilized polymer film has created the problem that the path length in the fluorometer has now been decreased from 1 cm to <1 mm. To overcome this problem, we are investigating a more three-dimensional immobilization into a smaller volume centered about the light path. In doing so, we hope to increase the light path to approach 1 cm while still maintain a small sample volume.

Conclusions

While we are still optimistic that the system will work, we have come to realize that there are certain issues we did not and could not have predicted. While we will continue to exhaust all options using the Nanoprobes gold system (since it creates are very closely, specifically bound gold), we realize that in may be necessary to investigate other immobilization techniques that would lock the gold into the hydrogel network without directly interacting with the enzyme.

Even if the system is altered to use a different gold product, the incorporation of a second, noninterfering fluorophore is a crucial technique. This will lend itself to making the final product (a portable, self-contained biosensing apparatus) more robust. The second fluorophore present for normalization allows for simpler optical alignment in the final system.

CHAPTER VI

FEASIBILITY OF DEVELOPING A SERS BASED SENSOR PLATFORM FOR SPECIFIC DETECTION OF β-AMYLOID

Introduction

The goal of this work is to examine the feasibility of the development of a new detection platform and methodology for early detection and characterization of β-amyloid peptide (Aβ), the primary protein component of senile plaques in Alzheimer's disease (AD). Definitive diagnosis of AD is still by postmortem examination of central nervous tissue for evidence of amyloid plaques and neurofibrillary tangles. Probable diagnosis is made based on tests of cognitive function, MRI, and functional PET. Currently, a number of investigators are developing fluorescent or PET imaging agents specific for Aβ that could be used for *in vivo*, pre mortem diagnosis of AD [91, 174 - 176]. In addition, a number of investigators are developing 2-D electrophoresis/mass spectrometry methods to look for early markers of AD in cerebral spinal fluid [98, 177 - 204]. However, at present, there are still no approved definitive tests for AD premortem.

A unique product has been developed by Nanospectra Biosciences that incorporates nanoshells on a surface providing a robust platform for analyte detection at trace levels using surface enhanced Raman spectroscopy. A variety of evidence indicates that Aβ peptide, in specific aggregation states, can be found in cerebral spinal fluid, and may be able to be used as a marker for AD progression [183, 187, 192, 199 –

201, 204]. For a SERS sensing strategy to be successful, an affinity surface for Aβ must be designed that is molecularly small, has high affinity for Aβ, has low affinity for irrelevant proteins, and whose spectral features do not significantly overlap with structure specific features of the Aβ Raman vibrational spectra. The development and testing of such an affinity surface is described.

Surface enhance Raman spectroscopy (SERS)

Surface Enhanced Raman Spectroscopy (SERS) is a Raman Spectroscopic technique that provides greatly enhanced Raman signal from analyte molecules that have been adsorbed onto certain specially prepared metal surfaces. Increases in the intensity can be as high as 10^8 and 10^{14} for some systems [46, 47]. Furthermore, the fact that SERS is surface-dictated spectroscopic technique justifies the use of SERS as a sensor platform.

Aβ structure associated with Alzheimer's disease

Aβ is a 39 to 43 amino acid long peptide that aggregates both *in vivo* and *in vitro* to form a variety of structures reported to be toxic and/or disease associated. These structures include a non-fibrillar species of approximately 17 to 42 kDa referred to as amyloid derived diffusible ligands (ADDLs) [90], protofibrils species [205] and fibril species. All the disease associated oligomers of Aβ have a high beta sheet content, in contrast to non-disease associated species. The currently most aggressively pursued Aβ oligomer target for both diagnostics and therapeutics is the ADDL [206].

In vivo, Aβ is known to accumulate in the cerebral cortex during disease, with deposition into mature amyloid plaques first in the entorhinal cortex and the hippocampus then later in the frontal cortex [91]. During disease, it is apparent that Aβ accumulates in other parts of the body that are easier to sample for *in vitro* diagnostic measurements [207]. Aβ circulates in both the blood and the cerebral spinal fluid. As disease progresses, there are significant changes in oligomeric Aβ in the cerebral spinal fluid [208 - 210].

Relationship between sialic acid and β-amyloid

While many investigators are developing structure specific antibodies for detection of disease associated Aβ [211-213], there may be biomimetic materials that can be developed with antibody like affinity but smaller molecular size, that may be more appropriate for the demands of a SERS based sensing system. A variety of evidence indicates that β-amyloid may bind to cells via an interaction with surface glycolipids or glycoproteins, and that the affinity of this interaction increases when the gangliosides or sialic acid molecules on the cell surface are clustered. [214-221]. Based on these data, we hypothesized that biomimetic surfaces could be synthesized which would reproduce the clustered sialic acid structure of the cell surface, and therefore recreate the Aβ binding seen to occur on neuronal cell membranes.

Using all the principles previously described, we have successfully proven the capability of SERS as a sensor platform. Furthermore, we have developed and characterized numerous surfaces for both binding affinity to Aβ and binding capacity

(both of which are important characteristics for a SERS-based sensor). Combining this information, we have all the background necessary to justify moving forward into SERS-based sensor development.

Materials and methods

Materials

The Aβ (1-40) was synthesized and purified by BioSource International (Camarillo, CA). The sequence is DAEFRHDSGYEVHHQKLVFFADVGSNKG-AIIGLMVGGVV. Molecular mass and purity were confirmed by mass spectroscopy and reverse phase HPLC (MW = 4356, >95 % purity). Bovine serum albumin (BSA) was purchased from Fisher Scientific (Fairlawn, NJ). The nanosphere gold substrates (to be referred to as "slides" henceforth) were supplied by Nanospectra Biosciences, Inc. (Houston, TX). The IODO-beads, G-5 desalting columns, 1-Ethyl-3-[3-dimethylaminopropyl]carbodiimide Hydrochloride (EDC), and sulfosuccinimydyl-3-(4-hydroxyphenyl) propionate (sulfo-SHPP) were purchased from Pierce Biotechnology, Inc. (Rockford, IL). The ^{125}I and G-25 Sephadex were purchased from Amersham Biosciences/GE HealthCare (Piscataway, NJ.). Disialyllacto-N-tetraose (DSLNT) was purchased from V-labs, Inc. (Covington, LA). The glycidyl methacrylate and tetrabutyl ammonium bormide were purchased from Acros Organics (Geel, Belgium). 5-(aminomethyl)fluorescein (5-AMF) was purchased from Molecular Probes (Eugene, OR). Scintillation counting was done using a Wallac MicroBeta Jet microplate scintillation counter from PerkinElmer Life and Analytical Sciences (Shelton, CT).

Sulfo-N-Hydroxy-Succinimido-Nanogold (sulfo-NHS-nanogold) and silver enhancing reagent were purchased from Nanoprobes (Yaphank, NY). All other materials and chemicals were purchased from Sigma-Aldrich Corporation (St. Louis, MO).

The nanosphere slides from Nanospectra are designed to allow them to be tuned to the frequency of the laser being using in the Renishaw microRaman system. The spheres have silica core around which gold is deposited layer by layer until the desired frequency is achieved. Figure 6.1 shows how the frequency of the spheres varies with shell thickness.

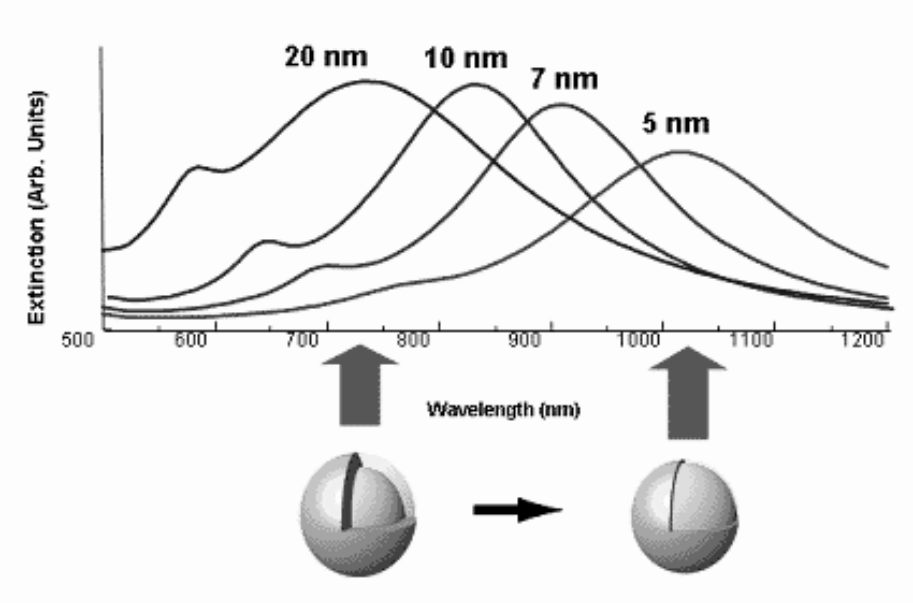

Fig 6.1. Relationship between absorbance and shell thickness for Nanospectra nanospheres. The curves show the absorption characteristics of four different shell thicknesses. As can be seen here, as the thickness increases, the absorption maximum blue shifts. Obtained from www.nanospectra.com/physics/physics.asp.

Gold labeling and silver enhancing of generation 4.0 PAMAM dendrimer

The procedures for the attachment of sulfo-NHS-nanogold to primary amines on the dendrimer were performed according to the peptide labeling procedure provided by Nanoprobes without modification [154]. The silver enhancement was performed according to the silver enhancement of nanogold for EM procedure from Nanoprobes without modification [154].

Collection of SERS spectra

30 μl of each of the samples (sample 1 = Au-Ag-Dendrimer, sample 2 = Au-Ag-Dendrimer-Aβ) were pipetted onto the surface of a microscope glass coverslip (22×22 mm, Fischer Scientific Co.) and the water was allowed to evaporate for 30-45 min, until a thin solid crust of the sample remained on the surface of the coverslip. The coverslip was then placed onto the stage of the Leica *DMLM* microscope that was coupled to a Renishaw System 1000 Raman spectrometer. The laser used for the SERS studies was the 514.5 nm line of an Ar^+ laser (Spectra Physics Model 263C) with approximately 5 mW of laser power delivered to the sample. The incident laser beam was incident on the sample via the 50X air objective (NA =0.75) of the microscope. The SERS spectra were collected with the diffraction grating centered at 900 cm^{-1} and integration time of 90 secs.

Formation of self-assembled monolayer (SAM)

All monolayers were formed using the same procedure. The monolayer material was dissolved in ethanol to form a 2mM solution. The slide was submerged in the ethanolic solution and allowed to react for 24 hours at room temperature. The slide was then removed from the solution and rinsed thoroughly with ethanol and dried under nitrogen. The monolayer materials used all had the following general form: HS-R-COOH, where R = $(CH_2)_2$, $(CH_2)_{10}$, or $(CH_2)_{15}$. The exception to this rule is 4-aminothiol phenol (4-ATP). 4-ATP has the following structure: HS-R-NH_2, where R = benzene. Figure 6.2 depicts how the self-assembly occurs. FTIR was used to confirm the assembly of the monolayer. Figure 6.3 shows a representative spectrum of a monolayer with relevant peaks pointed out.

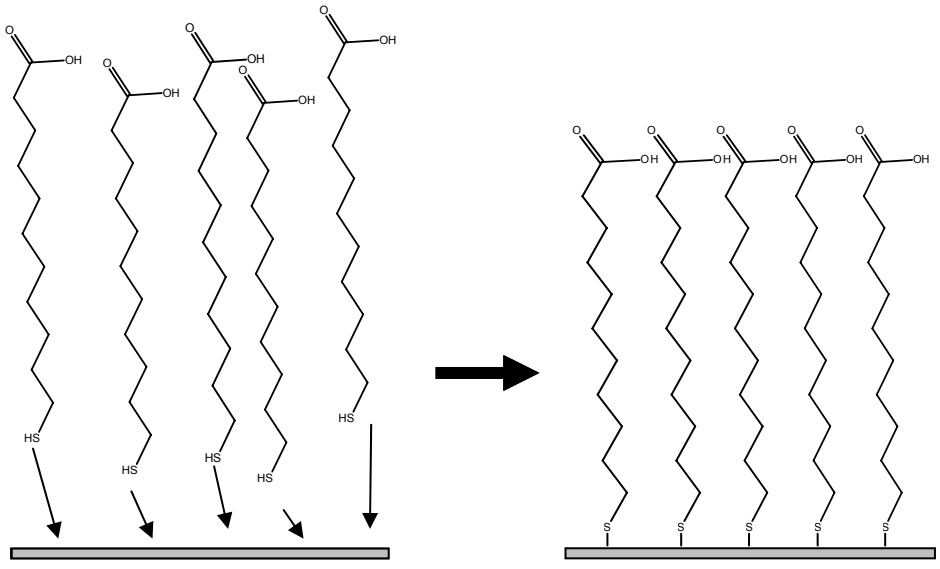

Fig 6.2. Schematic of self assembly process. The monolayer compound floats freely in solution until coming in contact with the metaled surface (Ag, Au, or Ni usually). Upon contact, the thiol reacts with the surface, covalently binding the molecule to the surface. This layer is fluid in nature and will move around and continue to assemble until a tightly packed structure is created. This creates the lowest energy state for the system and completes the self assembly process.

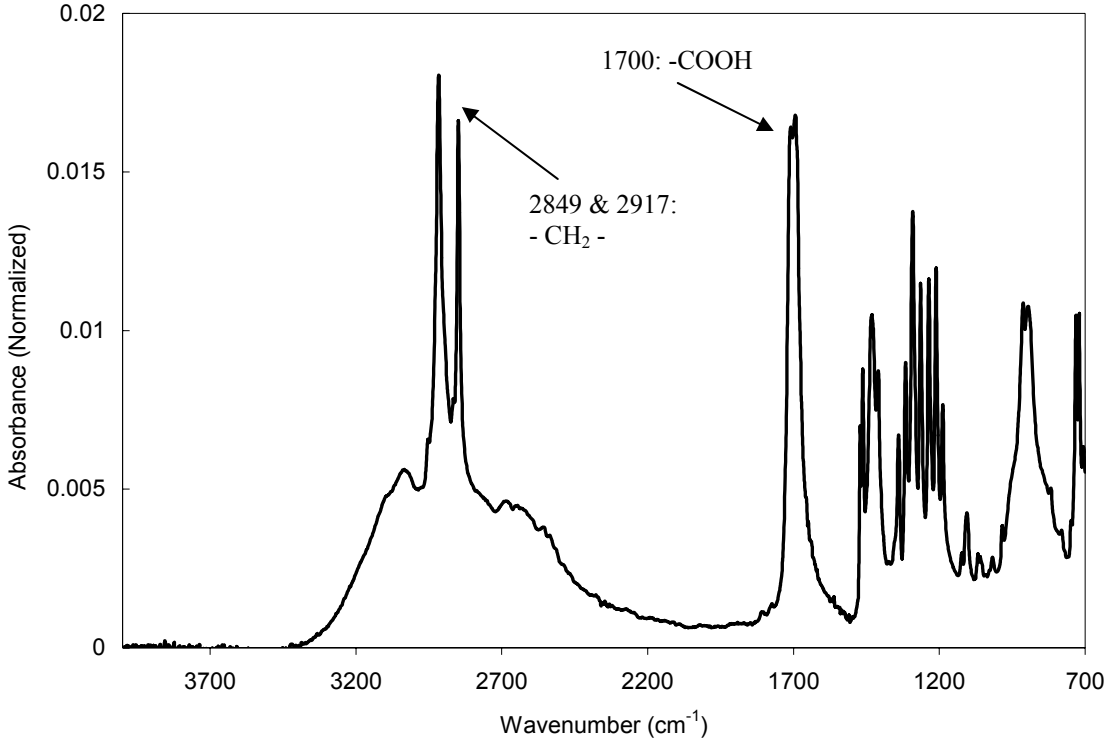

Fig 6.3. FTIR spectrum of 11-MUDA SAM. The most interesting peaks occurred at 1700 (carboxylic acid) and a doublet at 2849 & 2917 (CH_2).

Determination of monolayer stability

One slide of each monolayer was placed in two different conditions: in nitrogen, in the dark and exposed to light and air. A third 16-MHDA slide was stored in nitrogen, but exposed to light to test for the effect of photobleaching the fluorophore. After 24 hour exposure, the surfaces were thoroughly rinsed with deionized water and dried under nitrogen before imaging using a fluorescence microscope. The images were analyzed using Matlab.

Attachment of dendrimer or 5-AMF to carboxy-terminated monolayer

The dendrimers were attached using EDC chemistry described by Pierce Biotechnology [222] with minor modifications. These modifications were the concentrations used (since the surface concentration of monolayer could not be known). The EDC was added to a concentration of 10 mg/mL (give molar concentration) with dendrimer or 5-AMF added to the same molar concentration and reacted overnight. Upon completion, the slide was rinsed thoroughly with deionized water and dried under nitrogen for storage. Figure 6.4 shows the mechanism for EDC chemistry. Figure 6.5 represents a dendrimer surface. Figure 6.6 represents the FTIR spectra from attaching dendrimer.

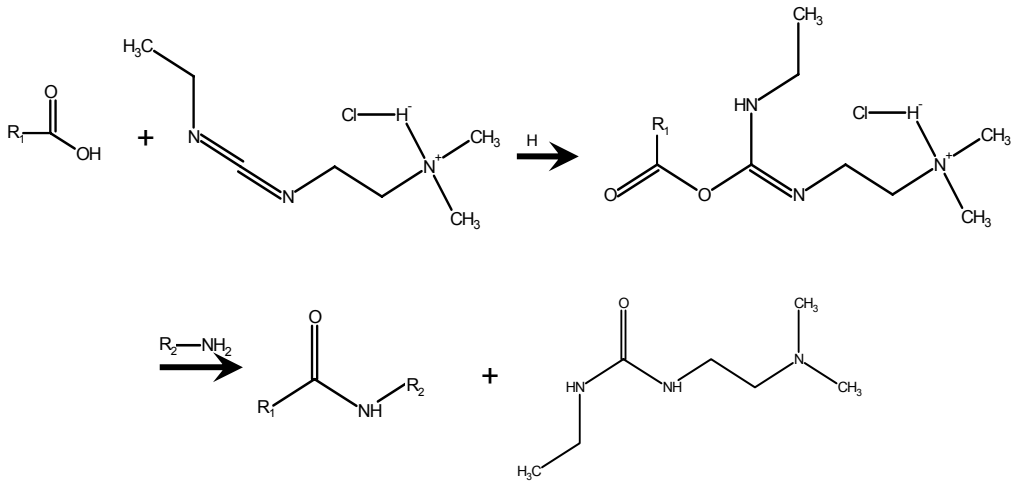

Fig. 6.4. Schematic of EDC chemistry. The carboxylic acid-terminated compound reacts with EDC to form an amine-reactive intermediate. This intermediate then reacts with the amine-terminated compound to create and amide bound leaving only the spent EDC.

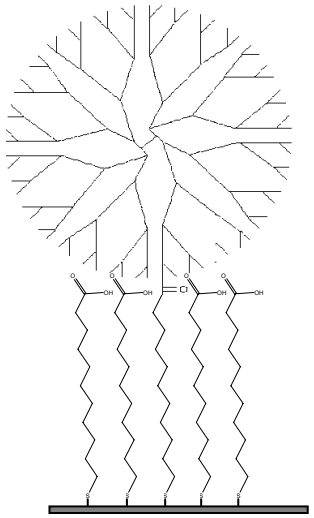

Fig. 6.5. Schematic of dendrimer surface. The figure depicts a generation 4.0 amine-terminated dendrimer attached to a carboxylic acid terminated surface (11-MUDA) via EDC chemistry. This leads to the formation of amide bounds.

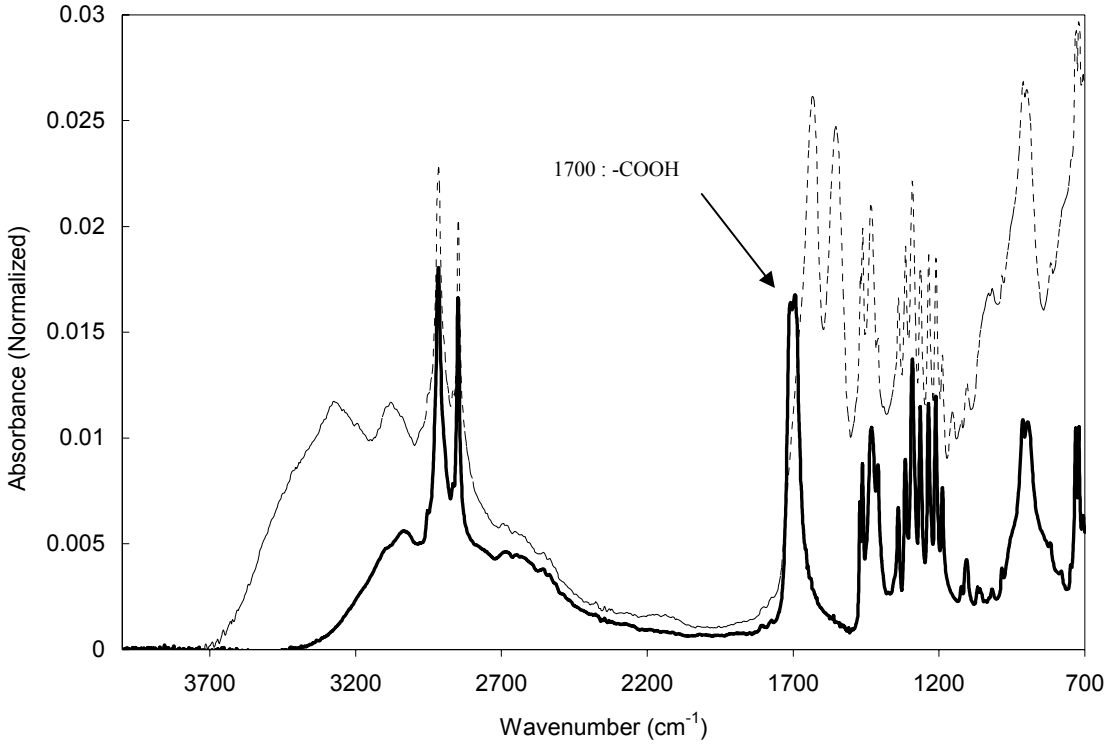

Fig. 6.6. FTIR spectra of 11-MUDA and 11-MUDA/Den 4.0 on surface. The FTIR spectra of 11-MUDA (d, solid line) and 11-MUDA/Den 4.0 (thin, dashed line) show how the EDC chemistry works. The strong spectrum from the dendrimer obscures any amide peaks that may have formed (due to secondary amides being present in the dendrimer). However, the loss of the 11-MUDA peak at ~1700 indicates that there is a loss of the carboxylic acids at the surface. This can be attributed to the formation of amides to link the dendrimer.

Production of DSLNT "artificial ganglioside"

A solution containing 100uL of deionized water containing 1mg DSLNT, 2.2uL triethylamine, 2.2uL glycidyl methacrylate, and 2.2mg tetrabutyl ammonium bromide was reacted overnight at room temperature. The solution was then incubated at 60^{o}C for one hour. After cooling to room temperature, the solution was diluted to 1 mL of total volume with deionized water. To the solution was added 15 mg of G-25 Sephadex to remove unreacted glycidyl methacrylate. This purification is based on simple quenching procedures. This works by introducing an excess of hydroxides to bind the excess methacrylate. The mixture was incubated at room temperature for one hour. The Sephadex was removed via centrifuge filtration over a 30 kDa membrane. The filtrate was then lyophilized to produce a sticky solid. The procedure was adapted from Leech et al [223]. The product of this reaction, a disialic acid terminated oligosaccharide with a methacrylate pendant group, could then be reacted with SAMs to make a disialic acid terminated monolayer, which is referred to as an artificial ganlioside in the following sections. With all the available hydroxyl groups available on DSLNT (due to the entire structure being composed of sugars), it is not possible to predict where the glycidyl methacrylate will attach. This makes representing the structure extremely difficult. However, Figure 6.7 represents the FTIR spectra of a)glycidyl methacrylate, b)DSLNT, and c)glycidyl methacrylate – DSLNT complex. The location of peaks in the spectra indicates the success of the attachment chemistry.

a)

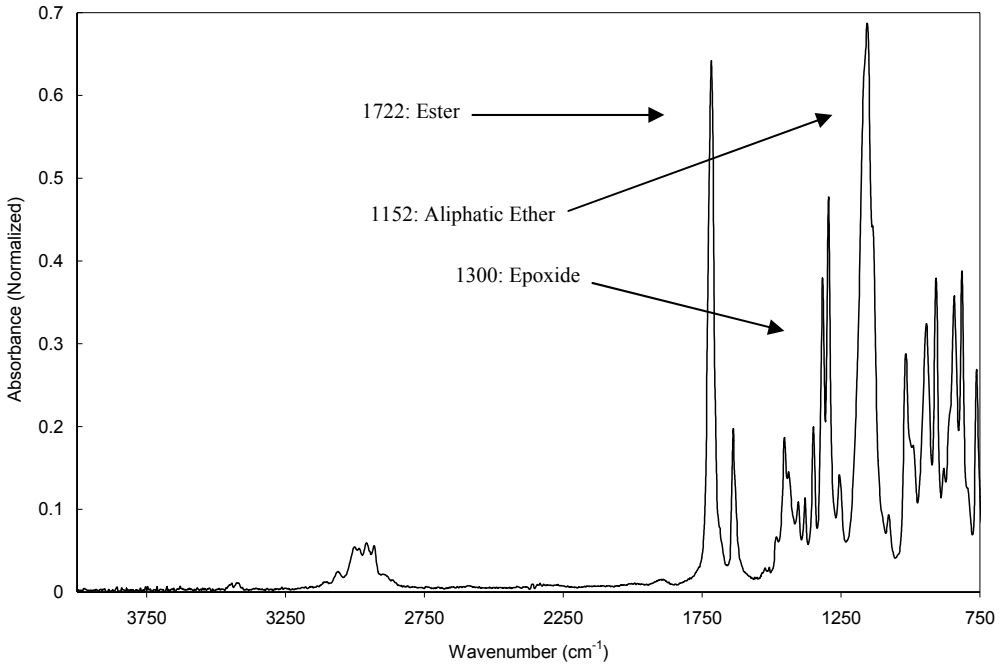

b)

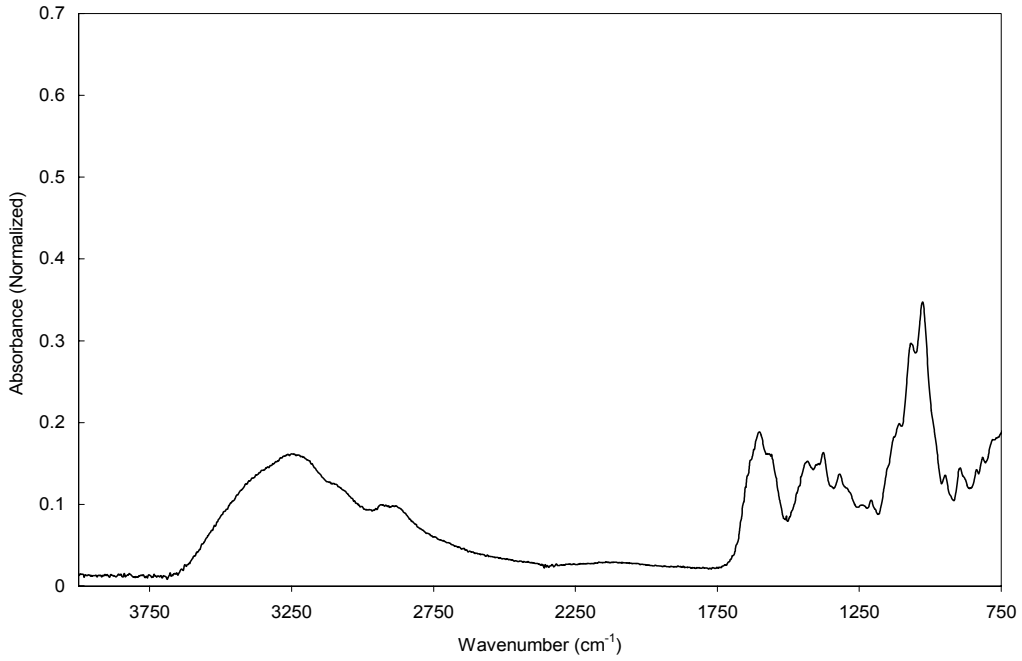

Fig. 6.7. FTIR spectra of a) glycidyl methacrylate, b) DSLNT, and c) glycidyl methacrylate – DSLNT complex. The ester peak, epoxide peak, and aliphatic ether peak in the gylcidyl methacrylate are the peaks of interest. In the methacrylate – DSLNT complex, we see the presence of numerous peaks characteristic of DSLNT. However, one thing we do notice is a strong ester peak without the presence of peaks from epoxides or aliphatic ethers.

c)

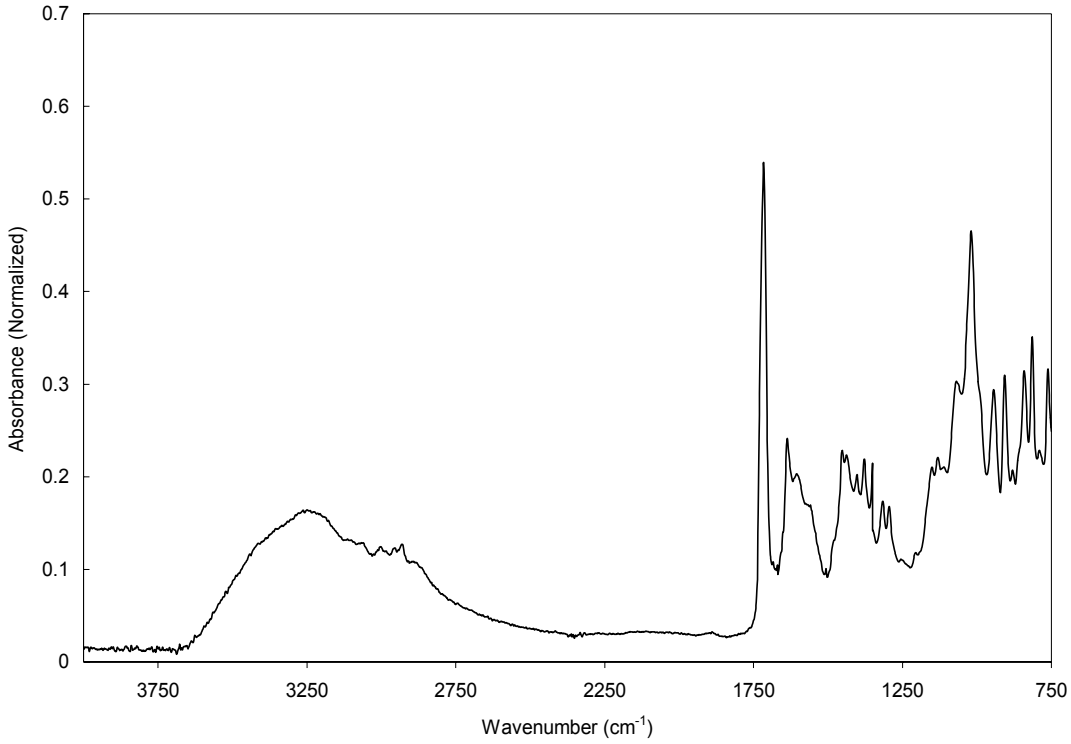

Fig 6.7. continued

From these spectra, you can see that the complex has both species present (as is clear from the characteristics of the DSLNT being present and the strong ester peak). However, the presence of the ester peak without the presence of the epoxide or aliphatic ester peaks indicates that the epoxide ring has reacted with the DSLNT, creating more ester bonds in the process. There is no noticeable decrease in the alcohol stretch from 2500 – 3500. This is due to the large number of alcohols available.

Production of GM_1 ganglioside or artificial ganglioside surface

The ganglioside, GM_1, or disialic acid terminated oligosaccharaide-methacrylate prepared as described previously was dissolved in hexane to a concentration of 0.1 mg/ml and slowly pipetted over DI water in a Petri dish. The hexane was allowed to evaporate, leaving the ganglioside or oligosaccharide on the surface of the water with the hydrophobic portion facing upward. A slide with a SAM developed as previously described was dipped SAM-side down to just contact the water air interface, allowing the hydrophobic tail of the ganglioside/oligosaccharide to interact with the alkane portion of the monolayer. The slide was then lifted away from the water and dried under nitrogen. Figure 6.8 gives the representation of a ganglioside layer. Representing the artificial ganglioside layer is again not possible (due to the large number of confirmations possible). However, the general form of the artificial ganglioside monolayer should closely mimic that of the ganglioside layer. FTIR spectra of the ganglioside and artificial ganglioside layers are shown in Figures 6.9 a and b.

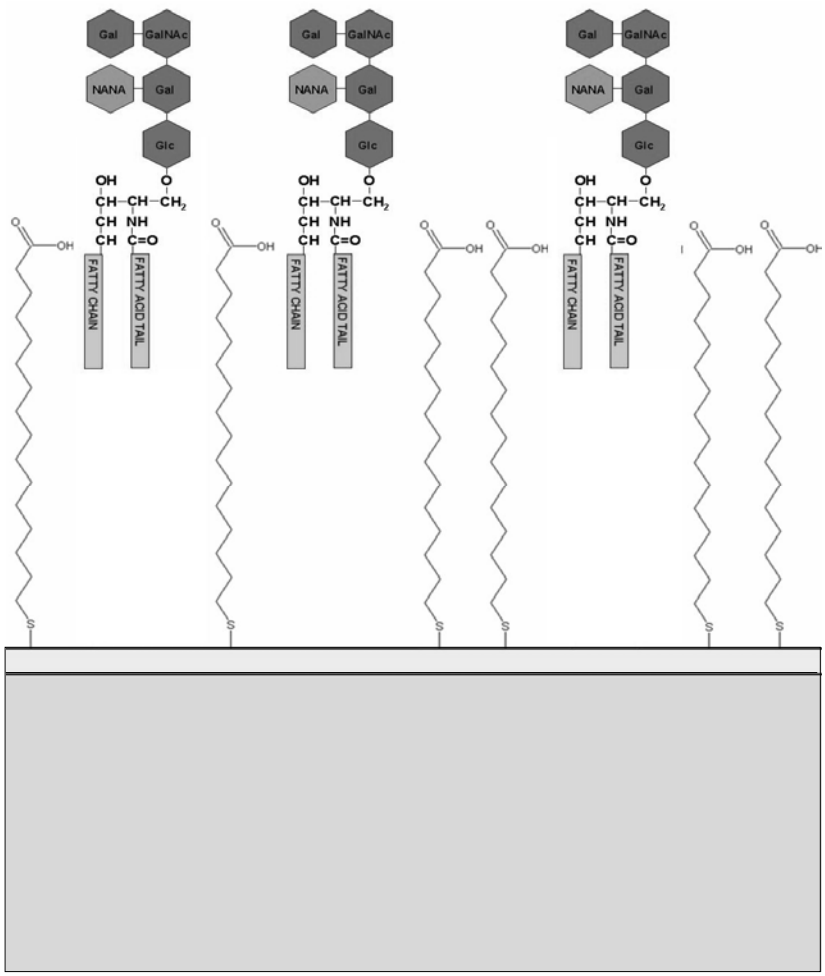

Fig. 6.8. Schematic of a ganglioside surface. The hydrophobic fatty acid tails of the ganglioside interact with the equally hydrophobic alkanes of the monolayer, tangling with them. Upon drying, the surface is left with the hydrophilic sugar molecules protruding from the monolayer while the hydrophobic tails stay embedded in the SAM.

a)

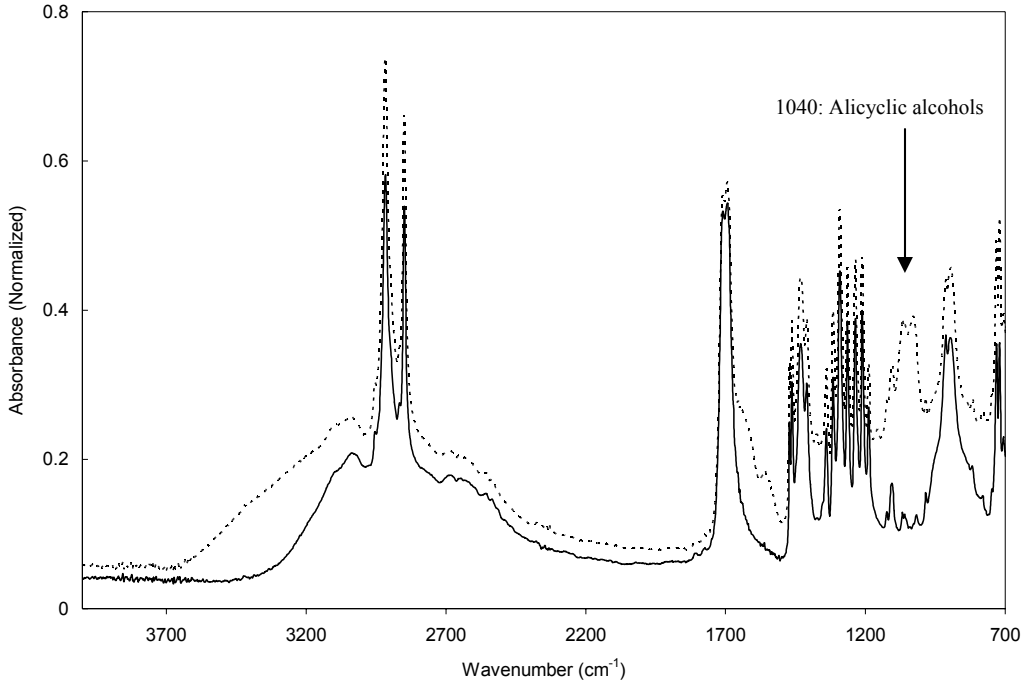

b)

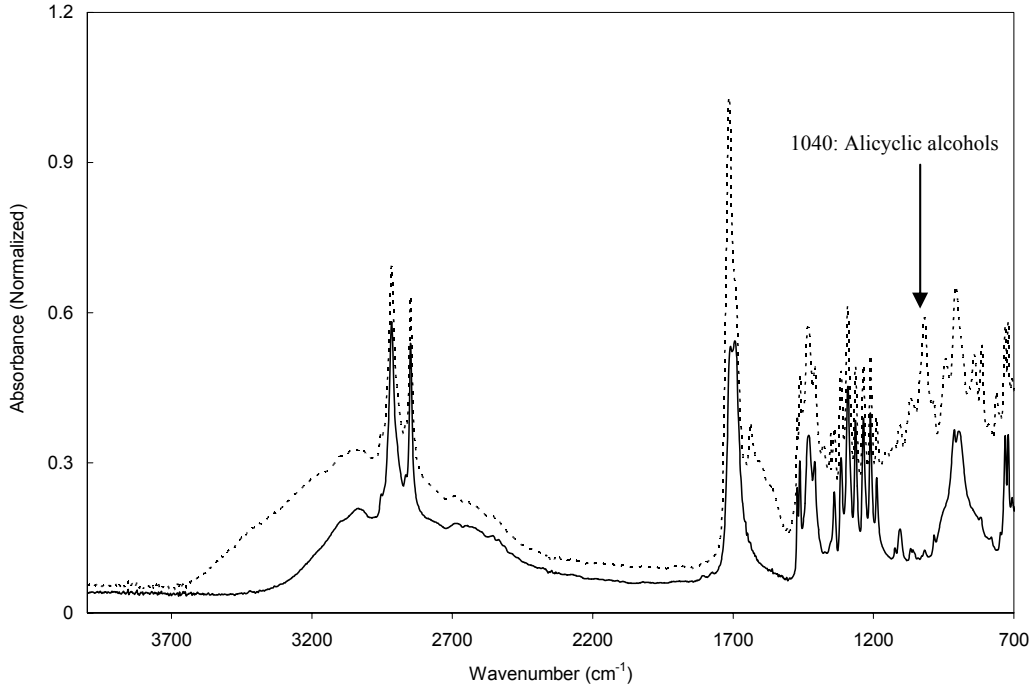

Fig 6.9. FTIR spectra of a) GM_1 and b) artificial ganglioside layers. The peaks of interest are labeled to indicated successful formation of the monolayers. The most interesting peak is at 1016 for the artificial ganglioside and 1040 for the GM_1 ganglioside. These represent alicyclic alcohol peaks. The dark line represents the 11-MUDA monolayer and the dsshed lines represent the monolayer and ganglioside conjugate.

Production of sialic acid labeled monolayer

The sialic acid was attached to amine terminated SAM using EDC chemistry described by Pierce Biotechnology [222] with minor modifications as described in the previous section. The EDC was added to a concentration of 10 mg/mL (give molar concentration) with sialic acid added to the same molar concentration. The monolayer used in this procedure was the amine-terminated 4-ATP. FTIR analysis of this sample was not performed due to limited material availability. However, successful labeling of the layer seems likely from previous success and binding studies presented later.

Stability of fluorecein labeled monolayer

The fluorescein monolayer was developed my creating 3-MPA, 11-MUDA, and 16-MHDA monolayers as previously described. The fluorescein was attached using standard EDC chemistry. The fluorescein slides were then a image used standard fluorescent microscopy techniques while employing a fluorescein filter. The field of vision used during analysis was kept constant at approximately a 3mm diameter circle. The images were then analyzed using Matlab.

Radiolabeling of β-amyloid

Aβ(1-40) was radioiodinated via a modified Bolton Hunter method. This method of iodination was chosen to preferentially label at the N terminus of the peptide. Labeling at other primary amines was inhibited by maintaining the pH below the pKa of those residues. 100 nmol of sulfo-SHPP was iodinated with 200 μCi of ^{125}I using the

IodoBead catalyst. The reaction was carried out for 15 minutes in pH 8 borate buffer in a volume of 140 μL. The catalyst was removed and 10 nmol (100 μL) of freshly prepared β-amyloid(1-40) (in water) was added to the iodinated sulfo-SHPP. The reaction was allowed to proceed for 3 hours at 4 C. The resulting condensation product was separated from free ^{125}I using a G-5 desalting column which also fractionated the peptide. The peptide was eluted from the column with phosphate buffer and stored at 4^{o}C until use. Iodinated Aβ(1-40) was typically used within one month of preparation. The free activity associated with radiolabeled Aβ(1-40) was determined by precipitation of the peptide with 5 wt% phosphotungstic acid in the presence of 5 mg/ml bovine serum albumin. Precipitable activity was 70 to 80%.

Peptide concentration was determined from the activity of the ^{125}I-labelled Aβ(1-40) by assuming that 50% of the peptide was recovered in from the desalting column using one column volume of the eluting buffer and that the peptide concentration was proportional to the precipitable activity of that fraction. No attempt was made to remove unlabelled peptide from labeled peptide. Relative aggregation state of the peptide was assessed using native polyacrylamide gel electrophoresis, counting activity of sliced sections of gel to determine relative abundance of different molecular weight species. The iodinated peptide was approximately 70% monomer or dimer, with the balance being large (above 100 kDa) aggregate.

Determination of binding affinity ($K_{A\beta}$) and surface saturation (N_{sat})

Freshly prepared nanogold-monolayer surfaces were incubated with sufficient

^{125}I-labeled Aβ(1-40) to completely wet the surface (typically 120 μL) at a constant temperature with rocking for two hours. Bovine serum albumin was added at a final concentration of 1 mg/ml to block nonspecific binding. Free Aβ(1-40) was removed from the surface, then the surface was washed twice with phosphate buffered saline. The bound surface was removed from the glass slide using a cotton swab. The activities of free peptide and bound surface (plus cotton swab) were counted separately, and binding constants were determined from equilibrium binding isotherms via fitting to a langmuir isotherm (Equation 6.1) using a non-linear least squares regression using Polymath 5.0.

$$N_{bound} = \frac{K_{A\beta}[A\beta]_{free} N_{sat}}{1 + K_{A\beta}[A\beta]_{free}} \qquad (6.1)$$

where: N_{bound} = nanomoles of Aβ on surface

$K_{A\beta}$ = equilibrium binding coefficient (M^{-1})

$[A\beta]_{free}$ = concentration of Aβ in solution at equilibrium

N_{sat} = nanomoles of Aβon surface at saturation

Results and discussion

Determination of SERS detection feasibility

The first step of this study was to determine two things. The first is whether Aβwould give an acceptable signal through SERS. The second was to determine if the signal from the recognition unit (dendrimer, ganglioside, etc.) would interfere with the signal from the Aβ.

These two things were determined by first gold labeling the dendrimer and then silver enhancing the dendrimer after reacting with Aβ fibrils (dendrimer and Aβ at 100μM concentrations in PBS at pH = 7.4). The SERS analysis was performed by Mustafa Chowdhury in Dr. Gerry Coté's lab at Texas A&M University. The results of this study can be seen in Figure 6.10.

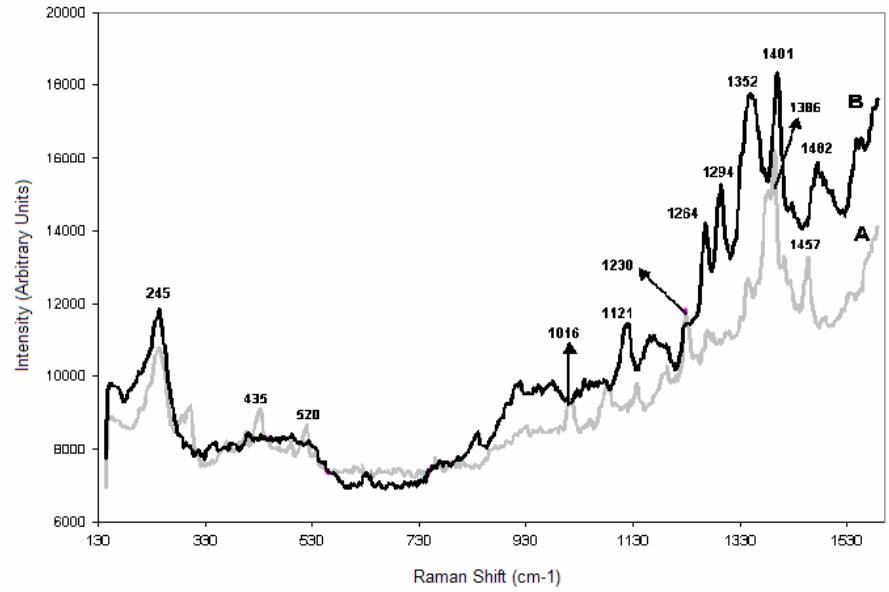

Fig 6.10. SERS feasibility study. A representative SERS spectrum for the dendrimer alone (gray line) and the dendrimer bound to Aβ (black line) are shown. Several peaks are present in the Aβ spectrum that are not present with just the dendrimer. The area of most interest occurs in the 1350-1400 range. This area is indicative of amide bonds (a very strong signature in amyloid proteins that provide structure information).

In the spectral region from 1350-1400 cm^{-1} in Figure 6.10, the dendrimer spectrum has a peak at 1386 cm^{-1} indicating the presence of amides in the internal structure of the dendrimer. However, the peak shifts to around 1352 cm^{-1} when Aβ is preesent, indicating the presence of amides in a β-sheet structure. Both the presence of

Aβ and information on its structure are needed for an effective diagnostic for Alzheimer's disease. The amide region of the Raman spectra can be used for structure determination of Aβ [224, 225]. The shifting of this peak and its clear presence with dendrimer present indicates a SERS based sensor that incorporates a dendrimer as recognition element for Aβ is both reasonable and feasible.

Effect of distance from surface on SERS signal

It was important to recognize the impact that distance has on SERS. We analyzed this behavior by attaching aniline (a very strong Raman active substrate) to the ends of three different monolayers (3-MPA, 11-MUDA, and 16-MHDA) using EDC chemistry. We then analyzed the aniline Raman signal from the surfaces to determine how the aniline SERS signal intensity changed with distance from the surface. Figure 6.11 shows the behavior.

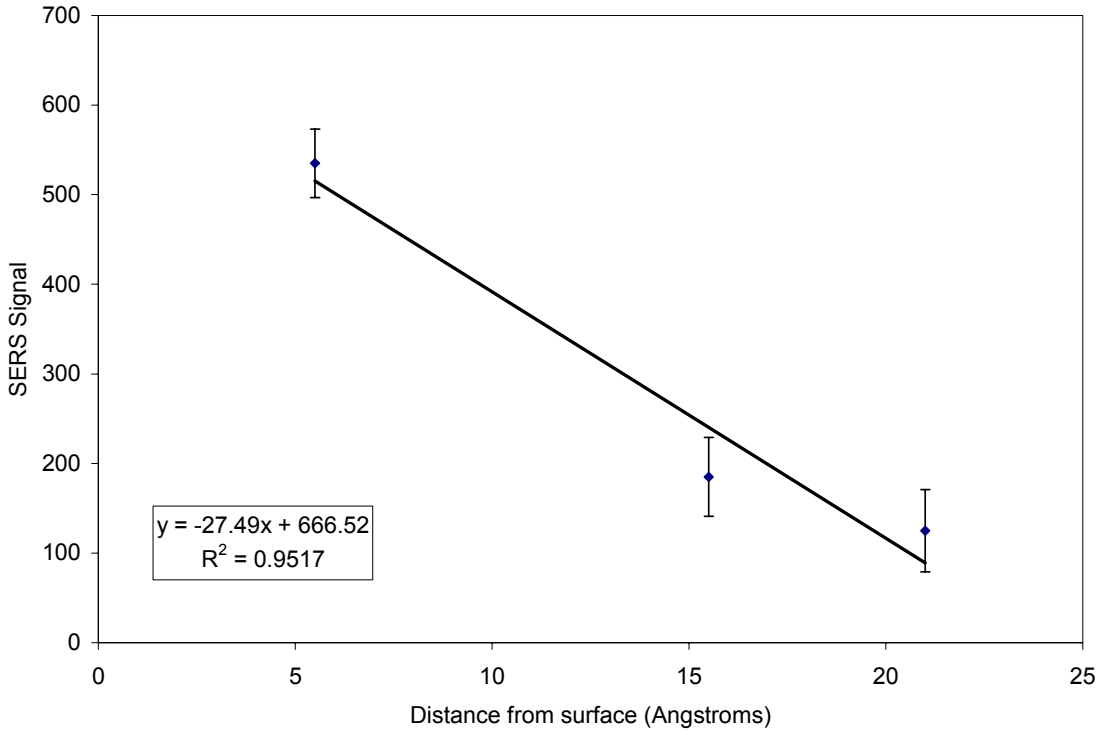

Fig 6.11. Distance dependence of SERS intensity. The system tested had aniline attached to different length alkanethiol SAMS. A linear fit to the data gave the trend line indicated on the graph.

Using the equation 6.2 to describe the SERS intensity:

$$I = a\left(\frac{r - x}{r}\right)^{n} \qquad (6.2)$$

where: a is some scaling factor

r is the radius of the particle

x is the length of the spacer arm (distance from surface)

n is the power for the distance decay

The numerator of equation 6.2 expands to Pascal's Triangle (Figure 6.12), which is as follows:

n=0	1
n=1	1 1
n=2	1 2 1
n=3	1 3 3 1
n=4	1 4 6 4 1
n=5	1 5 10 10 5 1

Fig 6.12. Pascal's Triangle. This triangle represents the expansion of equation of the form $(x-y)^n$. This figure represents the first 5 expansions.

These numbers represent the coefficients of subsequent r and x terms (where the exponent of r decreases as you go from left to right). Since r >> x, we can reduce any of these expansions to first two terms of the form in equation 6.3.

$$r^n + C_2\, r^{(n-1)}x \qquad (6.3)$$

where: C_2 is the second term in the row

By substituting into the general SERS dependence equation, we arrive at equation 6.4.

$$I = a\left(\frac{r^n - C_2 r^{(n-1)}x}{r^n}\right) \qquad (6.4)$$

Which reduces to (equation 6.5):

$$I = a\left(1 - \frac{C_2 x}{r}\right) = a - \frac{aC_2 x}{r} \qquad (6.5)$$

This means that intensity should be linear with x if the system fits this form. Figure 6.11 shows the linear relationship of the data. From the equations described previously, we can see that the y-intercept is "a", and the slope is aC_2/r. From the trend line values for slope and intercept, we conclude that a = 667 and $C_2 = 3.08$ (assuming the particle radius is 75nm, as is true in our system). Referencing back to Pascal's Triangle to arrive at a 3rd order distance dependence for the substrate we are using.

Monolayer stability

Literature indicates that monolayers are unstable in the presence of oxygen [226]. This is due to the reaction of oxygen with sulfur at the metal surface. This causes the formation of sulfates (which no longer bind to the gold surface). To test the stability of the monolayers on proprietary gold nanoshell surfaces made by Nanospectra, we formed standard monolayers of 3-mercaptopropionic acid (3-MPA), 11-mercaptoundecanoic acid (11-MUDA), and 16-mercaptohexadecanoic acid (16-MHDA) and then attached 5-AMF as described above. The result of this analysis can be seen in Figure 6.13.

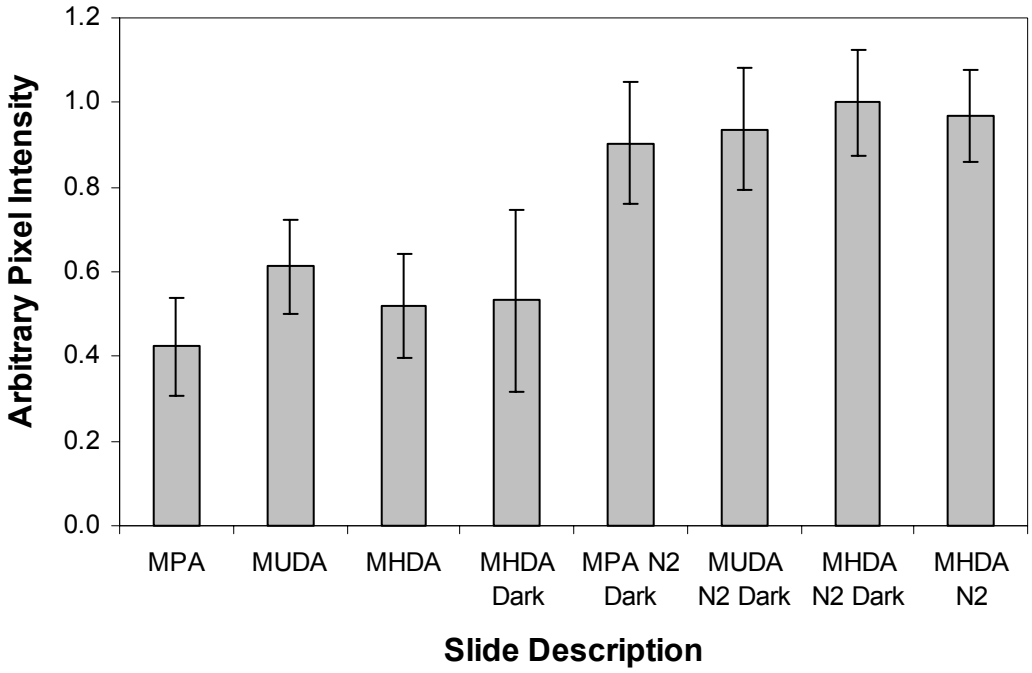

Fig 6.13. 24 hour monolayer degradation study. The surfaces were exposed to both light and air unless otherwise noted. The arbitrary pixel intensity is normalized based on the highest surface signal (MHDA, N_2, Dark). The error bars represent a one standard deviation for the data. All samples have n>10,000. All means are statistically different from one another based on studentized t-tests ($p < 0.00025$).

As seen in Figure 6.13, the signal intensity for all three monolayer types (3, 11 and 16 carbon chains) that fluorescence signal intensity from the attached fluorescein were equivalent at the first measurement within experimental error when stored in nitrogen in the dark. All three monolayers also showed similar loses of surface signal after 24 hours when stored in air in the light, with the fluorescence signal loss ranging from 39% for 11-MUDA to 58% for 3-MPA. Exposure to just light (MHDA, N_2) led to no appreciable degradation of the surface, while exposure to just air (MHDA, Dark) led to similar levels of signal loss and surface degradation as exposure to both nitrogen and

light. These results suggest that the monolayer with fluorescein attached degrades significantly in the presence of air.

Degradation of the fluorescein-SAM was followed as a function of time in both the presence and absence of air, as shown in Figure 6.14.

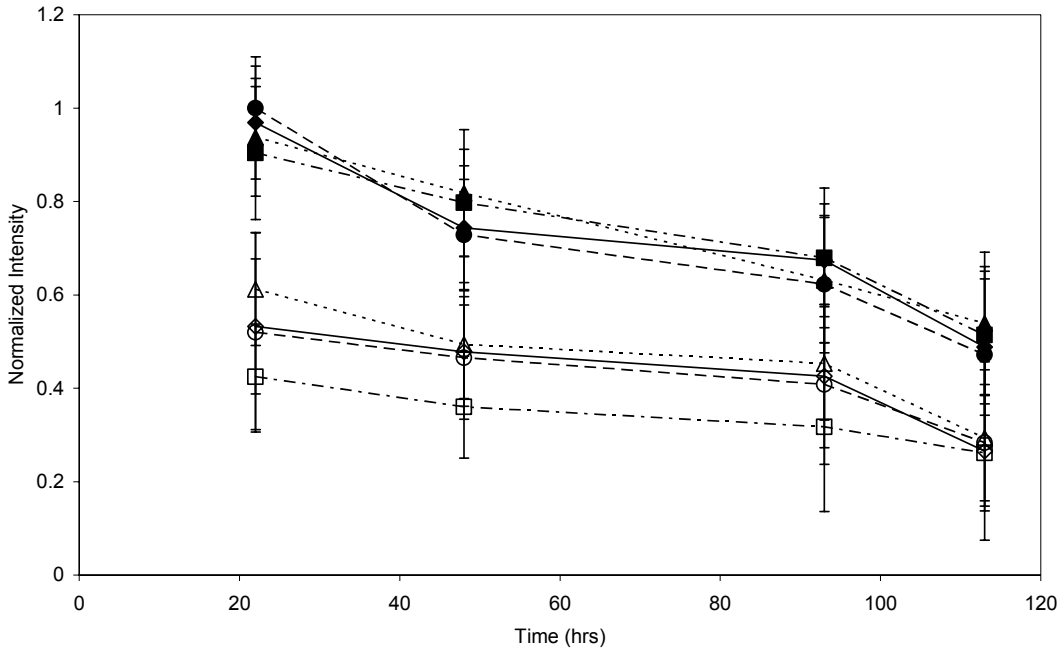

Fig. 6.14. Long term monolayer degradation study. The study was performed by storing in the appropriate environment in between readings. The slides were rinsed and dried before each reading. Open symbols represent slides stored in air and light, and filled symbols represent slides stored in N_2 and dark (unless otherwise noted). The symbols and lines are as follows: filled diamond and solid line, 16-MHDA in light; open diamond and solid line, 16-MHDA in dark; circle and dashed line, 16-MHDA; triangle and dotted line, 11-MUDA; square and broken dashed line, 3-MPA. Error bars represent one standard deviation.

As can be seen from Figure 6.14, all samples stored in similar environments showed similar amounts of degradation with time (within experimental error). This was

determined by analyzing a linear curve fit to the data points. The degradation appears to be zero order indicating the rate is only related to oxygen concentration. Samples that were stored in nitrogen showed similar degradation rates but lower total degradation than those stored in air. This is can be attributed to the fact that 1) the surfaces exposed to air continuously had less surface to lose after 24 hours than those stored in nitrogen and 2) the washing and reading procedures allowed the samples stored in nitrogen to be exposed to air for considerable lengths of time.

While these results clearly indicate that fluorescein labeled monolayers degrade or detach from the gold surface as a function of time, and that degradation, at least initially, is faster in air than in the presence of nitrogen, they do not indicate at what position in the monolayer degradation occurs. Degradation could be at the amide bond where fluorescein was attached to the SAM, or more likely, at the gold surface, where the sulfur attaches to the gold. Others have shown that oxidation occurs at this position [226].

Determination of binding affinity ($K_{A\beta}$) and surface saturation (N_{sat})

After analyzing the monolayer stability, we tested the binding affinity and surface capacity at saturation of different surfaces for β-amyloid. The surfaces tested were as follows: unblocked gold surface, unblocked 11-MUDA monolayer, blocked 11-MUDA monolayer, blocked dendrimer-labeled 11-MUDA monolayer (generations 2.0, 3.0, and 4.0), blocked artificial ganglioside layer, blocked GM_1 ganglioside layer, blocked 4-ATP monolayer, and blocked sialic acid-labeled 4-ATP monolayer. The Langmuir binding isotherm fits to these surfaces can be seen in Figures 6.14-6.17.

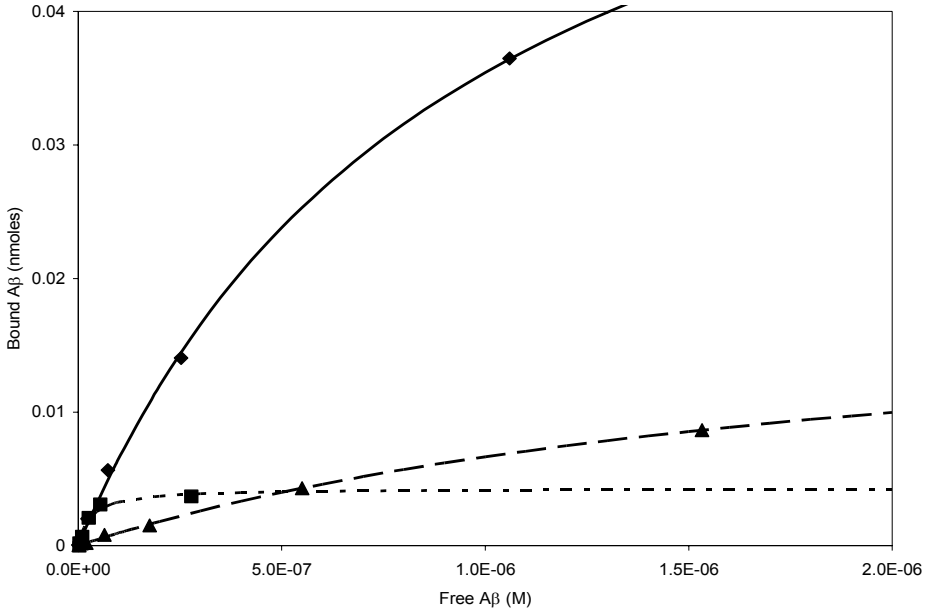

Fig. 6.15. Binding isotherm for unblocked gold, unblocked 11-MUDA, and blocked 11-MUDA. The symbols represent the experimental data, while the lines represent the calculated langmuir isotherms. The symbols and lines are as follows: ♦ and solid line – unblocked gold; ■ and small dashed line – unblocked monolayer; ▲ and large dashed line – blocked monolayer.

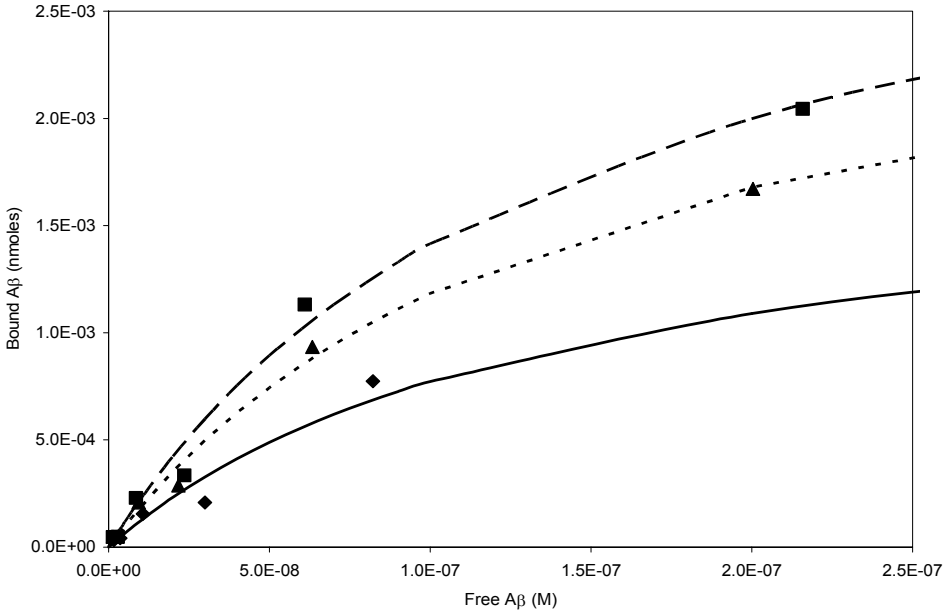

Fig. 6.16. Binding isotherm for blocked 11-MUDA monolayers with dendrimer generations 2.0, 3.0, and 4.0. The symbols represent the experimental data, while the lines represent the calculated langmuir isotherms. The symbols and lines are as follows: ♦ and solid line – generation 2.0; ■ and small dashed line – generation 3.0; ▲ and large dashed line – generation 4.0.

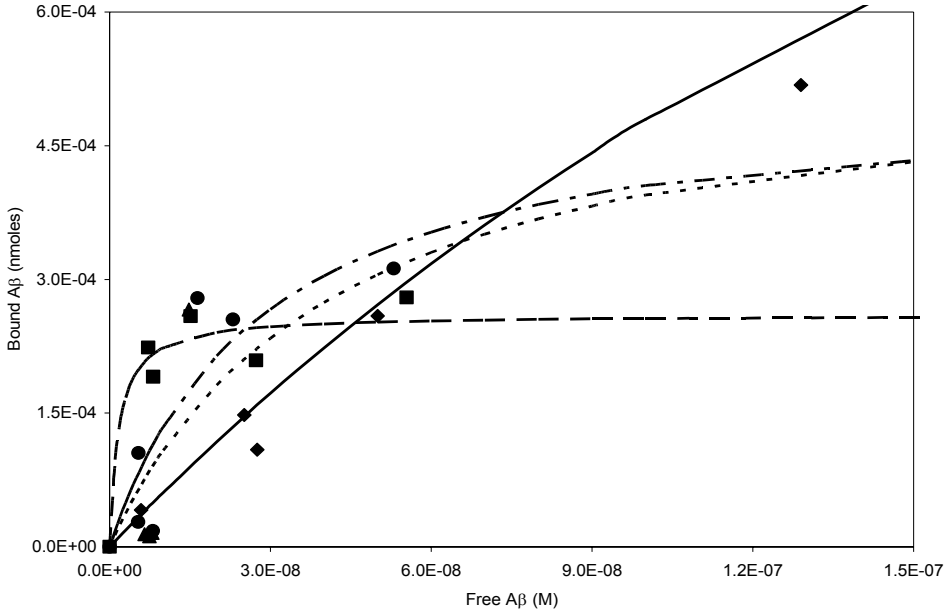

Fig. 6.17. Binding isotherm for blocked 4-ATP monolayers with and without sialic acid attached, GM_1 ganglioside layers, and artificial ganglioside layers. The symbols represent the experimental data, while the lines represent the calculated langmuir isotherms. The symbols and lines are as follows: ♦ and solid line – 4-ATP; ■ and large dashed line – 4-ATP with sialic acid; ▲ and small dashed line – GM_1; ● and slternating dashed line – artificial ganglioside.

From these isotherms, it was possible to obtain values for $K_{A\beta}$ and N_{sat} for each surface. The results can be found in Table 6.1.

Table 6.1. Summary of binding information for different surfaces

Substrate	$K_{A\beta}$ (M^{-1})	N_{sat} (pmoles)
Gold Surface	$1.05 \pm 0.02 \times 10^{6}$	69.3 ± 0.8
11-MUDA	$3.2 \pm 0.3 \times 10^{7}$	4.3 ± 0.2
Blocked 11-MUDA	$5.0 \pm 0.1 \times 10^{5}$	20.0 ± 0.8
Blocked Gen 2.0	$7.2 \pm 0.7 \times 10^{6}$	1.85 ± 0.08
Blocked Gen 3.0	$7.1 \pm 0.5 \times 10^{6}$	3.0 ± 0.1
Blocked Gen 4.0	$6.9 \pm 0.4 \times 10^{6}$	2.89 ± 0.08
Blocked artificial ganglioside	$3.471 \pm 0.001 \times 10^{7}$	0.5222 ± 0.0001
Blocked GM_1 ganglioside	$2.4 \pm 0.8 \times 10^{7}$	0.6 ± 0.1
Blocked 4-ATP	$3.1 \pm 0.3 \times 10^{6}$	2.0 ± 0.4
Blocked sialic acid	$6 \pm 3 \times 10^{8}$	0.261 ± 0.005
Blocked Gen 2.0/SA	$1.01 \pm 0.03 \times 10^{7}$	N/A
Blocked Gen 3.0/SA	$1.1 \pm 0.8 \times 10^{7}$	N/A
Blocked Gen 4.0/SA	$2.5 \pm 0.7 \times 10^{7}$	N/A

95% Confidence intervals for each constant has the same units as the constant to which they apply.

As seen in Figure 6.15 and Table 6.1, the unmodified gold surface was capable of binding the greatest amount of Aβ, approximately 70 pmols, but without specificity. Experiments were done with the unmodified gold surface to determine the upper limit of binding capacity for the system. A comparison of the two 11-MUDA surfaces (blocked and unblocked) shows that the self assembled monolayer has a relatively high binding capacity for Aβ, however, the addition of BSA leads to a 100 fold decrease in binding affinity, suggesting that the binding observed was nonspecific. In preparation of all other binding isotherms, BSA was used to block nonspecific binding.

All three generations of dendrimer show specific binding to Aβ at around a value of $K_{A\beta}$ of 7×10^{6} M (Figure 6.16, Table 6.1). Comparing this to a highly specific molecule, like an antibody ($K = 1 \times 10^{9}$ M), indicates that the dendrimer is approximately two orders of magnitude less specific. This indicates that there is room

for improvement. From patent data, we estimate that the binding affinity of the PAMAM dendrimers for infectious prions to be on the order of 10^8 M^{-1} [227]. Both Aβ and infectious prions form extended β-sheet (amyloid) structures, thus is it possible that binding affinity of the dendrimers may be higher for more aggregated Aβ species.

Also of note is the binding capacity for the dendrimers. Generation 3 and 4 dendrimers have the same binding capacity for Aβ, while generation 2 binds significantly less Aβ at saturation. Given that we infer that the binding of Aβ to the unmodified dendrimers is via electrostatic interactions and the larger generation dendrimers have greater charges, this difference in binding capacity was expected. Similar trends have been shown for oligonucleotides binding to dendrimers via electrostatic interactions [228]. Total binding capacity at saturation may be important in determining limits of detection of Aβ via a SERS based sensor.

A variety of evidence suggests that Aβ binds specifically to gangliosides on the cell surface; therefore we made a number of ganglioside-like surfaces that could be used in our sensor platform. As seen in Figure 6.17 and Table 6.1, all of the sialic acid containing surfaces had greater binding affinity than the surfaces that did not contain sialic acid. Furthermore, as the amount of sialic acid per structure increased, so did the binding affinity (SA > AG > GM_1). This is expected with the sialic acid surface approaching the "perfect" clustered surface. It's possible that by increasing the chain length of the monolayer, we may be able to increase the binding affinity of the surface. Work by Kakio and others [229-231] demonstrated that Aβ has an affinity on the order of

10^6 M^{-1} for GM_1 gangliosides which contain sialic acid residues (an order of magnitude less than what we were able to achieve). Affinity was highest for gangliosides with several sialic acid residues and when the gangliosides were clustered together in cholesterol rich microdomains, with affinity values in excess of 10^7 for tetrasialated gangliosides [231]. These numbers are comparable to what we found when designing the therapeutic dendrimer. As for the artificial ganglioside, it shows a five fold increase in binding affinity over the dendrimer alone and a 3 fold increase in the binding affinity of sialic acid-labeled dendrimer. This indicates that labeling the dendrimer is a step in the right direction, and that increasing the labeling ratio (currently only around 20%) could increase the dendrimer to levels comparable to those of gangliosides. This work is currently being investigated.

Conclusions

Initial investigations indicate that using SERS will work as a sensing system for the detection of β-amyloid. SERS shows both high sensitivity and structural analysis allowing for the determination of the structure of the bound protein. However, the system is going to be dependant upon the size, selectivity, and binding capacity of the recognition molecule being used.

It appears that by labeling the dendrimer with sialic acid, we are able to produce a molecule that is both highly selective for Aβ ($K_{A\beta} > 1 \times 10^7$ M) and closely mimics the cell surface structures (gangliosides). With some further work and turning, the system could prove to be more effective than just using gangliosides or sialic acid monolayers as

recognition molecules (since the dendrimer will effectively increase the surface area for binding.

CHAPTER VII

ATTENUATION OF β-AMYLOID INDUCED TOXICITY BY SIALIC ACID-CONJUGATED DENDRITIC POLYMERS

Overview

Beta-amyloid (Aβ) is the primary protein component of senile plaques in Alzheimer's disease and is believed to be associated with neurotoxicity in the disease. We have shown that Aβ binds with relatively high affinity to clustered sialic acid residues on cell surfaces and propose that artificial sialic acid clusters conjugated to dendritic polymers can compete with clustered sialic acid residues on cell surface gangliosides for Aβ binding. In the current work, we assess the ability of these sialic acid conjugated dendrimers to prevent Aβ toxicity. Flow Cytometry was used to analyze viability of SH-SY5Y neuroblastoma cells and the effects of soluble and clustered Sialic acid mimics on Aβ cell toxicity. Soluble Sialic acid attenuation of Aβ induced toxicity are highly Aβ concentration dependent and less effective at higher concentrations. The clustered Sialic acid mimics are more effective at protecting cells from Aβ toxicity at the higher concentrations of Aβ and looks promising as a possible therapy. This work may lead to and increased understanding of the mechanism of Aβ-sialic acid or ganglioside interaction, which is the first step towards developing therapeutic agents for prevention of Alzheimer's disease.

Introduction

Alzheimer's disease (AD) is the leading cause of neurodegeneration in the United States, affecting approximately 4.5 million Americans in 2003 [232], with an annual cost of care for these individuals estimated at over $100 billion [233]. This study cites figures based on 1991 data, which were updated in the journal's press release to 1994 figures, cited in *2001 – 2002 Alzheimer's Disease Progress Report* [234]. One of the pathological hallmarks of AD is the formation of amyloid plaques in the cerebral cortex, the primary protein component of which is the 39-43 amino acid peptide β-amyloid (Aβ) [235]. Aβ, in a number of aggregated states including fibrils, protofibrils, and spherical oligomers, has been shown to be toxic to neurons and neuron like cells in culture [99, 236, 237]. It is believed that Aβ may play a major role in neurodegeneration associated with AD. To that end, agents which either sequester Aβ or interfere with Aβ interaction/binding to cells have been sought after as a means to reduce the pathological effects of Aβ [97, 101–104].

A variety of evidence indicates that Aβ may bind to cells via an interaction with surface glycolipids or glycoproteins [100, 217, 229, 231, 238-241], and that the affinity of this interaction increases when the gangliosides or sialic acid molecules on the cell surface are clustered [229, 231]. Based on these data, we hypothesized that membrane mimics could be synthesized which would reproduce the clustered sialic acid structure of the cell surface, and therefore compete with the cell surface for Aβ binding. To that end, we prepared sialic acid conjugated dendritic polymers and tested their ability to attenuate Aβ toxicity in a cell culture model. The sialic acid conjugated dendritic polymers were,

in all cases, more effective than polymer alone at reducing Aβ toxicity. Attenuation of Aβ toxicity was achieved at lower concentrations for sialic acid conjugated dendrimers with greater sialic acid functionality when compared to dendrimers with lower sialic acid functionality. These results could have implications for the design of new agents that bind pathogenic Aβ peptides for the treatment of neurodegenerative disease.

Materials and methods

Materials

Aβ(1-40) was purchased from Biosource International (Camarillo, CA). Human neuroblastoma SH-SY5Y cells and rat pheochromaocytoma PC12 cells were purchased from ATCC (Manassas, VA). Cell dissociation buffer and cell culture reagents were purchased from Gibco-Invitrogen (Grand Island, NY). Propidium iodide (PI) was purchased from Molecular Probes (Eugene, OR). Human recombinant nerve growth factor – β (NGF-β), sialic acid (N-Acetylneuraminic acid) and polyamidoamine (PAMAM) dendrimer polymers generation 2.0, 3.0 and 4.0 were purchased from Sigma-Aldrich (St. Louis, MO). 1-Ethyl-3-[3-dimethylaminopropyl]carbodiimide Hydrochloride (EDC) was purchased from Pierce Biotechnology (Rockford, IL). Ultrafiltration membranes were purchased from Millipore (Billerica, MA). All other chemicals were purchased from Sigma-Aldrich.

Peptide preparation

Aβ(1-40) stock solutions were prepared by dissolving the lyophilized peptide in one of two solvents, either 0.1% (vol/vol) trifluoroacetic acid in water or anhydrous dimethyl sulfoxide (DMSO) to make 10 mg/ml stock solutions. After incubating for 30 minutes to 1h at 25^{o}C, the peptide stock solutions were diluted to a concentration of 0.5 mg/ml in sterile phosphate-buffered saline (PBS; 0.01 M NaH_2PO_4, 0.15 M NaCl, pH 7.4) with antibiotics. These solutions were rotated at 25^{o}C for 24 h. These solutions were further diluted to the final concentrations of between 5 and 20 μM in sterile medium and rotated for an additional 24 h prior to being added to cells. Alternatively, stock solutions of Aβ were diluted directly to their final concentrations in sterile cell culture medium and rotated at 25^{o}C for 24 h prior to addition to cells. Both methods of peptide preparation yielded Aβ fibril and other aggregated species containing samples that were consistently toxic to cells in culture culture [242, 243].

Cell culture

For experiments involving free sialic acid, rat pheochromaocytoma PC 12 cells were used. These cells were cultured in RPMI medium supplemented with 10% (vol/vol) horse serum, 5% (vol/vol) fetal bovine serum, 3 mM L-glutamine, 100 U/ml penicillin, 100 μg/ml streptomycin and 2.5 μg/ml amphotericin B (fungizone) in a humidified 5% CO_2/air, 37^{0}C incubator.

For all other experiments, human neuroblastoma SH-SY5Y cells were used. Cells were cultured in a humidified 5% CO_2/air incubator at 37^{o}C in MEM,

supplemented with 10% (vol/vol) fetal bovine serum, 2.2mg/ml NaHCO3, and antibiotics/antifungals at the same concentrations as used with PC12 cells. SH-SY5Y cells were NGF differentiated prior to use in toxicity experiments by addition of 20 ng/mL NGF to cells for 5-7 days.

Synthesis and purification of sialic acid-conjugated dendritic polymers

Sialic acid was conjugated to amine terminated PAMAM dendrimers using EDC chemistry [222]. Sialic acid and EDC were both dissolved in 2mL of DI water to final concentrations of 30 mg/mL (200 mM). This system was allowed to react for 1 h at room temperature. After one hour, dendrimer was added to a final concentration of 2mM. The reaction was then allowed to continue overnight to reach completion. The reaction solution was then ultrafiltered using 1000 NMWL filters using the Millipore Model 8003 Ultrafiltration Stirred Cell to remove unreacted sialic acid and EDC. The reaction mixture was ultrafiltered using six 2 mL washes of DI water, such that the final concentration of free sialic acid in the mixture was less than 6% of the total sialic acid (free and covalently bound to dendrimer). Reduction of sialic acid levels in the washes was verified using UV absorbtion at 250 nm. After purification, the sialic acid conjugated dendrimer was resuspended in DI water for later use. Verification of the presence of sialic acid on dendrimers was done by FT-IR spectroscopy using a ThermoNicolet Avatar 3710 FTIR with Pike Miracle ATR Accessory (Thermo Electron Corporation, Waltham, MA). As seen in Figure 7.1, peaks at 1034 cm^{-1}, 1380 cm^{-1} and

between 2700 cm^{-1} and 3100 cm^{-1} confirm the presence of alcohols and acids consistent was a sugar and loss of primary amines from the reaction of the dendrimer with the acid.

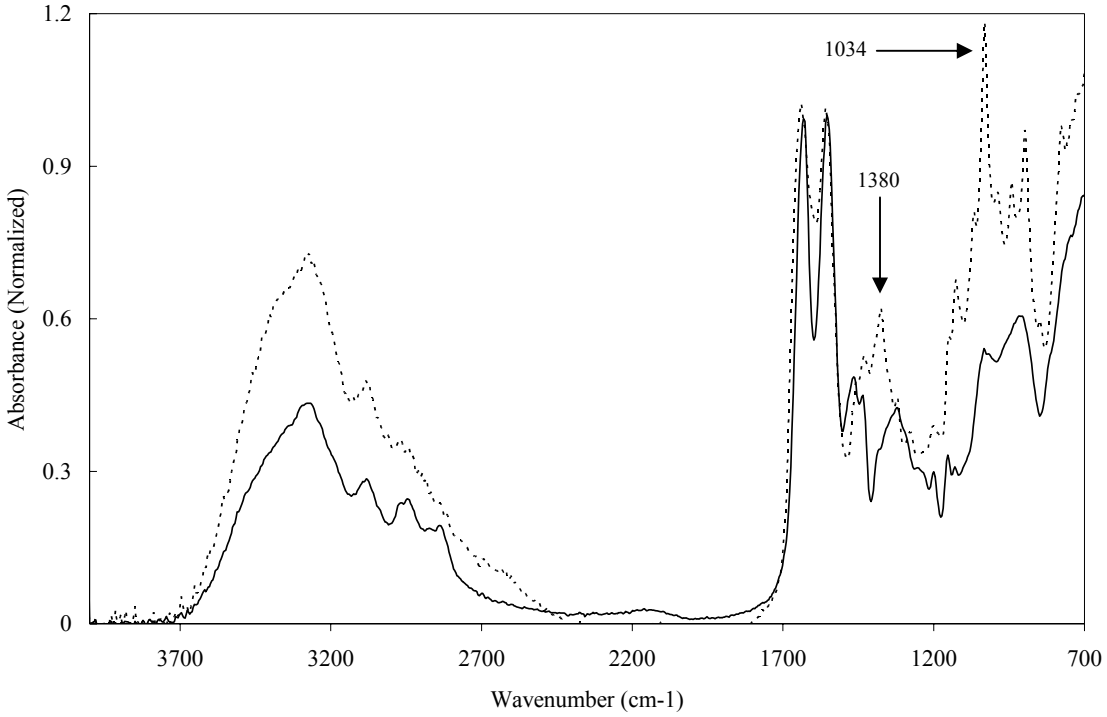

Fig. 7.1. FTIR of conjugated and unconjugated PAMAM dendrimer generation 3.0. The FTIR spectrum of unconjugated dendrimer (solid line) shows a characteristic doublet between 2700 and 3100 cm^{-1} representing the primary amines of the dendrimer termini. For the conjugated dendrimer (dashed line), along with the disappearance of the amine doublet, which indicates a "capping" of the primary amines by sialic acid, there are the appearance of peaks at 1380 and 1034 cm^{-1} from the C-O-C structure and alicyclic alcohols from sialic acid, respectively.

Toxicity assays

MTT assay

PC 12 viability was measured using the MTT (3-(4,5-dimethylthiazol-2-yl)-2,5-diphenyltetrazolium bromide) reduction assay. Viable, redox-active cells reduce MTT to a colored formazan product, the formation of which is generally linearly related to the

concentration of viable cells within the population. For these experiments cells were plated at a density of 10^5 cells/ well in a 96 well plate. After 24 h, the medium in each well was replaced with the Aβ peptide solutions and sialic acid and then incubated for another 24 h at 37^{o}C. MTT was then added to the medium to yield a final concentration of 0.5mg/ml in each well. The cells were allowed to interact with the MTT for 4 h, after which 100 μL of 5:2:3 N,N-dimethylformamide/SDS/water solution (pH 4.7) was added to dissolve the formed formazan crystals. After 18 h in a humidified CO_2 incubator, absorbances were read at 585 nm (Emax Microplate reader,Molecular Devices, Sunnyvale, CA). Percent viability was determined by comparing absorbances for Aβ peptide or peptide-sialic acid treated samples to untreated controls. The fractional increase in viability was estimated as viability of cells treated with both peptide and sialic acid relative to viability of cells just treated with Aβ peptide.

PI assay

SH-SY5Y viability was measured by staining cells with PI, a nucleic acid dye that only binds to cells with permeable membranes, and measuring fluorescence of the cell population using flow cytometry. SH-SY5Y cells were plated at a density of 2 X 10^4 cells/well in 96 well plates and NGF differentiated. After 7 days differentiation, culture medium was replaced with medium containing NGF and the compound to be tested, either Aβ, dendrimer, sialic acid, sialic acid conjugated dendrimer, or a combination of the above. 24 hours after addition of Aβ or other agent, cells were prepared for viability measurement by first detaching cells from the well by incubating

with 150 μL dissociation buffer at 25^0C for 15 minutes. 10 μL of 33 μM PI was added to each well and left to incubate at 25^0C for 20 minutes in the dark after brief shaking. Immediately after, cell fluorescence was measured with the FACSArray Bioanalyzer (Becton-Dickonson, Bedford, MA). Cells were excited with a 532 nm laser and fluorescence was detected using a 564-606 nm filter. Gating was done so as to obtain percentages of the total cell population that were viable. Normalized viability values were obtained by dividing the percentage of viable cells in the sample by that in the control samples with no Aβ or other agent.

Estimation of LD_{50} values and toxicity inhibition parameters.

LD_{50} values, defined here as concentrations of dendrimer or dendrimer sialic acid conjugate that led to a 50% reduction in cell viability, were obtained by linear interpolation of viability as a function of concentration data about the region of 50% viability. The uncertainty of the concentration of dendrimer was estimated by determining the 95% confidence interval of concentration from the viability curves, and using that to determine a coefficient of variation of the measurement.

In order to estimate the toxicity inhibition effects of dendrimers and sialic acid conjugated dendrimers, but also to take into account potential toxicity of the dendrimer constructs we developed the following empirical model (equation 7.1) that correlates the normalized viability (V), defined as the ratio of percentage of viable population in a sample to that in the sample with no Aβ or dendrimer present to the concentration of

sialic acid-conjugated dendrimer in terms of equivalent sialic acid (bound sialic acid (SA)) concentration:

$$V = V_0 + \frac{SA(V_{\max} - V_0)}{SA + K_i} - \frac{k_t SA}{K_i} \qquad (7.1)$$

where V_o is the viability at zero dendrimer-sialic acid complex concentration, V_{max} is the maximum normalized viability, and K_i and k_t are empirical constants associated with sialic acid binding to Aβ (and inhibition of its toxicity), and with the intrinsic toxicity of the dendrimer conjugates, respectively.

It should be noted that this model does not take into account the concentration of Aβ and is therefore valid only for 50 μM Aβ. The data were fitted to the model and constants V_{max} K_i and k_t were estimated using the Levenberg-Marquardt non-linear regression method (Polymath 5.1, CACHE Corporation, Austin, TX)

Results and discussion

Attenuation of Aβ-induced toxicity by free sialic acid

Work from a number of laboratories suggests that Aβ binds to sialic acid containing gangliosides with a moderately high affinity [241, 244-247]. In our lab, we have previously shown that depletion of membrane-associated sialic acid residues or inhibition of sialic acid-containing ganglioside synthesis protects PC 12 cells from Aβ-induced toxicity [217]. Based on these results, we hypothesized that we should be able to inhibit Aβ binding to cells and Aβ toxicity by providing a soluble source of sialic acid in

the culture medium, which would compete with the cell membrane for Aβ binding. As a control, we examined the effects of sialic acid from 0 to 2 or 5 mM on differentiated SH-SY5Y or PC12 cell viability. At these concentration ranges, sialic acid had no effect on cell viability (data not shown). We then examined the ability of free sialic acid to attenuate Aβ toxicity in PC12 cells. As can be seen in Figure 7.2, at the lowest concentration of Aβ used, 5 μM, the cell viability increased as a function of sialic acid dosage, up to a saturation viability level. This protective effect was a strong function of the concentration of Aβ, with little protection offered by the sialic acid for concentrations of Aβ equal to or above 10 μM. There are several probable reasons why free sialic acid did not protect cells from toxicity at high Aβ levels. Based on the viability data shown in Fig. 7.2, a binding affinity of Aβ for free sialic acid can be estimated to be on the order of 10^{-4} M, while Aβ affinity for gangliosides has been estimated to be of the order 10^{-6} M [231, 239] suggesting that even higher concentrations of free sialic acid would be needed to compete with Aβ-ganglioside binding. Moreover, based on stoichiometric arguments, the data indicate that Aβ binds to more than one sialic acid molecule. This interpretation is consistent with findings that Aβ affinity is greatest for gangliosides that are clustered in cholesterol rich microdomains [229].

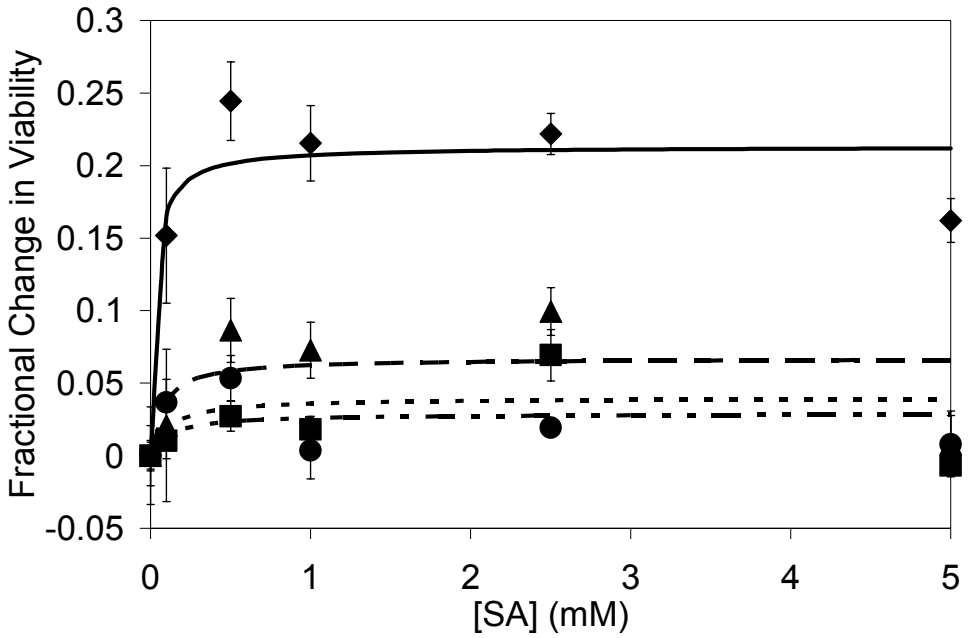

Fig. 7.2. Attenuation of Aβ induced toxicity by free sialic acid. 5 μM Aβ (♦) shows an increase in viability of 30% from control (0 sialic acid) for sialic acid concentrations above 0.5 mM (Tukey, $p < 0.005$). 10 μM (▲), 15 μM (●), and 20 μM (■) show no significant difference from control.

We next synthesized sialic acid containing dendridic polymers of varying size and sialic acid functionality to test if the clustered sialic acid residues presented by these polymers would better protect cells from Aβ toxicity than soluble sialic acid. Others have used similar types of sialic acid modified dendridic polymers to prevent viral adhesion (infection) both *in vitro* and *in vivo* [248-250], suggesting that such a strategy might be fruitful in treating disease.

Dendrimer toxicity

Generation 2.0, 3.0 and 4.0 PAMAM dendrimers were used in our studies. Toxicity of dendrimers at concentrations ranging up to either 250 μM, 125 μM and 130 μM for generation 2.0, 3.0, and 4.0 dendrimers, respectively, were assessed using differentiated SH-SY5Y cells. The LD_{50} values estimated from the results of these experiments are shown in Table 7.1. The intrinsic dendrimer toxicity increased with generation number implying that the toxicity of the dendrimer was related to either molecular weight of the molecule, the number of terminal amine groups, or both. The detrimental influence of dendrimers has been discussed in previous works [248, 251]. We also evaluated the toxicity of the sialic acid-conjugated dendrimers (all generations) in experiments analogous to those performed with unmodified dendrimers. LD_{50} values for the sialic acid modified dendrimers are also shown in Table 7.1.

Table 7.1. LD_{50} values for conjugated and unconjugated dendrimers of different generations

Generation	Unconjugated Dendrimer (μM)	Conjugated Dendrimer (μM)
2.0	50 ± 40	84 ± 17
3.0	10 ± 7	42 ± 14
4.0	1.7 ± 0.2	3.5 ± 1.2

All generations show a decline in intrinsic toxicity upon conjugation with sialic acid. All values are found to be statistically different from all other values (studentized-t, $p < 0.05$).

In all cases, sialic acid modification significantly decreased the toxicity or LD_{50} value of the dendrimer. This result is consistent with work by a number of other groups which showed that polycation toxicity was a strong function of both mass and charge [251,

252] and that increased surface modification of amine terminated dendrimers led to a decrease in their toxicity [248]. Together, these results support the idea that the dendrimer surface charges is one of the factors attributing to intrinsic toxicity.

Attenuation of toxicity of Aβ by dendrimer-SA complexes

In Figure 7.3, we show the effect of unmodified dendrimers and dendrimer-sialic acid conjugates on Aβ toxicity in differentiated SH-SY5Y cells. In all cases, cells were treated with 50 μM Aβ. Increase in cell viability relative to cells just treated with Aβ is plotted. Typical cell viability after 24 hour treatment with 50 μM Aβ as prepared in our laboratory is about 60 %. It can be seen that for generation 2.0, the protective effect of the dendrimer-sialic acid complex increases with concentration up to around 5.5 μM, and then saturates. For generation 3.0, the protective effect increases with dendrimer-sialic acid complex concentration up to 11 μM and then starts to decrease. For generation 4.0, the protective effect increases up to a concentration of about 1.5μM and then decreases rapidly. This phenomenon of decreasing protection at the higher concentrations of dendrimer, especially for the higher generation dendrimer, may be explained by the relatively high intrinsic toxicity of the generation 3.0 and 4.0 dendrimers. It should be noted that for the unconjugated dendrimers, there is significant protection exhibited against Aβ toxicity. However, upon sialic acid-conjugation, the protection levels increase by up to 200%.

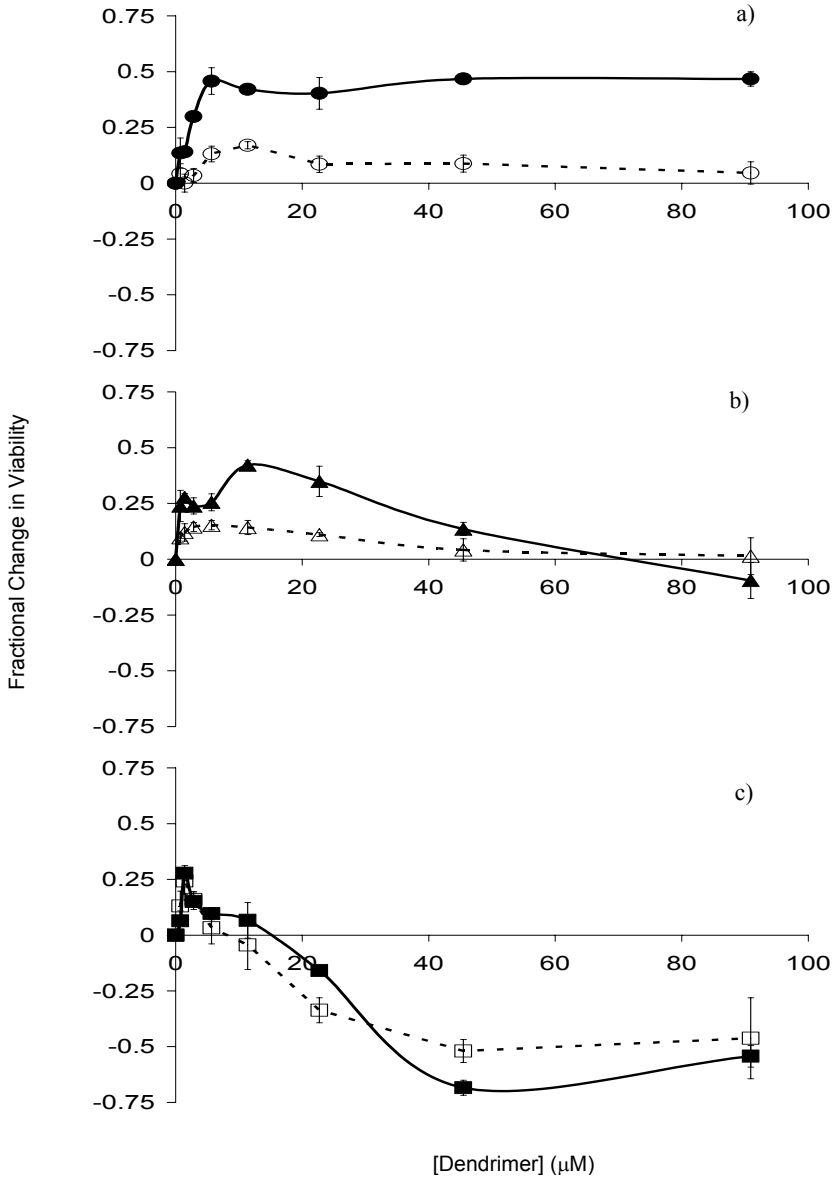

Fig 7.3. Attenuation of Aβ toxicity by conjugated and unconjugated dendritic compounds of different generations. a) Conjugated (solid line, filled) generation 2.0 shows a substantial increase in protection compared to unconjugated dendrimer(dashed line, open). While for generations 3.0 (b) and 4.0 (c), there is an initial improvement in protection followed by a waning at higher concentrations.

This small protective interaction of the unconjugated dendrimer is not surprising. It has been suggested that cell surface binding of Aβ is dictated by electrostatic

interactions, and preventing these interactions decreases Aβ toxicity [97]. We suggest that both forms of the dendrimer (conjugated and unconjugated) protect cells from Aβ toxicity in different ways. The presence of the primary amines and large positive surface charge on the unconjugated dendrimer leads to an electrostatic interaction of the dendrimer with the negatively charged cell membrane, preventing the Aβ from binding and, therefore, blocking toxicity. Unfortunately, this dendrimer interaction with the cell surface can lead to cell death, as found here and in Fischer et. al. [251]. Conversely, we postulate that the conjugated dendrimer prevents the interaction of Aβ with the cell surface not by blocking the cell surface, but by sequestering the Aβ.

Efficiences of the different generations of dendrimer-sialic acid complexes

Taking into account both the protectiveness and intrinsic toxicity of conjugated polymers, we developed an empirical model that correlates the normalized viability provided by modified and unmodified dendrimers for Aβ treated cells. Two constants were obtained from fitting the model to the experimental data shown in Figure 7.3, K_i, which represents the inhibition by the sialic acid containing dendrimer of Aβ toxicity, and k_t, which represents the intrinsic toxicity of the dendrimer conjugate. Table 7.2 shows the constants K_i and k_t of this model for the different generations of sialic acid-conjugated dendrimer.

Table 7.2. Model constants for different generations of sialic acid-conjugated dendrimers

Generation	K_i (μM)	k_t (μM)
2.0	33.06 ± 0.17	$0.45 \pm 0.013 \times 10^{-3}$
3.0	14.64 ± 0.04	$2.89 \pm 0.008 \times 10^{-6}$
4.0	13.36 ± 0.20	$18.0 \pm 0.3 \times 10^{-3}$

The binding constant, K_i, decreases with increasing generation number, indicating greater binding affinity for Aβ. The toxicity constant, k_t, increases by an order of magnitude with each increase in generation number. Model fits showed R^2 values of 0.93, 0.86, and 0.96 for generations 2,3, and 4, respectively. All values reported represent a 95% confidence interval. Statistical differences of K_i and k_t of different generations are found to be significant ($p < 0.0001$).

It is clear that the protective property constant K_i decreases with increase in generation number, indicating that generation 4.0 is more efficient than generation 3.0, which in turn is more efficient than generation 2.0 at protecting cells from Aβ toxicity. K_i was estimated per mole equivalent sialic acid, not per mole dendrimer. If estimated per mole dendrimer, Ki values would vary from approximately 2 μM, 0.5 μM and 0.2 μM for generations 2.0, 3.0 and 4.0 sialic acid modified dendrimers, respectively, further accentuating the significance of the differences in toxicity attenuation properties of the different generation dendrimer constructs. However, on examination of the k_t values, it is evident that generation 4.0 is an order of magnitude more toxic than generation 3.0, which is another order of magnitude more toxic than generation 2.0. This explains why the increase in viability by the generation 2.0 complex saturates, while the increase in viability by the generation 3.0 and 4.0 complexes decreases at higher concentrations up to the extent that no protection is observed.

One plausible reason as to why clusters of sialic acid are more efficient than free sialic acid molecules in protecting cells from Aβ induced toxicity is that the clustered

sialic acid compounds more closely mimic cell surface gangliosides. It has been shown that Aβ binds with highest affinity to gangliosides that either contain multiple sialic acid residues or that are clustered in cholesterol rich membranes [229, 231]. Also, clustering sialic acid greatly improves the probability of interaction between clustered sialic acids "tethered" to the already bound sialic acid molecule and virial particles [248, 250, 253]. Similar phenomena probably occur during Aβ sialic acid dendrimer interactions. Finally, unlike free sialic acid, clustered sialic acid molecules are more stable and are not vulnerable to enzymatic breakdown when exposed to biological fluids [248].

To date, there have been many attempts at developing either a prevention or cure for AD, each involving different stages of pathogenesis. Strategies which alter APP processing and thereby reduce formation of Aβ have had some success in animal models at reducing Aβ(1-40) levels, but have not been without some significant limitations [253, 254]. Agents which prevent Aβ aggregation and/or reverse fibril formation have had success *in vitro* and have potential as *in vivo* therapeutics [230, 255, 256]. Immunotherapies involving clearance of aggregated Aβ showed early promise in both animal models and humans, but are currently associated with unacceptable side effects [101-103]. However, there is evidence that agents which sequester Aβ in the plasma may actually be effective at reducing Aβ levels in the cortex and may have the potential of reducing cognitive decline associated with disease [104, 257]. These studies suggest that sialic acid based molecules that have a high affinity for Aβ such as the ones we describe here may contribute to the array of therapeutic agents being developed for treatment of AD.

Conclusions

It is clear that interactions between Aβ and membrane-bound sialic acid play an important role in neurotoxicity, and it is possible that by introducing sialic acid for direct competition with the cell surface, the neurotoxic effects of Aβ can be mitigated. Moreover, by clustering sialic acid residues, we can more closely mimic cell surfaces to create improve competition efficiency. The results from all three dendrimer generations tested support these claims. The findings encourage further investigation into the development of biomimetic compounds for use in prevention of Aβ toxicity.

CHAPTER VIII

DEVELOPMENT OF NOVEL SIALIC ACID LABELED DENDRIMERS AS A POSSIBLE THERAPEUTIC TOOL FOR THE PREVENTION OF β-AMYLOID TOXICITY ASSOCIATED WITH ALZHEIMER'S DISEASE

Introduction

As previously discussed, Alzheimer's disease (AD) is the leading cause of neurodegeneration in the United States, affecting approximately 4.5 million Americans in 2003 [232], with an annual cost of care for these individuals estimated at over $100 billion [233]. With the cause of the neurotoxicity being linked to to the presence of Aβ fibrils [99, 235 - 237], we propose that by targeting these fibrils, we can prevent toxicity via sequestering these fibrils. This technique has been demonstrated by previous work [97, 101-104], but little has been done to make these sequestering agents more biomimetic. It is this area we look to explore.

A variety of evidence indicates that Aβ may bind to cells via an interaction with surface glycolipids or glycoproteins with increased binding occurring in the presence of gangliosides or other sialic acid containing molecules that cluster the sialic acids [100, 217, 229, 231, 238-241]. Based on these data, we hypothesized that membrane mimics could be synthesized which would reproduce the clustered sialic acid structure of the cell surface, and therefore compete with the cell surface for Aβ binding. It is this work that we will discuss.

Materials and methods

Materials

All materials purchased from Sigma Aldrich Corporation (St. Louis, MO).

Dendrimer labeling - acetylation of sialic acid (compound 1)

The acetyl protection was performed by first dissolving 250 mg of NANA in 10 mL of pyridine. To this solution was added 537 mg (497 uL) of acetic anhydride and 37 mg of 4-(dimethylamino)pyridine (DMAP). The solution was reacted at room temperature for 3 hours. After 3 hours, a 1 mL solution of hydrazine acetate in dimethyl formamide (DMF) was added to the pyridine solution. The mixture was reacted at 55^{o}C for 15 min. A 1 mL volume of trichloroacetonitrile and 45.3 uL of 1,8-diazabicyclo[5.4.0]undec-7-ene (DBU) were then added, and the system was reacted at 0^{o}C for 1.5 hours. The final solution was stored at -80^{o}C until used. This procedure was adapted from Ren et al. [258].

Dendrimer labeling – production of 2-(2-isothiocyanatoethoxy ethanol) (compound 2)

A solution containing 700 uL of 2-(2-aminoethoxy)ethanol and 2 mL of triethylamine in 10 mL of chloroform was added slowly over the course of an hour to a stirred solution containing 540 uL of thiophosgene in 40 mL of chloroform. The solvent was removed *in vacuo*. The resulting residue was dissolved in 10 mL of deionized water. A two-step extraction was performed using two 10 mL volumes of dichloromethane. The organic phases from the extraction were combined and washed

twice with deionized water (2 x 10 mL). The organic layer was then dried over magnesium sulfate and filtered. The solvent was removed *in vacuo*. The resulting yellowish oil was stored at -80^{o}C until used. This procedure was adapted from Woller et al. [259, 260].

Dendrimer labeling – attachment of compound 2 to dendrimer (compound 3)

A 100 uL solution of generation 4.0 polyamidoamine (PAMAM) (0.57 μmol of dendrimer) was evaporated under reduced pressure. The resulting residue was dissolved in 5 mL of dimethyl sulfoxide (DMSO). A ten-fold molar excess of compound 2 was added to the DMSO mixture (this excess is based on the number of terminal amines available on the dendrimer and not the amount of dendrimer). The solution was reacted at room temperature for 8 hours. The solvent was removed *in vacuo.* This procedure was adapted from Woller et al. [259, 260].

Dendrimer labeling – attachment of sialic acid (compound 4)

The residue of compound 3 was dissolved in 20 mL of dichloromethane with 10 mg of 4Å molecular sieves under nitrogen. To the solution, 50 μmoles (1 mL) of compound 1 and 200uL boron trifluoride-diethyl etherate was added slowly. The solution was reacted at room temperature for 7 hours. Sodium bicarbonate (100 mg) was added to the solution, and the solution was filtered over celite. The solvent was removed *in vacuo*. The resulting compound was stored at -80^{o}C until used. This procedure was adapted from Woller et al. [259, 260].

Dendrimer labeling – deprotection of sialic acid

Compound 4 was dissolved in 20 mL of a methanol/deionized water mixture (1:1). Methanolic base (1 M, 180 uL) was added, and the solution was mixed overnight until all solid was dissolved. The solution was neutralized with Amberlite IR-120 and filtered using a glass filter. The solvent was removed *in vacuo*. The resulting residue was dissolved in deionized water, and purified using 10 kDa centrifuge filter units. The resulting solution was stored at 4^{o}C until used. This procedure was adapted from Woller et al. [259, 260].

Determination of sialic acid labeling

The extent of sialic acid labeling was determined using the procedure described by Warren [261] with minor modifications. As opposed to stopping the reaction, we just cooled the samples under tap water, centrifuged, and read. This step was performed after FTIR verification of sialic acid attachment to the dendrimer.

Results and discussion

FTIR analysis of dendrimer-sialic acid compound

Using standard FTIR techniques, an evaporated sample of the dendrimer-sialic acid compound was analyzed for characteristic peaks. The results of this analysis can be found in Figure 8.1

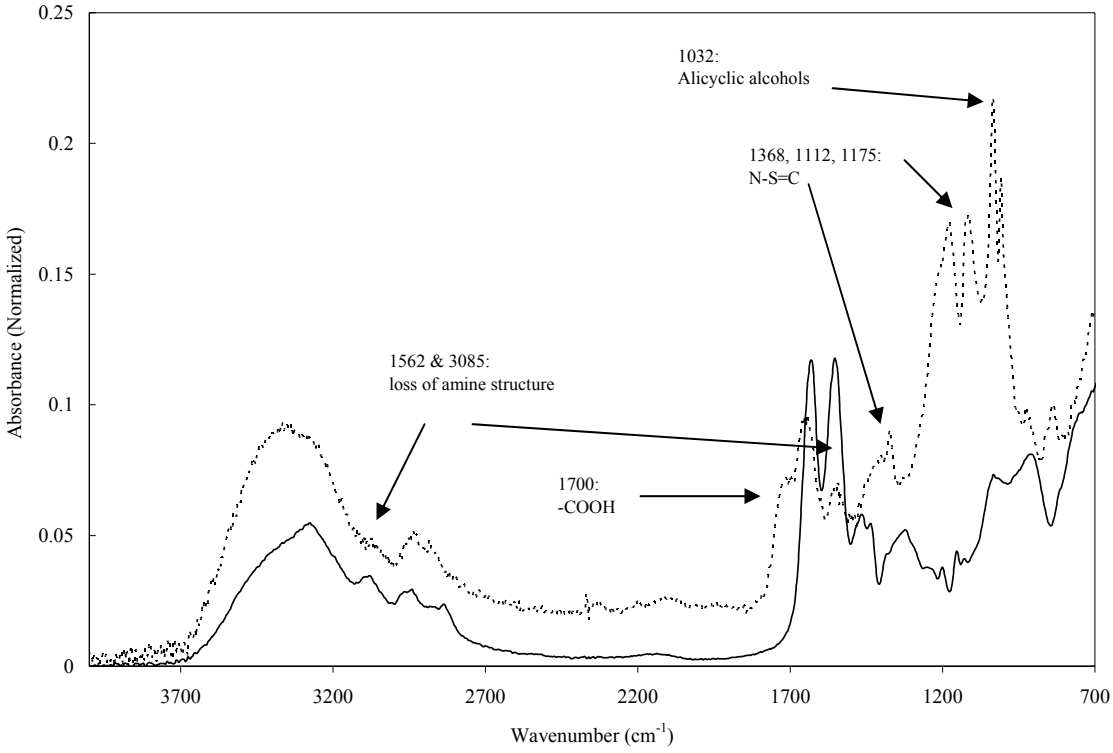

Fig 8.1. FTIR analysis of sialic acid-labeled dendrimer. The solid line represents generation 4.0 dendrimer. The dashed line represent the sialic acid-labeled dendrimer. The peaks of interest are as follows: 1562 & 3085 – loss of primary amines in the dendrimer; 1700 – presence of carboxylic acids from the sialic acid; 1112, 1175 & 1368 – formation of thiourea structure; 1032 – alicyclic alcohols from sialic acid.

From the FTIR analysis, it is apparent by the presence of certain characteristic structures (thiourea, carboxylic acids, and alicyclic alcohols) and the loss of other peaks (amine structure loss) that the chemistry was successful. Determination of sialic acid labeling via the Warren assay indicates that we have complete labeling. This is commensurate with what has been found by others [259, 260].

Initial studies with the new sialic acid-labeled dendrimer indicate that is has higher protective properties than those produced through EDC chemistry (Chapter VII).

Furthermore, the protection curves indicate that the binding is via a different mechanism. However, there is currently not enough data to make any definitive statements.

Conclusions

If the preliminary data holds up, then this is an indication that both the labeling amount and sialic acid confirmation influence the binding properties of these dendrimers to Aβ. Based on the work presented in Chapter VII, it would be useful to analyze other generations of dendrimers for similar characteristics and less intrinsic toxicity. Eventually, it would be necessary to address the ability of the compound to pass the blood-brain barrier, but this is a distant concern.

CHAPTER IX

CONCLUSIONS

This project has tied together many different aspects important to sensor design. First, we utilized standard kinetic and spectroscopic principles to develop models that could be use for general sensor design. We then successfully applied these principles and results of the modeling toward several different biomedically relevant sensing platforms and targets. We have proven the flexibility and robustness of the systems we have developed and laid the ground work for substantial future work in the area.

We were successful in using a commercially available antibody for the development of a prion sensor. Through experimental and theoretical analysis, we determined that the detection limits for the prion sensor, or any competitive sensor, are always dictated by the equilibrium bind coefficient. Regardless of how the system model was modified, these limitations always applied. We realized that to achieve lower detection limits, we would have to develop a direct sensing method.

Using what we learned from the prion sensor, we worked at developing a direct sensor for Aβ using SERS as the detection method. With the strong distance dependence of SERS, we had to develop a recognition molecule that was smaller than an antibody, but still maintained high specificity. We accomplished this by creating sialic acid-labeled materials. These materials included sialic acid-labeled monolayers, ganglioside and artificial ganglioside monolayers, and sialic acid-labeled dendrimers.

The latter structures were developed to more closely mimic biological structures. We found that as the number of sialic acids increased, so did the binding affinity of Aβ. We demonstrated the feasibility of using these materials in a sensing platform. We also tested the use of some of these materials *in vitro* toxicity studies to examine is such materials could protect cells from Aβ toxicity. While the sialic acid labeled dendrimers could prevent Aβ neurotoxicity at low concentrations, there use was limited by their toxicity at high concentrations.

With success from the first attempts with sialic acid attachment, we investigated the issue of sialic acid conformation (to more closely mimic biological arrangement). Using an adaptation of techniques developed by synthetic chemists, we successfully altered the conformation of sialic acid attachment to more closely mimic that found in gangliosides and other biological molecules. Furthermore, this altered attachment showed substantially greater protective properties than the simpler attachment used previously to attenuate Aβ neurotoxicity. These materials may be useful as therapeutics for Alzheimer's disease treatment.

I feel this project demonstrates a firm understanding of material design, analysis and application techniques. It incorporates a broad base of knowledge form several disciplines (biomedical engineering, biochemical engineering, material science, food engineering, and optical design). It is this cross-disciplinary work that lends itself to successful expansion of the field of biosensors.

Future Work

As with any project, there is always more you wished you could have done, but time is always a limitation. I feel that all the work I have done has laid the groundwork for many advances.

For the prion sensor, the background and design principles have been investigated.. A working platform has been developed, but there is substantial room for optimization. The sensor, as it currently stands, is not selective for infectious prion only. By altering the recognition unit to an antibody that targets only infectious prion, this can be addressed. Furthermore, by altering the fluorophore that is used, we could improve the signaling capability of the sensor by selecting a fluorophore appropriate for the system we are working with (high quantum efficiency for quenching, low quantum efficiency for enhancement). Finally, we need to address the response of the system with actually sample. This may require some adjustments for sample pretreatment, fluorophore detection, and antibody selection, just to name a few. I intend to pursue this in my future works.

With the OPH sensor, we have been more successful in understanding the shortcomings of the systems than in determining its strengths. However, this leaves the project wide open for possible advancements. Based on the modeling the results, the system shows a lot of promise, but due to budgetary constraints, time constraints, and experimental complications, this promise has not come to fruition. I hope to do further investigations in enzymatic sensors in the future.

Finally, the work in detection and treatment of Alzheimer's disease (via Aβ interaction) has shown tremendous potential. All indications are that sialic acid interaction with Aβ is highly successful and well thought out. With trends in our data indicating that increased clustering of sialic acid being more effective, we definitely appear to be heading in the right direction. However, I propose that there are other molecules outside gangliosides that may be influencing the binding of Aβ (neuronal cell adhesion molecule (NCAM)).

Additionally, this project has addressed the use of SERS as a sensing platform in a way the previously had not been attempted. In combination with our foray into synthetic chemistry, I feel this project significantly demonstrates the importance of looking beyond your current boundaries and knowledge. With the success of initial experiments in this project, I believe that this system could have major impacts on both diagnosis and treatment of Alzheimer's disease.

REFERENCES

[1] J. Chow, N.N. Dingra, E. Baker, B.C. Helmly, D.A. Nivens, W.E. Lynch, Nanoparticle mediated photodefluorination monitored by ^{19}F NMR, J. Photochem. Photobio. A 173 (2005) 156-160.

[2] Y. Liu, Z. Liu, Y. Yang, H. Yang, G. Shen R. Yu, Simple synthesis of $MgFe_2O_4$ nanoparticles as gas sensing materials, Sensors and Actuators B 107 (2005) 600-604.

[3] A. Salomonsson, S. Roy, C. Aulin, J. Cerdà, P. Käll, L. Ojamäe, M. Strand, M. Sanati, A.L. Spetz, Nanoparticles for long-term stable, more selective MISiCFET gas sensors, Sensors and Actuators B 107 (2005) 831-838.

[4] O. Bomatí-Miguel, M.P. Morales, P. Tartaj, J. Ruiz-Cabello, P. Bonville, M. Santos, X. Zhao, S. Veintemillas-Verdaguer, Fe-based nanoparticulate metallic alloys as contrast agents for magnetic resonance imaging, Biomaterials 26 (2005) 5695-5703.

[5] A. Valanne, S. Huopalahti, T. Soukka, R. Vainionpää, T. Lövgren, H. Härmä, A sensitive adenovirus immunoassay as a model for using nanoparticle label technology in virus diagnostics, J. Clin. Vir. 33 (2005) 217-223.

[6] G. Tosi, F. Rivasi, F. Gandolfi, L. Costantino, M.A. Vandelli, F. Forni, Conjugated poly(D,L-lactide-co-glycolide) for the preparation of in vivo detectable nanoparticles, Biomaterials 26 (2005) 4189-4195.

[7] T. Green-Sadan, Y. Kuttner, T. Lublin-Tennenbaum, N. Kinor, Y. Boguslavsky, S. Margel, G. Yadid, Glial cell line-derived neurotrophic factor-conjugated nanoparticles suppress acquisition of cocaine self-administration in rats, Exp. Neuro. 194 (2005) 97-105.

[8] J.K. Kretsinger, L.A. Haines, B. Ozbas, D.J. Pochan, J.P. Schneider, Cytocompatibility of self-assembled β-hairpin peptide hydrogel surfaces, Biomaterials 26 (2005) 5177-5186.

[9] M.A. Lan, C.A. Gersbach, K.E. Michael, B.G. Keselowsky, A.J. García, Myoblast proliferation and differentiation on fibronectin-coated self assembled monolayers presenting different surface chemistries, Biomaterials 26 (2005) 4523-4531.

[10] H. Tian, C. Deng, H. Lin, J. Sun, M. Deng, X. Chen, X. Jing, Biodegradable cationic PEG–PEI–PBLG hyperbranched block copolymer: Synthesis and micelle characterization, Biomaterials 26 (2005) 4209-4217.

[11] B. Menz, R. Knerr, A. Göpferich, C. Steinem, Impedance and QCM analysis of the protein resistance of self-assembled PEGylated alkanethiol layers on gold, Biomaterials 26 (2005) 4237-4243.

[12] J.N. Ding, P.L. Wong, J.C. Yang, Friction and fracture properties of polysilicon coated with self-assembled monolayers, Wear (In Press).

[13] M.E. Anderson, C. Srinivasan, R. Jayaraman, P.S. Weiss, M.W. Horn, Utilizing self-assembled multilayers in lithographic processing for nanostructure fabrication: Initial evaluation of the electrical integrity of nanogaps, Microelec. Eng. 78-79 (2005) 248-252.

[14] X. Ju, M. Kurahashi, T. Suzuki, Y. Yamauchi, Fabrication of a gold pattern with a nanoscale edge by using heptanethiol self-assembled monolayers and a metastable helium beam, App. Surf. Sci. 241 (2005) 241-245.

[15] J. Xin, K. Mitsunori, S. Taku, Y. Yasushi, Positive and negative patterning of ethanethiol, decanethiol, and hexadecanethiol self-assembled monolayers by using a metastable helium beam, Thin Solid Films 464-465 (2004) 420-424.

[16] R.K. Smith, P.A. Lewis, P.S. Weiss, Patterning self-assembled monolayers, Prog. Surf. Sci. 75 (2004) 1-68.

[17] K.V. Gobi, C. Kataoka, N. Miura, Surface plasmon resonance detection of endocrine disruptors using immunoprobes based on self-assembled monolayers, Sensors and Actuators B 108 (2005) 784-790.

[18] B.D. Gupta, A.K. Sharma, Sensitivity evaluation of a multi-layered surface plasmon resonance-based fiber optic sensor: A theoretical study, Sensors and Actuators B 107 (2005) 40-46.

[19] R. Rella, J. Spadavecchia, M.G. Manera, P. Siciliano, A. Santino, G. Mita, Liquid phase SPR imaging experiments for biosensors applications, Biosens. Bioelectron. 20 (2004) 1140-1148.

[20] W. Lee, D. Lee, B. Oh, W. Lee, J. Choi, Nanoscale fabrication of protein A on self-assembled monolayer and its application to surface plasmon resonance immunosensor, Enzyme Microb. Tech. 35 (2004) 678-682.

[21] S.H. Choi, J.W. Lee, S.J. Sim, Enhancement of the sensitivity of surface plasmon resonance (SPR) immunosensor for the detection of anti-GAD antibody by changing the pH for streptavidin immobilization, Enzyme Microb. Tech. 35 (2004) 683-687.

[22] S.H. Choi, J.W. Lee, S.J. Sim, Enhanced performance of a surface plasmon resonance immunosensor for detecting Ab–GAD antibody based on the modified self-assembled monolayers, Biosens. Bioelectron. (In Press).

[23] S. Kim, H. Suh, K. Koh, S. Suck, H. Choi, H. Kim, Surface plasmon resonance study on the interaction of photochromic spironaphthoxazine with L-phenylalanine in self-assembled monolayers on gold, Dyes and Pigments 62 (2004) 93-97.

[24] J. Lakowicz, I. Gryczynski, Z. Gryczynski, K. Nowaczyk, C. Murphy, Time resolved spectral observations of cadmium enriched cadmium sulfide nanoparticles and the effect of DNA oligomer binding, Anal. Biochem. 280 (2000) 128-136.

[25] W. Chan, S. Nie, Quantum dot bioconjugates for ultrasensitvie isotopic detection, Science 281 (1998) 2016-2018.

[26] A. Valanne, H. Lindroos, T. Lövgren, T. Soukka, A novel homogeneous assay format utilising proximity dependent fluorescence energy transfer between particulate labels, Anal. Chim. Acta 539 (2005) 251-256.

[27] K. Sokolov, G. Chumanov, T. Cotton, Enhancement of molecular fluorescence near the surface of colloidal metal films, Anal. Chem. 70 (1998) 3898-3905.

[28] T. Schalkhammer, F.R. Aussenegg, A. Leitner, H. Brunner, G. Hawa, C. Lobmaier, F. Pittner, Ion channels in artificial bolaamphiphilic membranes deposited on sensor chips - optical detection in an ion channel based biosensor, SPIE 2976 (1997) 129-136.

[29] J. Kummerlen, A. Leitner, H. Brunner, F.R. Aussennegg, A. Wokaun, Enhanced dye fluorescence over silver island films: Analysis of the distance dependence, Molecular Physics 80 (1993) 1031-1046.

[30] A.P. Silverman, E.T. Kool, Quenched probes for highly specific detection of cellular RNAs, Trends Biotech. 23 (2005) 225-230.

[31] S.D. Pas, S. Noppornpanth, A.A. van der Eijk, R.A. de Man, H.G.M. Niesters, Quantification of the newly detected lamivudine resistant YSDD variants of

Hepatitis B virus using molecular beacons, J. Clin. Vir. 32 (2005) 166-172.

[32] P. Manna, K. Grantham, S. Reddy, R. Nath, J. Dalal, Detection and quantitative Candida load monitoring using molecular beacon probe, Biol. Blood Marrow Trans. 11 (2005) 73-74.

[33] W. Tan, K. Wang, T.J. Drake, Molecular beacons, Curr. Opin. Chem. Biol. 8 (2004) 547-553.

[34] G. Yao, W. Tan, Molecular-beacon-based array for sensitive DNA analysis, Anal. Biochem. 331 (2004) 216-223.

[35] J.G.S. Lopes, P.S. Santos, The SERS spectrum of 1,2-diaminoanthraquinone studied on silver colloid, J. Mol. Struct. 744-747 (2005) 75-78.

[36] J.L. Castro, M.R. López-Ramírez, J.F. Arenas, J.C. Otero, Surface-enhanced Raman scattering of tartaric and malic acids adsorbed on silver colloids, Vib. Spec. (In Press).

[37] S. Choi, H. Park, Surface-enhanced Raman scattering (SERS) spectra of sodium benzoate and 4-picoline in Ag colloids prepared by γ-irradiation, App. Surf. Sci. 243 (2005) 76-81.

[38] E.A.C Flores, M.M.C Vallette, R.E.C. Clavijo, P. Leyton, G. Díaz, F. Koch, R. Koch, SERS spectrum and DFT calculations of 6-nitrochrysene on silver islands, Vib. Spec. 37 (2005) 153-160.

[39] R. Wen, Y. Fang, Adsorption of pyridine carboxylic acids on silver surface investigated by potential-dependent SERS, Vib. Spec. (In Press).

[40] A. M. Polubotko, Some anomalies in the regularities of the SER spectra of benzene and hexafluorobenzene, App. Surf. Sci. 239 (2005) 387-393.

[41] I. Lundstrom, Real-time biospecic interaction analysis, Biosens. Bioelectron. 9 (1994) 725.

[42] R.J. Green, R.A. Frazier, K.M. Shakeshe, M.C. Davies, C.J. Roberts, S.J.B. Tendler, Surface plasmon resonance analysis of dynamic biological interactions with biomaterials, Biomaterials 21 (2000) 1823.

[43] K. Matsubara, S. Kawata, S. Minami, A compact surface plasmon resonance sensor for water in process, Appl. Spectrosc. 42 (1988) 1375.

[44] J.R. Lakowicz, Principles of fluorescence spectroscopy, New York: Kluwer Academic / Plenum Publishers (1999).

[45] J. Wang, Glucose biosensors: 40 years of advances and challenges, Electroanalysis 13 (2001) 983– 988.

[46] K. Kneipp, H. Kneipp, I. Itzkan, R.R. Dasar, M.S. Feld, Ultrasensitive chemical analysis by Raman spectroscopy, Chem. Rev. 99 (1999) 2957-2975.

[47] M. Moskovits, Surface-enhanced spectroscopy, Rev. Mod. Phys. 57 (1985) 783-826.

[48] P. Kambhampati, C.M. Child, M.C. Foster, A. Campion, On the chemical mechanism of surface enhanced Raman scattering: Experiment and theory, J. Chem. Phys. 108 (1998) 5013-5026.

[49] R.L. Garrell, Surface-enhanced Raman spectroscopy, Anal. Chem. 61 (1989) 401A- 411A.

[50] A. Campion, P. Kambhampati, Surface-enhanced Raman scattering, Chem. Soc. Rev. 27 (1998) 241-250.

[51] M.J. Weaver, S. Zou, H.Y.H Chan, The new interfacial ubiquity of surface-enhanced Raman spectroscopy, Anal. Chem. 72 (2000), 38A-47A.

[52] G.C. Weaver, K.J. Norrod, Surface enhanced Raman spectroscopy: A novel physical chemistry experiment for the undergraduate laboratory, J. Chem. Ed. 75 (1998) 621-624.

[53] G.K. Jennings, P.E. Laibinis, Self-assembled monolayers of alkanethiols on copper provide corrosion resistance in aqueous environments, Colloids and Surfaces A 116 (1996) 105-114.

[54] K.Y. Suh, J. Seong, A. Khademhosseini, P.E. Laibinis, R. Langer, A simple soft lithographic route to fabrication of poly(ethylene glycol) microstructures for protein and cell patterning, Biomaterials 25 (2004) 557-563.

[55] S. Lee, P.E. Laibinis, Protein-resistant coatings for glass and metal oxide surfaces derived from oligo(ethylene glycol)-terminated alkyltrichlorosilanes, Biomaterial 19 (1998) 1669-1675.

[56] M. Matsuzawa, K. Umemura, W. Knoll, D. Beyer, K. Sugioka, Micropatterning of neurons using organic substrates in culture, Thin Solid Films 305 (1997) 74-79.

[57] Z. Miqin, T. Desai, M. Ferrari, Proteins and cells on PEG immobilized silicon surfaces, Biomaterials 19 (1998) 953-960.

[58] M. Källtorp, S. Oblogina, S. Jacobsson, A. Karlsson, P. Tengvall, P. Thomsen, In vivo cell recruitment, cytokine release and chemiluminescence response at gold, and thiol functionalized surfaces, Biomaterials 20 (1999) 2123-2137.

[59] B. Kasemo, Biological surface science, Curr. Op. Solid State Mat. Sci. 3 (1998) 451-459.

[60] G.D. Pins, F.H. Silver, A self-assembled collagen scaffold suitable for use in soft and hard tissue replacement, Mat. Sci. Eng. 3 (1995) 101-107.

[61] I.K. Ko, K. Kato, H. Iwata, Parallel analysis of multiple surface markers expressed on rat neural stem cells using antibody microarrays, Biomaterials 26 (2005) 4882-4891.

[62] S. Lan, M. Veiseh, M. Zhang, Surface modification of silicon and gold-patterned silicon surfaces for improved biocompatibility and cell patterning selectivity, Biosens. Bioelectron. 20 (2005) 1697-1708.

[63] R. Bashir, BioMEMS: State-of-the-art in detection, opportunities and prospects, Adv. Drug Del. Rev. 56 (2004) 1565-1586.

[64] A.T. Woolley, Biomedical microdevices and nanotechnology, Trends Biotech. 19 (2001) 38-39.

[65] E. Alocilja, S. Radke, Market analysis of biosensors for food safety, Biosens. Bioelectron. 18 (2003) 841-846.

[66] R.G. Will, J.W. Ironside, M. Zeidler, K. Estibeiro, S.N. Cousens, P.G. Smith, A. Alperovitch, S. Poser, M. Pocchiari, A. Hofman, A new variant of Creutzfeldt-Jacob disease in the UK, Lancet 347 (1996) 921-955.

[67] G. Chazot, E. Broussole, C.I Lapras, T. Blättler, A. Aguzzi, N. Kopp, New variant of Creutzfeldt-Jacob disease in a 26 year-old French man, Lancet 347 (1996) 1181.

[68] National Center for Infectious Disease, Bovine spongiform encephalopathy and Creutzfeldt – Jakob disease, website of the Center for Disease Control – www.cdc.gov (2005).

[69] S.B. Prusiner, M. Scott, D. Foster, K.M. Pan, D. Groth, C. Mirenda, M. Torchia, S.L. Yang, D. Serban, G.A. Carlson, P.C. Hoppe, D. Westaway, S.J. DeArmond, Transgenic studies implicate interactions between homologous PrP isoforms in scrapie prion replication, Cell 63 (1990) 673-686.

[70] L. Fishbein, Transmissible spongiform encephalopathies, hypotheses and food safety: An overview, The Science of the Total Environment 217 (1998) 71-82.

[71] B. Oesch, D. Westaway, M. Walchl, M.P. McKinley, B.H. Kent, R. Aebersold, A cellular gene encodes scrapie PrP 27-30 protein, Cell 40 (1985) 735-776.

[72] M. Jeffrey, G. McGovern, C. Goodsir, K. Brown, M. Bruce, Sites of prion protein accumulation in scrapie-infected mouse spleen revealed by immuno-electron microscopy, Journal of Pathology 191 (2000) 323-332.

[73] S. Mouillet-Richard, M. Ermonval, C. Chebassier, J.L. Laplanche, S. Lehmann, J.M. Launay, O. Kellermann, Signal transduction through prion protein, Science, 289 (2000) 1925-1928.

[74] K.M. Pan, M. Baldwin, J. Nguyen, M. Gasset, A. Serban, D. Groth, I. Mehlhorn, Z. Huang, R.J. Fletterick, F.E. Cohen, S.B. Prusiner, Conversion of α-helices into β-sheets features in the formation of the scrapie prion proteins, Proc. Natl. Acad. Sci. 90 (1993) 10962-10966.

[75] Canadian Blood Services, vCJD symptoms, website of the Canadian Blood Services – www.bloodservices.ca (2005).

[76] G. Sternbach, C. Dibble, J. Varon, From Creutzfeldt-Jakob disease to the mad cow epidemic. The Journal of Emergency Medicine, 15 (1997) 701-705.

[77] B. Ghetti, P. Piccardo, B. Frangione, O. Bugiani, G. Giaccone, K. Young, F. Prelli, M.R. Farlow, S.R. Dlouhy, F. Tagliaveni, Prion protein amyloidosis, Brain Pathol. 6 (1996) 127-145.

[78] S.B. Prusiner, P. Tremblay, J. Safar, M. Torchia, S.J. DeArmond, Prion biology and diseases, Cold Spring Harbor Laboratory Press (1999) 113.

[79] The evaluation of tests for the diagnosis of transmissible spongiform encephalopathy in bovines (8 July 1998), European Commision DG24, Directorate B, Unit B3.

[80] B.K. Nunnally, It's a mad, mad, mad, mad cow: A review of analytical methodology for detecting BSE/TSE, Trends in Analytical Chemistry 21 (2002) 82-88.

[81] Alzheimer's Association, What is Alzheimer's disease?, website of the Alzheimer's Association – www.alz.org (2005).

[82] K.L. Davis, S.C. Samuels, Pharmacological management of neurological and psychiatric disorders, McGraw-Hill (1998) 267–316.

[83] C. Lee, M. Kung, C. Hou, H.F. Kung, Dimethylamino-fluorenes: Ligands for detecting β-amyloid plaques in the brain, Nucl. Med. Biol. 30 (2003) 573-580.

[84] A. Monsonego, R. Maron, A. Bar-Or, J.I. Krieger, D. Selkoe, H.L. Weiner, The role of T cell reactivity to A-beta amyloid peptide in the pathogenic processes associated with Alzheimer's disease, Neurobiol. Aging 21 (2000) 23.

[85] A. Dedeoglu, K. Cormier, S. Payton, K.A. Tseitlin, J.N. Kremsky, L. Lai, X. Li, R.D. Moir, R.E. Tanzi, A.I. Bush, N.W. Kowall, J.T. Rogers, X. Huang, Preliminary studies of a novel bifunctional metal chelator targeting Alzheimer's amyloidogenesis, Exper. Geron. 39 (2004) 1641-1649.

[86] N.J. Clarke, A.J. Tomlinson, Y. Ohyagi, S. Younkin, S. Naylor, Detection and quantitation of cellularly derived amyloid β peptides by immunoprecipitation-HPLC-MS, FEBS Letters 430 (1998) 419-423.

[87] E.M. Sigurdsson, Y.Z. Wadghiri, J.A. Blind, E. Kundsen, A. Asuni, M. Sadowski, D.H. Tarnhull, T. Wisniewski, In vivo magnetic resonance imaging of amyloid plaques in mice with a non-toxic Aβ derivative, Neurobiol. Aging 25 (2004) S57.

[88] A.A. Cupizzano, M.G. Furman, T.A. Bekinschtein, L. Acion, H.A. Gomila, Leuokoaraiosis and cortical atrophy in Alzheimer's disease: A quantitated study using volumetric magnetic resonance imaging, Neurobiol. Aging 21 (2000) 178.

[89] C. Köhler, U. Ebert, K. Baumann, H. Schröder, Alzheimer's disease-like neuropathology of gene-targeted APP-SLx PS1mut mice expressing the amyloid precursor protein at endogenous levels, Neurobiol. Dis. (In Press).

[90] M.P. Lambert, A.K. Barlow, B.A. Chromy, C. Edwards, R. Freed, M. Liosatos, T.E. Morgan, I. Rozovsky, B. Trommer, K.L. Viola, P. Wals, C. Zhang, C.E. Finch, G.A. Krafft, W.L. Klein, Diffusible, nonfibrillar ligands derived from A-beta 1-42 are potent CNS neurotoxins, Proc. Nat. Acad. Sci. 95 (1998) 6448-6453.

[91] K. Shoghi-Jadid, J.R. Barrio, V. Kepe, H. Wu, G.W. Small, M.E. Phelps, S. Huang, Imaging β-amyloid fibrils in Alzheimer's disease: A critical analysis

through simulation of amyloid fibril polymerization, Nucl. Med. Biol. 32 (2005) 337-351.

[92] C. Czech, V. Blanchard, N. Clavel, S. Moussaoui, G. Tremp, B. Bonici, N. Touchet, L. Pradier, A. Pharma, Expression of amyloid precursor protein and presenilin-1 in transgenic mice, Neurobiol. Aging 21 (2000) 20.

[93] G.E. Gibson, V. Haroutunian, H. Zhang, L.C. Park, R.C. Mohs, R.K.F. Sheu, J.P. Blass, The importance of mitochondrial damage in Alzheimer's disease varies according to APOE genotype, Neurobiol. Aging 21 (2000) 90.

[94] Q. Duan, X.C.H. Wang, X.M. Wang, S.S. He, J.Z.H. Wang, Development of an ultrasensitive elisa-dienzyme visible substrate recycle assay for measurement of cerebrospinal fluid tau, Neurobiol. Aging 25 (2004) S36.

[95] D.G. Cook, S. Craft, J.B. Leverenz, R.A. Roth, Insulin degrading enzyme expression is reduced in hippocampus of Alzheimer's disease patients, Neurobiol. Aging 21 (2000) 120.

[96] G.C. Gregory, J.B. Kwok, J. Xuereb, P.R. Schofield, G.M. Halliday, Beta amyloid toxicity in Alzheimer's disease, Neurobiol. Aging 25 (2004) S157-S158.

[97] C. Hertel, E. Terzi, N. Hauser, R. Jakob-Rotne, J. Seelig, J.A. Kemp, Inhibition of the electrostatic interaction between β-amyloid peptide and membranes prevents β-amyloid-induced toxicity, Proc. Natl. Acad. Sci. 94 (1997) 9412-9416.

[98] The Ronald and Nancy Reagan Research Institute of the Alzheimer's Association and the National Institute on Aging Working group, Consensus report of the working group on ''Molecular and biochemical markers of Alzheimer's disease'', Neurobiol. Aging 16 (1998) 109–116.

[99] B. Seilheimer, B. Bohrmann, L. Bondolfi, F. Muller, D. Stuber, H. Dobeli, The toxicity of the Alzheimer's β-amyloid peptide correlates with a distinct fiber morphology, J. Struct. Biol. 119 (1997) 59–71.

[100] J. Mclaurin, A. Charkrabartty, Membrane disruption by Alzheimer β-amyloid peptides mediated though specific binding to either phospholipids of gangliosides, J. Biol. Chem. 271 (1996) 26482-26489.

[101] D. Gelinas, K. DaSilva, D. Fenili, P. George-Hyslop, J. McLaurin, Immunotherapy for Alzheimer's disease, Proc. Natl. Acad. Sci. 101 (2001) 14657-14662.

[102] C. Hock, U. Konietzko, J.R. Streffer, J. Tracy, A. Signorell, B. Müller-Tillmanns, U. Lemke, K. Henke, E. Moritz, E. Garcia, M.A. Wollmer, D. Umbricht, J. De Quervain, M. Hofmann, A. Maddalena, A. Papassotiropoulos, R.M. Nitsch, Antibodies against β-Amyloid slow cognitive decline in Alzheimer's disease, Neuron 38 (2003) 547–554.

[103] D. Schenk, M. Hagen, P. Seubert, Current progress in beta-amyloid immunotherapy, Curr. Op. Immun. 16 (2004) 599–606.

[104] Y. Matsuoka Y, M. Saito, G.K. LaFrancois, V. Olm, L. Wang, E. Casey, Y. Lu, C. Shiratori, C. Lmere, K. Duff, Novel therapeutic approach for the treatment of Alzheimer's disease by peripheral administration of agents with an affinity to β-amyloid, J. Neurosci. 23 (2003) 29-33.

[105] L.K. Korah, D.G. Ahn, K.A. Kang, Mini-antibody Production Process for the Purification of Protein C, Oxygen measurements in the 21st century: Basic techniques and clinical relevance, Advances in Experimental Medicine and Biology, (D.F. Wilson, S.M. Evans, J. Biaglow, A. Pastuszko, eds.) 150 (2003) 127-132.

[106] A. Menessy, S. Aref, Correlation of soluble interleukin-2 receptor (IL2R) and tumornecrosis factor & receptor (TNF & R) levels with severity of chronic hepatitis-C liver injury, J. Hepatology 32 (2000) 196.

[107] American Diabetes Association, All about diabetes, website of the American Diabetes Association - www.diabetes.org (2005).

[108] H. Kawazumi, K. V. Gobi, K. Ogino, H. Maeda, N. Miura, Compact surface plasmon resonance (SPR) immunosensor using multichannel for simultaneous detection of small molecule compounds, Sensors and Actuators B 108 (2005) 791-796.

[109] J. Přibyl, M. Hepel, P. Skládal, Piezoelectric immunosensors for polychlorinated biphenyls operating in aqueous and organic phases, Sensors and Actuators B (In Press).

[110] B. Oh, W. Lee, B. Chun, Y. Bae, W. Lee, J. Choi, Surface plasmon resonance immunosensor for the detection of Yersinia enterocolitica, Colloids and Surfaces A 257-258 (2005) 369-374.

[111] W. Tsai, I. Lin, Development of a piezoelectric immunosensor for the detection of alpha-fetoprotein, Sensors and Actuators B 106, (2005) 455-460.

[112] M. Michalzik, R.Wilke, S. Büttgenbach, Miniaturized QCM-based flow system for immunosensor application in liquid, Sensors and Actuators B (In Press).

[113] S. Suman, R. Singhal, A. Sharma, B. Malthotra, C. Pundir, Development of a lactate biosensor based on conducting copolymer bound lactate oxidase, Sensors and Actuators B 107 (2005) 768-772.

[114] N. Bistolas, U. Wollenberger, C. Jung, F. Scheller, Cytochrome P450 biosensors—a review, Biosens. Bioelectron. 20 (2005) 2408-2423.

[115] Rajesh, V. Bisht, W. Takashima, K. Kaneto, An amperometric urea biosensor based on covalent immobilization of urease onto an electrochemically prepared copolymer poly (N-3-aminopropyl pyrrole-co-pyrrole) film, Biomaterials 26 (2005) 3683-3690.

[116] I. Basu, R. Subramanian, A. Mathew, A. Kayastha, A. Chadha, E. Bhattacharya, Solid state potentiometric sensor for the estimation of tributyrin and urea, Sensors and Actuators B 107 (2005) 418-423.

[117] L. Campanella, A. Bonanni, E. Martini, N. Todini, M. Tomassetti, Determination of triazine pesticides using a new enzyme inhibition tyrosinase OPEE operating in chloroform, Sensors and Actuators B (In Press).

[118] I. Vostiar, J. Tkac, C. Mandenius, Intracellular monitoring of superoxide dismutase expression in an Escherichia coli fed-batch cultivation using on-line disruption with at-line surface plasmon resonance detection, Anal. Biochem. (In Press).

[119] I. Tothill, A. Turner, Developments in bioassay methods for toxicity testing in water treatment, Trends Anal. Chem. 15 (1996) 178–188.

[120] I. Tothill, A. Turner, Biosensors: New developments and opportunities in the diagnosis of livestock diseases, International Atomic Energy Agency (1998) 79–94.

[121] A. Turner, Immunosensors: The next generation, Nature Biotech. 15 (1997) 421.

[122] A. Heller, Amperometric biosensors, Curr. Opin. Biotechnol. 7 (1996) 50 - 54.

[123] S. Updike, G. Hicks, The enzyme electrode, Nature 214 (1967) 986-988.

[124] G. Guilbault, Handbook of immobilized enzymes, Marcel-Dekker, NewYork, 1984.

[125] H. Lei, B. Wu, C. Cha, H. Kita, Electro-oxidation of glucose on platinum in alkaline solution and selective oxidation in the presence of additives, J. Electroanal. Chem. 382 (1995) 103-110.

[126] D. Cullen, R. Sethi, C. Lowe, A multi-analyte miniature conductance biosensor, Anal. Chim. Acta 231 (1990) 33–40.

[127] J.E. Pearson, A. Gill, P. Vadgama, Analytical aspects of biosensors, Ann Clin Biochem. 37 (2000) 119–145.

[128] J. Eckfeldt, A.S. Levine, C. Greiner, M. Kershaw, Urinary urea: Are currently available methods adequate for revival of an almost abandoned test?, Clin Chem 28 (1982) 1500– 1502.

[129] L. Grigore, G. Ensell, A. Evans, Microfabrication of sensors with magnetic resonating elements for further application in molecular probe chemistry, Sensors and Actuators A (In Press).

[130] S. Babacan, P. Pivarnik, S. Letcher, A.G. Rand, Evaluation of antibody immobilisation methods for piezoelectric biosensor application, Biosens Bioelectron 15 (2000) 615–621.

[131] D. Griffiths, G. Hall, Biosensors—what real progress is being made?, TIBTECH 11 (1993) 122–130.

[132] B. Draft, Acoustic wave technology sensors, Sensors, 17 (2000) 68-83.

[133] V.K. Yadavalli, R.J. Russell, M.V. Pishko, M.J. McShane, G.L. Coté, A Monte Carlo simulation of photon propagation in fluorescent poly(ethylene glycol) hydrogel microsensors, Sensors and Actuators B 105 (2005) 365-377.

[134] M.J. McShane, B.D. Cameron, G.L. Coté, M. Motamedi, C.H. Spiegelman, A novel peak-hopping stepwise feature selection method with application to Raman spectroscopy, Anal. Chim. Acta 388 (1999) 251-264.

[135] N.D. Botkin, V.L. Turova, Mathematical models of a biosensor, App. Math. Model., 28 (2004) 573-589.

[136] V. Rossokhaty, N. Rossokhata, Mathematical model of a biosensor with multilayer charged membrane, Comp. Phys. Comm., 147 (2002) 366-369.

[137] A. Ramakrishnan, A. Sadana, A mathematical analysis using fractals for binding interactions of nuclear estrogen receptors occurring on biosensor surfaces, Anal. Biochem. 303 (2002) 78-92.

[138] J. de Gracia, M. Poch, D. Martorell, S. Alegret, Use of mathematical models to describe dynamic behaviour of potentiometric biosensors: Comparison of deterministic and empirical approaches to an urea flow-through biosensor, Biosens. Bioelectron. 11 (1996) 53-61.

[139] G. Jobst, I. Moser, G. Urban, Numerical simulation of multi-layered enzymatic sensors, Biosens. Bioelectron. 11 (1996) 111-117.

[140] A. Neikov, S. Sokolov, Generalized model for enzyme amperometric biosensors, Anal. Chim. Acta 307 (1995) 27-36.

[141] G. Chumanov, K. Sokolov, B.W. Gregory, T.M. Cotton, Collodial metal films as a substrate for surface enhanced spectroscopy, J. Phys. Chem. 99 (1995) 9466–9471.

[142] K. Sokolov, G. Chumanov, T.M. Cotton, Enhancement of molecular fluorescence near the surface of colloidal metal films, J. Anal. Chem. 70 (1998) 3898–3905.

[143] L.A. Luck, M.J. Moravan, J.E. Garland, B. Salopek-Sondi, D. Roy, Chemisorptions of bacterial receptors for hydrophobic amino acids and sugars on gold for biosensor applications: A surface plasmon resonance study of genetically engineered proteins, Biosens. Bioelectron. 19 (2003) 249–259.

[144] E. Vogel, R. Geßner, M.H.B. Hayes, W. Kiefer, Characterisation of humic acid by means of SERS, J. Mol. Struct. 482–483 (1999) 195–199.

[145] S. Cristoph, F.J. Meyer-Almes, Novel fluorescence based receptor binding assay method for receptors lacking conjugates with preserved affinity: Study on estrogen receptor alpha, Biopolymers 72 (2003) 256–263.

[146] I.Y. Wang, Y.Y. Zhou, C.Q. Zhu, M.C. Mang, H.S. Tao, L. Wang, Fluorescence enhancing method for the determination of human serum albumin with functionalized CdS nanoparticles as fluorescence probes, Chem. J. Chin. Univ. 24 (2003) 612–614.

[147] N. Lochner, F. Pittner, M. Wirth, F. Gabor, Wheat germ agglutinin binds to the epidermal growth factor receptor of artificial Caco-2 membranes as detected by silver nanoparticles enhanced fluorescence, Pharm. Res. 20 (2003) 833–899.

[148] H. Harma, A.M. Pelkkikangas, T. Soukka, P. Huhtinen, S. Huopalahti, T. Lovgren, Sensitive miniature single-particle immunoassay of prostate-specific antigen using time-resolved fluorescence, Anal. Chim. Acta 482 (2003) 157–164.

[149] W. Chen, G. Martinez, A. Mulchandani, Molecular beacons: A real-time polymerase chain reaction assay for detecting salmonella, Anal. Biochem. 280 (2000) 166–172.

[150] D.J. Lichlyter, S.A. Grant, O. Soykan, Development of a novel FRET immunosensor technique, Biosens. Bioelectron. 19 (2003) 219–226.

[151] J. Kummerlen, A. Leitner, H. Brunner, F.R. Aussenegg, A. Wokaun, Enhanced dye fluorescence over silver island films: Analysis of the distance dependence, Mol. Phys. 80 (1993) 1031–1046.

[152] Instructions for ImmunoPure Fab preparation kit, Pierce Chemical Co. (December 2001).

[153] Product information for monomaleidmido nanogold labeling reagent, Nanoprobes Rev. 1.6 (June 2001).

[154] Product information for sulfo-N-hydroxy-succinimido-nanogold labeling reagent, Nanoprobes Rev. 1.4 (March 2000).

[155] Product information for monoamino nanogold labeling reagent, Nanoprobes Rev. 1.4 (September 2000).

[156] A. Anand, Development of a bio-sensing technique for the detection of prions in foods, Master's Thesis, Texas A&M University, 2003.

[157] M. Groschup, S. Harmeyer, E. Pfaff, Antigenic features of prion proteins of sheep and of other mammalian species, J. Immunol. Methods 207 (1997) 89–101.

[158] S. Kaluz, M. Kaluzova, A.P.F. Flint, Sequencing analysis of prion genes from red deer and camel, Gene 199 (1997) 283–286.

[159] Molecular Probes, Handbook of fluorescent probes and research products, web edition.

[160] J.W. Kelley, The environmental dependency of protein folding best explains prion and amyloid diseases, Proc. Natl. Acad. Sci. 95 (1998) 930–932.

[161] J.M. Prausnitz, Molecular thermodynamics of fluid-phase equilibria, Prentice-Hall, Englewood Cliffs, NJ, 1969.

[162] K.J. Laidler, Chemical kinetics, Harper Collins Publishers, New York, 1987.

[163] J.Y. Madec, M.H. Groschup, D. Calavas, F. Junghans, T. Baron, Protease-resistant prion protein in brain and lymphoid organs of sheep within a naturally scrapie-infected flock, Microb. Pathog. 28 (2000) 353–362.

[164] M. Bernabei, C. Cremisini, M. Mascini, G. Palleschi, Determination of organophosphorus and carbamic pesticides with a choline and acetylcholine electrochemical biosensor, Analytical Letters 24 (1991) 1317-1331.

[165] K.R. Rogers, M. Foley, S. Alter, P. Koga, M. Eldefrawi, Light addressable potentiometric biosensor for the detection of anticholinesterases, Analytical Letters 24 (1991) 191-198.

[166] J. Kulys, E.J. D'Costa, Printed Amperometric sensor based on TCNQ and cholinesterase, Biosens. Bioelectron. 6 (1991) 109–115.

[167] E.I. Rainina, E.N. Efremenco, S.D. Varfolomeyev, A.L. Simonian, J. R. Wild, The development of a new biosensor based on recombinant E. coli for the direct detection of organophosphorus neurotoxins, Biosens. Bioelectron. 11 (1996) 991-1000.

[168] A.L. Simonian, B.D. diSioudi, J.R. Wild, An enzyme based biosensor for the direct determination of diisopropyl fluorophosphates, Anal. Chim. Acta 389 (1999) 189-196.

[169] A.L. Simonian, J.K. Grimsley, A.W. Flounders, J.S. Schoeniger, T.C. Cheng, J.J. DeFrank, J.R. Wild, Enzyme-based biosensor for the direct detection of fluorine-containing organophosphates, Anal. Chim. Acta 442 (2001) 15-23.

[170] A.W. Flounders, A.K. Singh, J.V. Volponi, S.C. Carichner, K. Wally, A.S. Simonian, J.R. Wild J.S. Schoeniger, Development of sensors for direct detection of organophosphates.: Part II: Sol–gel modified field effect transistor with immobilized organophosphate hydrolase, Biosens. Bioelectron. 14 (1999) 715-722.

[171] R.J. Russell, M.V. Pishko, A.L Simonian, J.R. Wild, Poly(ethylene glycol) hydrogel-encapsulated fluorophore-enzyme conjugates for direct detection of organophosphorus neurotoxins, Anal. Chem. 71 (1999) 4909 – 4912.

[172] J. Henry, A. Anand, M. Chowdhury, G. Coté, R. Moreira, T. Good, Development of a nanoparticle-based surface-modified fluorescence assay for the detection of prion proteins, Anal. Biochem. 334 (2004) 1-8.

[173] A.L. Simonian, T.A. Good, S.-S. Wang, J.R. Wild, Nanoparticle-based optical biosensors for the direct detection of organophosphate chemical warfare agents and pesticides, Anal. Chim. Acta 534 (2005) 69-77.

[174] B.J. Bacskai, J. Skoch, W.E. Klunk, E. Nesterov, T.M. Swager, C.A. Mathis, A. Dunn, B.T. Hyman, Novel approaches for non-invasive optical detection of amyloid-β plaques in vivo, Neurobiol. Aging 25 (2004) S57-S58.

[175] Z. Zhuang, M. Kung, C. Hou, K. Plössl, D. Skovronsky, T.L. Gur, J.Q. Trojanowski, V.M.Y. Lee, H.F. Kung, IBOX(2-(4′-dimethylaminophenyl)-6-iodobenzoxazole): A ligand for imaging amyloid plaques in the brain, Nucl. Med. Biol. 28 (2001) 887-894.

[176] R.A.Fishman, Cerebrospinal fluid in diseases of the nervous system, WB Saunders, Philadelphia, 1980.

[177] E.J. Thompson, The CSF proteins: A biomedical approach, Elsevier (1988) 117–20.

[178] M. Vandermeeren, M. Mercken, E. Vanmechelen, Detection of tau proteins in normal and Alzheimer's disease cerebrospinal fluid with a sensitive sandwich enzyme-linked immunosorbent assay, J. Neurochem. 61 (1993) 1828– 1834.

[179] K. Blennow, A. Wallin, H. Agren, C. Spenger, J. Siegfried, E. Vanmechelen, Tau protein in cerebrospinal fluid: A biochemical marker for axonal degeneration in Alzheimer disease? Mol. Chem. Neuropathol. 26 (1995) 231–245.

[180] C. Vigo-Pelfrey, P. Seubert, R. Barbour R, Elevation of microtubule-associated protein tau in the cerebrospinal fluid of patients with Alzheimer's disease, Neurology 45 (1995) 788– 93.

[181] A.J. Green, R.J. Harvey, E.J. Thompson, M.N. Rossor, Increased tau in the cerebrospinal fluid of patients with frontotemporal dementia and Alzheimer's disease, Neurosci. Lett. 259 (1999) 133–135.

[182] L. Molina, J. Touchon, M. Herpe, Tau and apo E in CSF: Potential aid for discriminating Alzheimer's disease from other dementias, Neuroreport 10 (1999) 3491– 3495.

[183] N. Andreasen, L. Minthon, P. Davidsson, Evaluation of CSF-tau and CSF-Aβ42 as diagnostic markers for Alzheimer disease in clinical practice, Arch. Neurol. 58 (2001) 373–379.

[184] T. Tapiola, M. Overmyer, M. Lehtovirta, The level of cerebrospinal fluid tau correlates with neurofibrillary tangles in Alzheimer's disease, Neuroreport 8 (1997) 3961– 3963.

[185] M. Sjogren, P. Davidsson P J.Gottfries, The cerebrospinal fluid levels of tau, growth-associated protein-43 and soluble amyloid precursor protein correlate in Alzheimer's disease, reflecting a common pathophysiological process, Dement. Geriatr. Cogn. Disord. 12 (2001) 257–264.

[186] R. Motter, P.C. Vigo, D. Kholodenko, Reduction of beta-amyloid peptide 42 in the cerebrospinal fluid of patients with Alzheimer's disease, Ann. Neurol. 38 (1995) 643–648.

[187] A. Tamaoka, N. Sawamura, T. Fukushima, Amyloid beta protein 42(43) in cerebrospinal fluid of patients with Alzheimer's disease, J. Neurol. Sci. 148 (1997) 41–45.

[188] P.D. Mehta, T. Pirttila, S.P. Mehta, E.A. Sersen, P.S. Aisen, H.M. Wisniewski, Plasma and cerebrospinal fluid levels of amyloid beta proteins 1 – 40 and 1 – 42 in Alzheimer disease, Arch. Neurol. 57 (2000) 100–105.

[189] H. Vanderstichele, K. Blennow, N. D'Heuvaert, Development of a specific diagnostic test for measurement of β-amyloid(1–42) in CSF. In: Fisher A, Hanin I, Yoshida M, editors. Progress in Alzheimer's and Parkinson's diseases, New York: Plenum (1998) 773–778.

[190] K. Kanemaru, N. Kameda, H. Yamanouchi, Decreased CSF amyloid β 42 and normal tau levels in dementia with Lewy bodies, Neurology 54 (2000) 1875–1876.

[191] F. Hulstaert, K. Blennow, A. Ivanoiu, Improved discrimination of AD patients using beta-amyloid(1 – 42) and tau levels in CSF, Neurology 52 (1999) 1555–1562.

[192] M. Sjogren, P. Davidsson, A. Wallin, Decreased CSF-[beta]-amyloid 42 in Alzheimer's disease and amyotrophic lateral sclerosis may reflect mismetabolism of [beta]-amyloid induced by disparate mechanisms, Dement. Geriatr. Cogn. Disord. 13 (2002) 112–118.

[193] K. Ishiguro, H. Ohno, H. Arai, Phosphorylated tau in human cerebrospinal fluid is a diagnostic marker for Alzheimer's disease, Neurosci. Lett. 270 (1999) 91–94.

[194] R. Kohnken, K. Buerger, R. Zinkowski, Detection of tau phosphorylated at threonine 231 in cerebrospinal fluid of Alzheimer's disease patients, Neurosci. Lett. 287 (2000) 287 187–190.

[195] Y.Y. Hu, S.S. He, X. Wang, Levels of nonphosphorylated and phosphorylated tau in cerebrospinal fluid of Alzheimer's disease patients: An ultrasensitive bienzyme-substrate-recycle enzyme-linked immunosorbent assay, Am. J. Pathol. 160 (2002) 1269– 1278.

[196] M. Sjogren, P. Davidsson, M. Tullberg, Both total and phosphorylated tau are increased in Alzheimer's disease, J. Neurol. Neurosurg. Psychiatry 70 (2001) 624–630.

[197] L. Parnetti, A. Lanari, S. Amici, V. Gallai, E. Vanmechelen, F. Hulstaert, CSF phosphorylated tau is a possible marker for discriminating Alzheimer's disease from dementia with Lewy bodies. Phospho-Tau International Study Group, Neurol. Sci. 22 (2001) 77–78.

[198] D. Galasko, L. Chang, R. Motter, High cerebrospinal fluid tau and low amyloid β 42 levels in the clinical diagnosis of Alzheimer disease and relation to apolipoprotein E genotype, Arch. Neurol. 55 (1998) 937–945.

[199] M. Kanai, E. Matsubara, K. Isoe, Longitudinal study of cerebrospinal fluid levels of tau, Aβ 1– 40, and Aβ 1 – 42(43) in Alzheimer's disease: A study in Japan, Ann. Neurol. 44 (1998) 17– 26.

[200] N. Andreasen, L. Minthon, P. Davidsson, Evaluation of CSF-tau and CSF-AB42 as diagnostic markers for Alzheimer's disease in clinical practice, Arch. Neurol. 58 (2001) 373–379.

[201] N. Andreasen, L. Minthon, E. Vanmechelen, Cerebrospinal fluid tau and Abeta42 as predictors of development of Alzheimer's disease in patients with mild cognitive impairment, Neurosci. Lett. 273 (1999) 5–8.

[202] A. Kurz, M. Riemenschneider, K. Buch, Tau protein in cerebrospinal fluid is significantly increased at the earliest clinical stage of Alzheimer disease, Alzheimer Dis. Assoc. Disord. 12 (1998) 372–377.

[203] M. Riemenschneider, K. Buch, M. Schmolke, A. Kurz, W.G. Guder, Cerebrospinal protein tau is elevated in early Alzheimer's disease, Neurosci. Lett. 212 (1996) 212 209–211.

[204] M. Riemenschneider, M. Schmolke, N. Lautenschlager, Cerebrospinal beta-amyloid ((1 –42)) in early Alzheimer's disease: Association with apolipoprotein E genotype and cognitive decline, Neurosci. Lett. 284 (2000) 85–88.

[205] H.W. Wang, J. F. Pasternak, H. Kuo, H. Ristic, M.P. Lambert, B. Chromy, K.L. Viola, W.L. Klein, W.B. Stine, G.A. Krafft, B.L. Trommer, Soluble oligomers of beta amyloid (1-42) inhibit long-term potentiation but not long-term depression in rat dentate gyrus, Brain. Res. 924 (2002) 133-40.

[206] Business Wire Date, Acumen and Merck enter into Alzheimer's collaboration, January 13, 2004

[207] L.V. Johnson, W.P. Leitner, A.J. Rivest, M.K. Staples, M.J. Radeke, D.H Anderson, The Alzheimer's A beta -peptide is deposited at sites of complement activation in pathologic deposits associated with aging and age-related macular degeneration, Proc. Natl. Acad. Sci. 99 (2002) 11830-11835.

[208] C.M. Clark, S.Xie, J. Chittams, D. Ewbank, E. Peskind, D. Galasko, J.C. Morris, D.W. McKeel Jr, M. Farlow, S.L. Weitlauf, J. Quinn, J. Kaye, D. Knopman, H. Arai, R.S. Doody, C. DeCarli, S. Leight, V.M. Lee, J.Q. Trojanowski, Cerebrospinal fluid tau and beta-amyloid: How well do these biomarkers reflect autopsy-confirmed dementia diagnoses?, Arch. Neurol. 60 (2003) 1696–1702.

[209] H. Hampel, A. Goernitz, K. Buerger, Advances in the development of biomarkers for Alzheimer's disease: From CSF total tau and $A\beta_{1-42}$ proteins to phosphorylated tau protein, Brain Res. Bulletin 61 (2003) 243-253

[210] H. Zetterberg, L. Wahlund, K. Blennow, Cerebrospinal fluid markers for prediction of Alzheimer's disease, Neurosci. Lett. 352 (2003) 67-69.

[211] Y.S. Kim, J.A. Moss, K.D. Janda, P1-175 Development of conformation-specific antibodies for neutralization of β-amyloid oligomers, Neurobiol. Aging 25 (2004) S145.

[212] C.D. Hock, U. Konietzko, A. Papassotiropoulos, A. Wollmer, J. Streffer, R.C. von Rotz, G. Davey, E. Moritz, R.M. Nitsch, Generation of antibodies specific for β-amyloid by vaccination of patients with Alzheimer disease, Nat. Med. 8 (2002) 1270–1275.

[213] T. Town, J. Tan, N. Sansone, D. Obregon, T. Klein, M. Mullan, Characterization of murine immunoglobulin G antibodies against human amyloid-β_{1-42}, Neurosci. Lett. 307 (2001) 101-104.

[214] T. Ariga, R.Yu, GM-1 inhibits amyloid β-protein-induced cytokine release, Neurochem. Res. 24 (1999) 219-226.

[215] T. Ariga, K. Kobayashi, A. Hasegawa, M. Kiso, H. Ishida, T. Miyatake, Characterization of high-affinity binding between gangliosides and amyloid β-protein, Arch. Biochem. Biophys. 388 (2001) 225–230.

[216] N.A. Avdulov, S.V. Chochina, U. Igbavboa, C.S. Warden, V.A. Vassiliev, W.G. Wood, Lipid binding to amyloid β-peptide aggregates: Preferential binding of cholesterol as compared with phosphadidylcholine and fatty acids. J. Neurochem. 69 (1997) 1746-1752.

[217] S. Wang, D. Rymer, T. Good, Reduction in cholesterol and sialic acid content protects cells from the toxic effects of β-amyloid peptides, J. Biol. Chem. 276 (2001) 42027-42034.

[218] L. Choo-Smith, W. Garzon-Rodriguez, C.G. Glabe, W.K. Surewicz, Acceleration of amyloid fibril formation by specific binding of Aβ(1-40) peptide of ganglioside containing vesicles, J. Biol. Chem. 272 (1997) 22987-22990.

[219] A. Kakio, S.I. Nishimoto, K. Yanagisawa, Y. Kozutsumi, K. Matsuzaki, Cholesterol-dependent formation of GM1 fanglioside-bound amyloid β-protein, an endogenous seed for Alzheimer amyloid, J. Biol. Chem. 276 (2001) 24985-24990.

[220] J. Mclaurin, A. Chakrabartty, Membrane disruption by Alzheimer β-amyloid peptides mediated though specific binding to either phospholipids of gangliosides, J. Biol. Chem. 271 (1996) 26482-26489.

[221] K. Matsuzaki, C. Horikiri, Interactions of amyloid β-peptide (1-40) with ganglioside-containing membranes, Biochem. 38 (1999) 4137-4142.

[222] Product Instructions for EDC attachment to proteins, Pierce Chemical Co. (May 2002).

[223] J.B. Leach, K.A. Bivens, C.W. Patrick Jr., C.E. Schmidt, Photocrosslinked hyaluronic acid hydrogels: Natural, biodegradable tissue engineering scaffold, Biotech. Bioeng. 82 (2003) 578-589.

[224] T. Miura, S. Mitani, C. Takanashi, N. Mochizuki, Copper selectively triggers β-sheet assembly of an N-terminally truncated amyloid β-peptide beginning with Glu3, J. Inorg. Biochem. 98 (2004) 10-14.

[225] K. Suzuki, T. Miura, H. Takeuchi, Inhibitory Effect of copper(II) on zinc(II)-induced aggregation of amyloid β-peptide, Biochem. Biophys. Res. Comm. 285 (2001) 991-996.

[226] T.M. Willey, A.L. Vance, T. van Buuren, C. Bostedt, L.J. Terminello, C.S. Fadley, Rapid degradation of alkanethiol-based self-assembled monolayers on gold in ambient laboratory conditions, Surf. Sci. 576 (2005) 188-196.

[227] S.B. Prusiner, S. Supattapone, M.R. Scott, U.S. Patent 6,517,855 (2003).

[228] W. Wattanakaroon, Development of an interleukin 2 receptor targeted gene therapy vehicle, Doctoral Dissertation, Texas A&M University, College Station (2005).

[229] A. Kakio, S.I. Nishimoto, K. Yanagisawa, Y. Kozutsumi, K. Matsuzaki, Cholesterol-dependent formation of GM1 ganglioside-bound amyloid β-protein, an endogenous seed for Alzheimer amyloid, J. Biol. Chem. 276 (2001) 24985-90.

[230] C.W. Cairo, A. Strzelec, R.M. Murphy, L.L. Kiessling, Affinity based inhibition of β-amyloid toxicity, Biochemistry 41 (2002) 8620-8629.

[231] T. Ariga, K. Kobayashi, A. Hasegawa, M. Kiso, H. Ishida, T. Miyatake, Characterization of high-affinity binding between gangliosides and amyloid β-protein. Archives of Biochemistry and Biophysics 388 (2001) 225–230.

[232] L.E. Hebert, P.A. Scherr, J.L. Bienias, D.A. Bennett, D.A. Evans, Alzheimer disease in the U.S. population: Prevalence estimates using the 2000 census, Arch. Neurol. 60 (2003) 1119 – 1122.

[233] R.L. Ernst, J.W. Hay, The U.S. economic and social Costs of alzheimer's disease revisited, American Journal of Public Health 84 (1994) 1261 – 1264.

[234] R. Koppel, Alzheimer's disease: The costs to U.S. businesses in 2002. National Institutes of Health publication number 03-5333, Alzheimer's Association (2003) 2.

[235] D.J. Selkoe, Translating cell biology into therapeutic advances in Alzheimer's disease, J. Neuropathol. Exp. Neurol. 53 (1994) 438–447.

[236] D.M. Hartley, D.M. Walsh, C.P. Ye, T. Diehl, S. Vasquez, P.M. Vassilev, D.B. Teplow, D.J. Selkoe, Protofibrillar intermediates of amyloid β-protein induces acute electrophysical changes and progressive neurotoxicity in cortical neurons, J. Neurosci. 19 (1999) 8876–8884.

[237] R.V. Ward, K.H. Jennings, R. Jepras, W. Neville, D.E. Owen, J. Hawkins, G. Christie, J.B. Davis, A. George, E.H. Karran, D.R. Howlett, Fractionation and charecterization of oligomeric, protofibrillar and fibrillar forms of β-amyloid peptide, Biochem. J. 348 (2000) 137–144.

[238] N.A. Avdulov, S.V. Chochina, U. Igbavboa, C.S. Warden, A.V. Vassiliev, W.G. Wood, Lipid binding to amyloid β-peptide aggregates: Preferential binding of cholesterol as compared with phosphadidylcholine and fatty acids, J. Neurochem. 69 (1997) 1746-1752.

[239] L. Choo-Smith, W. Garzon-Rodriguez, C.G. Glabe, W.K. Surewicz, Acceleration of amyloid fibril formation by specific binding of Aβ(1-40) peptide of ganglioside containing vesicles, J. Biol. Chem. 272 (1997) 22987-22990.

[240] T. Ariga, R. Yu, GM-1 inhibits amyloid β-protein-induced cytokine release, Neurochem. Res. 24 (1999) 219-226.

[241] K. Matsuzaki, C. Horikiri, Interactions of amyloid β-peptide (1-40) with ganglioside-containing membranes, Biochemistry 38 (1999) 4137-4142.

[242] S. Lee, K. Carson, A. Rice-Ficht, T. Good, Hsp20, a novel α-crystallin, prevents Aβ fibril formation and toxicity, Protein Sci. (In Press).

[243] D. Rymer, T. Good, The role of G protein activation in the toxicity of amyloidogenic Aβ (1-40), Aβ (25-35), and bovine calcitonin, J. Biol. Chem. 276 (2001) 2523-2530.

[244] R. Linares, In vitro model of photodynamic therapy using IL-2-photosensitizer conjugate directed to IL-2 receptor-bearing T-cells, Doctoral Dissertation, Texas A&M University, College Station (2000).

[245] M. van Engeland, C.S. Ramaekers, B. Schutte, C.P.M. Reutelingsperger, A novel assay to measure loss of plasma membrane asymmetry during apoptosis of adherent cells in culture, Cytometry 24 (1996) 131-139.

[246] K. Yanagisawa, A. Odaka, N. Suzuki, Y. Ihara, GM1 ganglioside-bound amyloid β-protein (Aβ): A possible form of preamyloid in Alzheimer's disease, Nature Med. 1 (1995) 1062-1066.

[247] J. Mclaurin, T. Franklin, P. Frazer, A. Charkrabartty, Structural transitions associated with the interaction of Alzheimer β-amyloid peptides with gangliosides, J. Biol. Chem. 273 (1998) 4506-4515.

[248] J. Reuter, A. Myc, M. Hayes, Z. Gan, R. Roy, D. Qin, R. Yin, L.T. Piehler, R. Esfand, D.A. Tomalia, J.R. Baker, Inhibition of viral adhesion and infection by sialic acid-conjugated dendritic polymers, Bioconjugate Chem. 10 (1999) 271-278.

[249] T. Pritchett, J. Paulson, Basis for the potent inhibition of influenza virus infection by equine and guinea pig α_2-macroglobulin, J. Biol. Chem. 264 (1989) 9850-9858.

[250] J. Landers, Z. Cao, I. Lee, Prevention of influenza pneumonitis by sialic acid-conjugated dendritic polymers, J. Infect. Dis. 186 (2002) 1222-1230.

[251] D. Fischer, Y. Li, B. Ahlemeyer, J. Krieglstein, T. Kissel, In vitro cytotoxicity testing of polycations: Influence of polymer structure on cell viability and hemolysis, Biomaterials 24 (2003) 1121-1131.

[252] W.J. Lees, A. Spaltenstein, J.E. Kingery-Wood, J.M. Whitesides, Polyacrylamides bearing pendant α-sialoside groups strongly inhibit agglutination of erythrocytes by influenza A virus: Multivalency and steric stabilization of particulate biological systems, J. Med. Chem. 37 (1994) 3419-3433.

[253] P. Blumberg, Protein kinase C as the receptor for the phorbol ester tumor promoters: Sixth Rhoads memorial award lecture, Cancer Res. 48 (1988) 1-8.

[254] R. Etcheberringaray, M. Tan, I. Dewachter, C. Kuiperi, I. Van der Auwera, S. Wera, L. Qiao, B. Bank, T. Nelson, A. Kozikowski, F. Van Leuven, D. Alkon, Therapeutic effects of PKC activators in Alzheimer's disease transgenic mice, Proc. Natl. Acad. Sci. 101 (2004) 11141-11146.

[255] J. Ghanta, C. Shen, L.L. Kiessling, R.M. Murphy, A strategy for designing inhibitors of β-amyloid toxicity, J. Biol. Chem. 271 (1996) 29525-29528.

[256] B. Blanchard, A. Chen, L. Rozenboom, K. Stafford, P. Weigele, V. Imgram, Efficient reversal of Alzheimer's disease fibril formation and elimination of neurotoxicity by a small molecule, Proc. Natl. Acad. Sci. 101 (2004) 14326-14332.

[257] L. Bergamaxchini, E. Rossi, C. Storini, S. Pizzimenti, M. Distaso, C. Perego, A. De Luigi, C. Vergani, M. De Simoni, Peripheral treatment with enoxaparin, a low molecular weight heparin, reduces plaques and β-amyloid accumulation in a mouse model of Alzheimer's disease, J. Neurosci. 24 (2004) 4186-4181.

[258] T. Ren, D. Liu, Synthesis of targetable cationic amphiphiles, Tetrahedron Lett. 40 (1999) 7621-7625.

[259] E.K. Woller, M.J. Cloninger, The lectin-binding properties of six generations of mannose-functionalized dendrimers, Organic Lett. 4 (2002) 7-10.

[260] E.K. Woller, E.D. Walter, J.R. Morgan, D.J. Singel, M.J. Cloninger, Altering the strength of lectin binding interactions and controlling the amount of lectin clustering using mannose/hydroxy-functionalized dendrimers, J. Am. Chem. Soc. 125 (2003) 8820-8826.

[261] L. Warren, The thiobarbituric acid assay of sialic acids, J. Biol. Chem. 234 (1959) 1971-1975.

VITA

Name:	James Edward Henry
Address:	Gordon A. & Mary Cain Department of Chemical Engineering, Louisiana State University, 110 Chemical Engineering, South Stadium Rd., Baton Rouge, LA 70803
Email Address:	james_e_henry@yahoo.com
Education:	B.S., Chemical Engineering, The University of Arkansas at Fayetteville, 1997 M.S., Chemical Engineering, The University of Arkansas at Fayetteville, 2000 Ph.D., Chemical Engineering, Texas A&M University, 2005